

Aus dem Institut für Physiologie und Pathophysiologie
des Fachbereichs Medizin der Philipps-Universität Marburg
Geschäftsführender Direktor: Prof. Dr.Dr. J. Daut

Philipps



Universität
Marburg

Voltage sensitive phosphatases:
understanding their function and
expanding their potential use

Inaugural-Dissertation zur Erlangung des Doktorgrades der Naturwissenschaften
dem Fachbereich Medizin der Philipps-Universität Marburg

vorgelegt von

Angeliki Mavrantoni

aus Korfu

Marburg, 2016

**Angenommen vom Fachbereich Medizin der Philipps-Universität Marburg
am: 22.04.2016**

Gedruckt mit Genehmigung des Fachbereichs.

Dekan: Prof. Dr. Helmut Schäfer

Referent: Prof. Dr. Dominik Oliver

1. Korreferent: Prof. Dr. Bünemann

Table of Contents

i.	Figures	5
ii.	Tables.....	6
iii.	Abbreviations	7
iv.	Aminoacids.....	8
v.	Summary	9
vi.	Zusammenfassung.....	11
1	Introduction	13
1.1	Voltage sensitive phosphatases	13
1.2	Phosphoinositides.....	15
1.3	Experimental control of phosphoinositides	16
1.4	Structure of VSPs	17
1.5	Human VSPs.....	20
1.6	Physiological role of VSPs.....	21
1.7	PTEN	22
1.7.1	PTEN and disease.....	22
1.7.2	PTEN structure and PTEN _{CIV}	23
1.8	Experimental approaches to study VSPs.....	25
1.8.1	Measurement of sensing current	26
1.8.2	Measurement of catalytic activity	27
1.9	Aims of this work	29
2	Materials and Methods	32
2.1	Molecular Biology	32
2.2	Cell culture and transfection	33
2.3	Patch clamping	35
2.3.1	Background.....	35
2.3.2	Patch clamping protocols.....	37
2.4	Total Internal Reflection Fluorescence (TIRF) Microscopy	38
2.5	Confocal Laser Scanning Microscopy.....	40
2.6	Förster Resonance Energy Transfer (FRET)	42
2.7	Solutions and chemicals.....	43
2.8	Data analysis.....	44
3	Results	47

3.1	Functional characterization of VSPs	47
3.1.1	Generation of a functional human VSP chimera targeted to the plasma membrane	47
3.1.2	Functional characterization of a novel PTEN oncogenic mutation	51
3.1.3	The effect of intracellular pH and redox state on VSPs	53
3.2	Development of an experimentally simple method for manipulation of cellular PI concentrations and for analysis of PTEN	63
3.2.1	Activation of Ci-VSP in intact cells by membrane depolarization via cation channels.....	64
3.2.2	Monitoring Ci-VSP activity without imaging	68
3.2.3	PTEN _{CiV} chimera for functional analysis of the tumor suppressor PTEN ..	71
3.2.4	PTEN _{CiV} can be exploited to test PTEN inhibitors	74
3.2.5	PTEN _{CiV} activation allows for rapid control of PI3K downstream pathways.....	77
4	Discussion	79
4.1	Functional characterization of VSPs	79
4.1.1	Generation of chimera for targeting hVSP1 to the membrane	79
4.1.2	hVSP1 is a 5-phosphatase in living cells.....	81
4.1.3	Novel oncogenic gain-of-function PTEN mutant.....	81
4.1.4	Does pH affect the catalytic activity of VSPs?	82
4.1.5	Interaction between C363 and C310 possibly underlies the inhibition of Ci-VSP by oxidation.	83
4.2	Controlling VSPs and PTEN _{CiV} without electrophysiology	84
4.2.1	Comparison of our method with previously described PI manipulation techniques	85
4.2.2	Three different cation channels for induction of membrane depolarization.....	86
4.2.3	Analysis of PTEN mutants and inhibitors	86
4.3	Outlook.....	88
5	References	91
6	Acknowledgments.....	98
7	Publications.....	99
8	Curriculum vitae	100
9	List of academic teachers	101
10	Ehrenwörtliche Erklärung	102

i. Figures

Figure 1.1: Structure and metabolism of phosphoinositides.....	15
Figure 1.2: Schematic representation of a VSP.	17
Figure 1.3: Structure of Ci-VSP.	19
Figure 1.4: Human VSPs and their isoforms.	20
Figure 1.5: Simplified phosphatidylinositol 3-kinase (PI3K) signaling pathway.....	22
Figure 1.6: Ci-VSP, PTEN and PTEN _{CIV}	24
Figure 1.7: VSPs' sensing currents.	26
Figure 1.8: K ⁺ channels for monitoring the catalytic activity of VSPs.....	27
Figure 1.9: PI sensors for monitoring the catalytic activity of VSPs.	29
Figure 2.1: The whole-cell patch clamping technique.....	36
Figure 2.2: Protocol for Kir2.1/Dr-VSP measurements.....	38
Figure 2.3: TIRF microscopy function and measurements.....	39
Figure 2.4: Confocal microscopy.....	41
Figure 2.5: The FRET approach.	43
Figure 2.6: Data calculation and curve fitting.	45
Figure 3.1: Cellular localization and sensing currents of wild type and chimeric VSPs..	48
Figure 3.2: Enzymatic activity of hVSP1 _{CIV}	50
Figure 3.3: The PTEN A126G oncogenic mutant is causing a gain of function.....	52
Figure 3.4: Increased PI(4,5)P ₂ depletion at acidic pH with Dr-VSP.	55
Figure 3.5: Other VSPs present similar sensitivity to pH.	56
Figure 3.6: Intracellular pH does not affect the PI(3,4,5) ₃ depletion via Dr-VSP.	56
Figure 3.7: The sensing of Dr-VSP was not affected by the different pH _{int}	57
Figure 3.8: The kinetics of PI(4,5)P ₂ resynthesis are not affected by the pH _{int}	58
Figure 3.9: pH sensitivity of PI(4,5)P ₂ depletion is independent of the buffer.	59
Figure 3.10: Mutagenesis of histidines does not abolish the pH sensitivity of Dr-VSP. .	60
Figure 3.11: The effect of oxidation on the phosphatase activity of Ci-VSP.....	63
Figure 3.12: Activation of Ci-VSP by membrane depolarization through overexpressed cation channels.	66
Figure 3.13: Comparison of the three depolarization methods in HEK cells cotransfected with Ci-VSP, tubbyC and one of the different channels.	68
Figure 3.14: FRET sensors to monitor Ci-VSP activation.....	69
Figure 3.15: Selection of a suitable channel and sensor for studying PTEN _{CIV}	72
Figure 3.16: Analyzing PTEN mutations using PTEN _{CIV} and TRPV1 mediated membrane depolarization.....	73
Figure 3.17: PTEN _{CIV} is inhibited by bisperoxovanadate compounds.....	75
Figure 3.18: bpV(phen) and bpV(HOpic) abolish PTEN _{CIV} activity at micromolar concentrations when applied intracellularly.....	76
Figure 3.19: Activation of PTEN _{CIV} leads to rapid dephosphorylation of FOXO1.....	77
Figure 4.1: Summary of the regulation of VSPs by pH and oxidizing agents.	84

ii. Tables

Table 1: All characterized voltage sensitive phosphatases.....	14
Table 2: Different PIs, their cellular localization and their role in cellular function.	16
Table 3: Biosensors used in this work.....	28
Table 4: List of the plasmids used in this study.....	35

iii. Abbreviations

ASDs, autism spectrum disorders

AKT, protein kinase B, PKB

bpV, bisperoxovanadium

C-tail, the carboxyl-terminus domain

CBR3, calcium binding region 3

CCD camera, charged coupled device

CFP, cyan fluorescent protein

CHO, Chinese hamster ovary cells

ChR2, channelrhodopsin-2

Ci-VSP, *Ciona intestinalis* voltage sensitive phosphatase

COSMIC, catalogue of somatic mutations in cancer

CRY2-CIBN, cryptochrome 2- CRY2-interacting bHLH 1

Dr-VSP, *Danio rerio* voltage sensitive phosphatase

DTT: Dithiothreitol

EC₅₀, half maximal effective concentration

ER, endoplasmic reticulum

FHA1, forkhead-associated domain

FKBP-FRB, FK506 binding protein-fragment of mammalian target of rapamycin [mTOR]
that binds FKBP

FOXO1, forkhead box 1

FRET, Förster resonance energy transfer

GFP, green fluorescent protein

Gg-VSP, *Gallus gallus* voltage sensitive phosphatase

GSSG, glutathione disulfide

H₂O₂, hydrogen peroxide

HEK, human embryonic kidney 293 cells

hVSP, human voltage sensitive phosphatase

Kir2.1, inwardly rectifying potassium channel 2.1, IRK

mTOR, mammalian target of rapamycin

P-loop, phosphatase binding loop
 PBM, PIP₂ binding module
 PDK1, phosphoinositide dependent kinase 1
 PDZ, postsynaptic density protein–*Drosophila* disc large tumor suppressor–zonula occludens 1 protein domain
 PH, pleckstrin homology
 PI, phosphoinositide
 PIP, phosphoinositide phosphate
 PI3K, phosphatidylinositol 3-kinase
 PKB, protein kinase B, AKT
 PTEN, phosphatase and tensin homologue deleted from chromosome 10
 PTEN_{Civ}, PTEN with *Ciona intestinalis* voltage sensor
 RFP, red fluorescent protein
 ROS, reactive oxygen species
 TPIP, TPE and PTEN homologous inositol lipid phosphatase, hVSP1
 TPTE, transmembrane phosphatase with tensin homology, hVSP2
 TIRF, total internal reflection fluorescence
 TRPV1, transient receptor potential vanilloid 1
 τ, time constant
 V_{1/2}, voltage for half maximal current inhibition
 VSD, voltage sensor domain
 VSP, voltage sensitive phosphatase
 XI-VSP, *Xenopus laevis* voltage sensitive phosphatase
 YFP, yellow fluorescent protein

iv. Aminoacids

A, alanine	H, histidine	R, arginine
C, cysteine	K, lysine	S, serine
D, aspartic acid	L, leucine	V, valine
E, glutamic acid	N, asparagine	
G, glycine	P, proline	

v. Summary

Voltage sensitive phosphatases: understanding their function and expanding their potential use

Voltage sensitive phosphatases (VSPs) are proteins consisting of two distinct domains: a transmembrane voltage sensor domain (VSD) and a cytosolic phosphatase domain highly similar to the human tumor suppressor protein PTEN (phosphatase and tensin homologue deleted from chromosome 10). The first characterized VSP was isolated from the sea squirt *Ciona Intestinalis*, named Ci-VSP, one decade ago. Upon membrane depolarization, Ci-VSP has phosphatase activity against phosphoinositide (PI) substrates and acts predominantly as a 5-phosphatase of PI(4,5)P₂ and PI(3,4,5)P₃.

VSPs exist in several species, including human, and although their function and physiological role are not completely understood, they have been proven excellent tools to rapidly and reversibly alter the phosphoinositide content of the plasma membrane in living cells.

The first part of this work focuses on further characterizing and understanding the function of VSPs by using well established techniques. We used whole-cell patch clamping to control VSPs and total internal reflection fluorescent (TIRF) microscopy to record their activity.

We first investigated the human VSP isoform 1 (hVSP1). hVSP1 lacks plasma membrane localization and has not been characterized in depth. Here we attempted to target hVSP1 to the plasma membrane and examine its enzymatic activity. We found that complete replacement of the VSD of hVSP1 with that of Ci-VSP resulted in a membrane targeted, voltage activated 5-phosphatase of PI(4,5)P₂.

Given the similarity of VSPs with PTEN, the chimeric protein PTEN_{CiV} had been created previously by fusing the VSD of Ci-VSP with PTEN. PTEN_{CiV} fully represents the enzymatic activity of PTEN (3-phosphatase of PI(3,4)P₂ and PI(3,4,5)P₃) and by being voltage regulated it comprises a powerful tool for studying this tumor suppressor. Specifically, we characterized the enzymatic activity of a novel PTEN mutation, A126G, identified from a prostate cancer patient. This mutation was found to convert the substrate specificity of PTEN from a 3- to a 5-phosphatase.

VSPs are suggested to be involved in processes where pH and redox state changes are known to occur. Therefore we next investigated the effect of intracellular pH and redox state on VSPs activity. We saw that acidic pH increases the PI(4,5)P₂ depletion by VSPs, while oxidation inhibits the enzymatic activity. Thus, it seems possible that pH and oxidation can, in addition to voltage, contribute to a fine modulation of VSPs.

In the second part, we developed an easily applicable method to use VSPs for manipulation of PI levels without the use of patch clamping. We used different cation channels that upon activation led to membrane depolarization and consequently VSP activation. We then characterized methods to monitor PIs levels, using fluorescence microscopy or photometry. At last, we demonstrated the application of these techniques by employing PTEN_{CIV} to characterize the effect of known PTEN mutations and analyze the effect of PTEN inhibitors.

In conclusion, in this work we increased our understanding regarding several aspects of VSPs activity, including hVSP1 and PTEN substrate specificity as well as the regulation of VSPs by intracellular pH and redox state. Lastly, we established an approach that allows for rapid manipulation and monitoring of PI levels in a population of cells and facilitates the study of PTEN mutations and pharmacological targeting.

vi. Zusammenfassung

Spannungsempfindliche Phosphatasen: Verstehen ihrer Funktion und Ausweiten ihrer potenziellen Nutzung

Spannungsempfindliche Phosphatasen (englisch: Voltage Sensitive Phosphatases, VSPs) sind Proteine, die aus zwei unterschiedlichen Teilen bestehen: einer transmembranen Spannungssensor-Domäne (VSD) und einer zytosolischen Phosphatase-Domäne. Die Spannungssensor-Domäne steuert die katalytische Aktivität einer Phosphatase, sehr ähnlich wie bei dem menschlichen Tumorsuppressorprotein PTEN (Phosphatase- und Tensin-Homolog gelöscht von Chromosom 10). Die erste charakterisierte VSP, Ci-VSP, wurde vor einem Jahrzehnt, von der Seescheide *Ciona intestinalis* isoliert. Ci-VSP hat bei Membrandepolarisation eine Phosphatase-Aktivität gegenüber Phosphoinositid (PI) Substraten und sie wirkt vor allem als 5-Phosphatase von PI(4,5)P₂ und PI(3,4,5)P₃.

VSPs wurden in verschiedenen Spezies gefunden, einschließlich dem Menschen. Trotz des fehlenden vollständigen Verständnisses, sind VSPs ausgezeichnete Werkzeuge, um den Phosphoinositid-Gehalt der Plasmamembran in lebenden Zellen schnell und reversibel zu ändern.

Der erste Teil dieser Arbeit konzentriert sich auf die weitere Charakterisierung und das Verständnis der Funktion der VSPs mit Hilfe gut etablierter Techniken. Wir verwendeten die Whole-Cell-Patch-Clamp-Technik, um die VSPs zu kontrollieren und Interne Totalreflexionsfluoreszenzmikroskopie (englisch: Total Internal Reflection Fluorescence microscopy, TIRF) um ihre Aktivität aufzunehmen.

Zuerst untersuchten wir die menschliche VSP-Isoform 1 (hVSP1). hVSP1 zeigt keine Plasmamembran-Lokalisation und deshalb ist es nicht tiefergehend charakterisiert worden. Hier haben wir versucht, hVSP1 an die Plasmamembran zu bringen und ihre enzymatische Aktivität zu untersuchen. Wir stellten fest, dass eine vollständige Ersetzung der Spannungssensor-Domäne von hVSP1 durch die von Ci-VSP eine membranständige, spannungsaktivierte 5-Phosphatase von PI(4,5)P₂ ergibt.

Angesichts der Ähnlichkeit der VSPs mit PTEN wurde durch Verbindung der VSD von Ci-VSP mit PTEN das chimärische Protein PTEN_{CiV} erstellt. PTEN_{CiV} behält die vollständige enzymatische Aktivität von PTEN (PTEN wirkt als 3-Phosphatase von PI(3,4)P₂ und PI(3,4,5)P₃). Die zusätzliche Regulierbarkeit durch Spannung macht PTEN_{CiV} zu einem leistungsfähigen Werkzeug für die Untersuchung dieses Tumorsuppressors. Insbesondere haben wir die enzymatische Aktivität der neuen Prostatakrebs-PTEN-Mutation A126G charakterisiert. Wir fanden heraus, dass die A126G-Mutante die Substratspezifität von PTEN von einer 3-zu einer 5-Phosphatase konvertiert.

Es wird vermutet, dass VSPs in Prozessen, in denen pH- und Redox-Zustandsänderungen auftreten, beteiligt sind. Deshalb untersuchten wir als Nächstes die Wirkung von intrazellulärem pH-Wert und von Redox-Zustand auf VSPs. Wir sahen, dass ein saurer pH-Wert den PI(4,5)P₂ Abbau in allen getesteten VSPs erhöht, und dass Oxidation die enzymatische Aktivität von Ci-VSP hemmt. Es scheint daher möglich, dass zusätzlich zur Spannung auch pH-Wert und Oxidation zu einer feinen Modulation von VSPs beitragen.

Im zweiten Teil entwickelten wir eine leichtanwendbare Methode zur Manipulation von PI-Pegeln -unter Verwendung von VSPs aber ohne die Notwendigkeit der Patch-Clamp-Technik. Wir setzten verschiedene Kationenkanälen ein, die bei Aktivierung zu Membrandepolarisation führten und sequenziell zur VSP-Aktivierung. Als Nächstes charakterisierten wir Methoden um PI(4,5)P₂ und PI(3,4,5)P₃ unter Verwendung von Fluoreszenzmikroskopie oder Photometrie zu kontrollieren. Außerdem haben wir die Anwendbarkeit dieser Techniken gezeigt, um die Wirkung von bekannten PTEN-Mutationen und PTEN-Inhibitoren durch Verwendung der PTEN_{CiV} Chimäre zu untersuchen.

Als Ergebnis dieser Arbeit erhöhen wir das Verständnis über verschiedene Aspekte der VSP-Aktivität, einschließlich der Substrat Spezifität von hVSP1 und PTEN, sowie der Regulierung der VSP durch intrazellulären pH-Wert und Redox-Zustand. Außerdem haben wir einen Ansatz etabliert, der nicht nur zügige Manipulation und Kontrolle des PI-Gehalts in einer Population von Zellen zulässt, sondern der auch die Untersuchung von PTEN-Mutanten und Pharmakologie erleichtert.

1 Introduction

1.1 Voltage sensitive phosphatases

Voltage sensitive phosphatases are a family of enzymes presenting the unique feature of combining enzymatic activity and voltage sensitivity in a single protein. They consist of a voltage sensing domain (VSD), similar to those found in voltage-gated ion channels, linked to a phosphoinositides (PIs) phosphatase. The history of their discovery starts in 1999, when the first member of the VSP family was described; a putative transmembrane tyrosine phosphatase TPTE (transmembrane phosphatase with tensin homology, now termed hVSP2) cloned from human genome, demonstrating however no apparent phosphatase activity (Chen et al., 1999; Tapparel et al., 2003; Walker et al., 2001). Next members identified were a second human VSP protein, TPIP (TPTE and PTEN homologous Inositol lipid Phosphatase, also termed TPTE2 or hVSP1) and the murine VSP, mVSP (Walker et al., 2001; Wu et al., 2001). In contrast to hVSP2, these two VSPs displayed phosphoinositide phosphatase activity in *in vitro* phosphatase assays. However, the role of the transmembrane domain on the regulation of the phosphatase activity of the mammalian VSPs remained, and still remains, elusive.

Six years later, light was shed on the VSPs field when Murata et al., 2005, for the first time, achieved to demonstrate how the voltage sensor domain was able to control the phosphatase activity (Fig. 1.2). They isolated the VSP of the ascidian *Ciona intestinalis*, Ci-VSP, and demonstrated in living cells that Ci-VSP was changing the concentration of PI(4,5)P₂ in a manner that depends on the membrane potential.

Soon VSPs from *Danio rerio* (Zebrafish), *Xenopus laevis* and *Gallus gallus* (chicken) were isolated and characterized (Hossain et al., 2008; Ratzan et al., 2011; Yamaguchi et al., 2014). The table 1 demonstrates all the up-to-date characterized VSPs.

Extensive research substantially increased our understanding of three facets of VSPs' function; a) the operation of the voltage sensor, meaning the movement and the conformational changes during activation (Villalba-Galea et al., 2008; Kohout et al., 2008; Li et al., 2014), b) the electrochemical coupling, which describes the mechanism

through which the voltage sensor conveys the activation to the phosphatase (Kohout et al., 2010; Hobiger et al., 2012; Liu et al., 2012) and c) the enzymatic activity, mainly regarding the substrate specificity (Halaszovich et al., 2009; Matsuda et al., 2011; Kurokawa et al., 2012).

Name	Species	Cellular localization	Tissue distribution	Predominant activity	Voltage activated	Citation
Ci-VSP	<i>Ciona intestinalis</i>	PM	sperm, neuronal tissue, blood	5-phosphatase of PI(4,5)P ₂ /PI(3,4,5)P ₃ (<i>in vivo</i>)	yes	1, 2
hVSP1 (4 isoforms)	Human	ER, Golgi	testis, brain, stomach	3-phosphatase of PI(3,4,5)P ₃ (<i>in vitro</i>)	not shown	3
hVSP2 (4 isoforms)	Human	ER, Golgi, PM	testis, spermato-cytes	non	not shown	4, 5
Dr-VSP	<i>Danio rerio</i>	PM	not shown	5-phosphatase of PI(4,5)P ₂ /PI(3,4,5)P ₃ (<i>in vivo</i>)	yes	6
XI-VSP (2 genes)	<i>Xenopus laevis</i>	PM	testis, ovary, liver, kidney	5-phosphatase of PI(4,5)P ₂ /PI(3,4,5)P ₃ (<i>in vivo</i>)	yes	7
Gg-VSP	<i>Gallus gallus</i>	PM	developing kidney	5-phosphatase of PI(4,5)P ₂ /PI(3,4,5)P ₃ (<i>in vivo</i>)	yes	8, 9
mVSP	mouse	Golgi	Testis	3-phosphatase of PI(3,5)P ₂ /PI(3,4,5)P ₃ (<i>in vitro</i>)	not shown	10

Table 1: All characterized voltage sensitive phosphatases. References: 1, (Murata et al., 2005); 2, (Halaszovich et al., 2012); 3, (Walker et al., 2001); 4, (Chen et al., 1999); 5, (Tapparel

et al., 2003); 6, (Hossain et al., 2008), 7; (Ratzan et al., 2011); 8,(Neuhaus and Hollemann, 2009); 9, (Yamaguchi et al., 2014); 10, (Wu et al., 2001). ER, endoplasmic reticulum; PM, plasma membrane.

1.2 Phosphoinositides

The substrate of VSPs, phosphoinositides (PIs), are phospholipids of the cellular membranes found in all eukaryotes. Although they are only a minor component of the membrane they play an important role in a variety of cellular processes including signaling, migration, proliferation, membrane trafficking and regulation of ion channels (Balla, 2013). They consist of a diacylglycerol (DAG) molecule linked to an inositol ring via a phosphodiester bond (Fig. 1.1A).

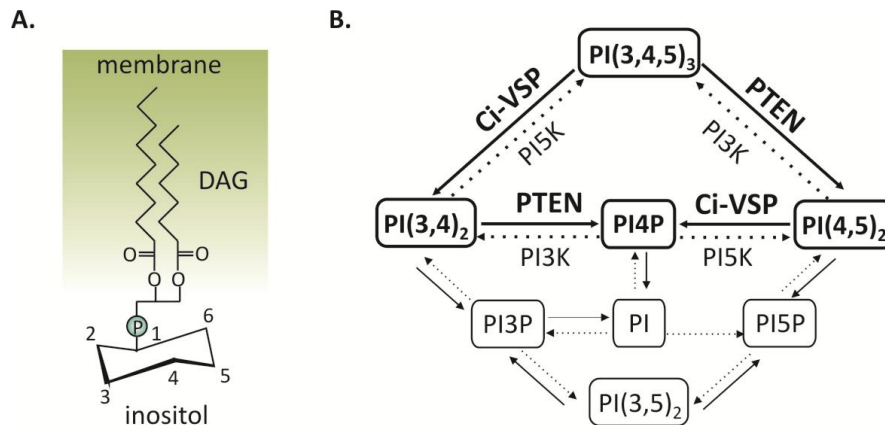


Figure 1.1: Structure and metabolism of phosphoinositides. **A:** PIs consist of two fatty acid chains linked to an inositol ring. Phosphorylation of the ring at positions 3, 4 and 5 can generate the seven different PI species. **B:** Schematic representation of PIs and their interconversion by metabolizing enzymes. For simplicity, only the PIs and enzymes mentioned in this work are highlighted. Full arrows are demonstrating phosphatases and dashed arrows kinases.

Phosphorylation of the inositol ring in several positions generates seven species of PIs, which demonstrate different membrane localizations and roles in cellular function (Table 2) (Falkenburger et al., 2010a; Devereaux and Di Paolo, 2013). A plethora of kinases and phosphatases strictly regulates the levels of each PI by interconversion between the different species (Fig. 1.1B). Impaired function of these metabolizing

enzymes has been connected to several diseases, including cancer, Lowe Syndrome, myopathies and many more (McCrea and De Camilli, 2009).

Lipid	Localization	Role
PI(3)P	late endosome, MVB	endosome trafficking
PI(4)P	trans Golgi	golgi trafficking
PI(5)P	nucleus, ER, Golgi	migration
PI(4,5)P ₂	plasma membrane	channels regulation, endocytosis, actin dynamics
PI(3,5)P ₂	late endosome	endosome trafficking
PI(3,4)P ₂	early endosome	cell survival, proliferation
PI(3,4,5) ₃	plasma membrane	cell survival, proliferation

Table 2: Different PIs, their cellular localization and their role in cellular function. MVB, multivesicular bodies; ER, endoplasmic reticulum.

1.3 Experimental control of phosphoinositides

To further address their roles in cell biology, a number of experimental techniques has been developed to control PI levels in living cells. These techniques vary from pharmacological means and genetic manipulations, like overexpression or knock-down of PI metabolizing enzymes, to more dynamic approaches that allow temporal control over PI levels. There are three such techniques for acute PI manipulation available, all displaying certain limitations that need to be considered.

The first technique is the FRB-FKBP (FK506 binding protein-fragment of mammalian target of rapamycin [mTOR] that binds FKBP) heterodimerization system that recruits a PI metabolizing enzyme (e.g., PI(4,5)P₂ 5-phosphatase) to the membrane by application of the drug rapamycin (Varnai et al., 2006; Suh et al., 2006). The timing of recruitment, which then results in e.g. acute PI(4,5)P₂ depletion, can be precisely controlled. However, recruitment and hence the alteration of PI levels is irreversible. Furthermore, the use of the rapamycin-induced dimerization system is limited to cell types that do not express large amounts of FKBP or FRB protein domains endogenously (Coutinho-Budd et al., 2013). Additionally, unwanted effects via endogenous rapamycin targets have to be considered (Brown et al., 1994).

The second technique is also based on the acute recruitment of a 5-phosphatase to the membrane, this time by using the blue light-induced dimerization of CRY2-CIBN (cryptochrome 2- CRY2-interacting bHLH 1) domains (Idevall-Hagren et al., 2012). This system allows for PI(4,5)P₂ depletion that is reversible within minutes, but imposes limitations on the analysis of PI levels using well established fluorescent biosensors, as the system is highly sensitive to blue and green light.

A third strategy to manipulate PI levels in living cells utilizes VSPs. For example, Ci-VSP was used to study the PI-dependent regulation of ion channels (Yudin et al., 2011; Lindner et al., 2011). This approach allows for temporally precise, robust and quickly reversible changes in PI levels. However, it requires electrophysiological instrumentation, not available in many laboratories, and is time consuming since it only allows for single cell recordings. These limitations have restricted the broad use of VSPs as tools for manipulation of PIs. Part of this thesis will present a novel approach to overcome the above limitations and establish VSPs as an easy-to-use tool for controlling PI levels in living cells.

1.4 Structure of VSPs

Voltage sensitive phosphatases consist of a voltage sensor domain and a catalytic domain connected via a short amino acid sequence called the linker (Fig. 1.2).

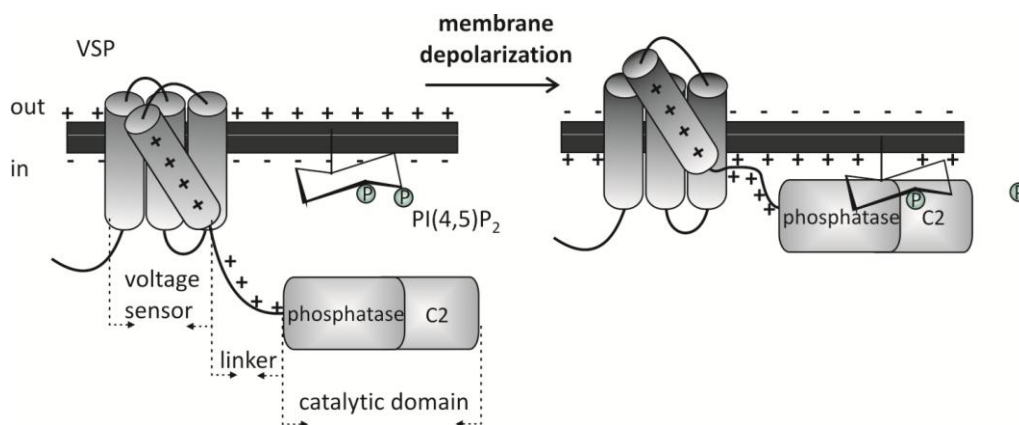


Figure 1.2: Schematic representation of a VSP. VSPs comprise two distinct domains, the voltage sensor and the catalytic domain connected to each other by a short linker. The voltage sensor consists of four transmembrane helices, S1-S4, responsible for the activation by

membrane potential. S4 contains four positively charged amino acids (arginines) that act as sensing charges. Membrane depolarization changes the transmembrane electrical field and causes displacement of S4. The linker, also called PBM (PIP₂ binding module), is an approximately 18 amino acids sequence rich in positively charged amino acids (arginines and lysines). These positively charged amino acids are shown to interact electrostatically with the negatively charged PI headgroups of the membrane, facilitating the transmission of the activation from the voltage sensor to the phosphatase domain. The catalytic domain consists of the phosphatase and C2 part (carboxyl-terminus). Here a 5-phosphatase activity against PI(4,5)P₂ is illustrated as an example.

Their voltage sensor domain consists of four transmembrane segments (S1-S4) with the fourth segment, S4, bearing four charged residues (arginines), which are responsible for the voltage sensing. Changes in the membrane potential can induce relocation of these charges and lead to conformational alternations in the protein itself.

According to the crystal structure of Ci-VSP, the S4 undergoes an upward displacement and a rotation during activation (Li et al., 2014). This movement is facilitated by electrostatic interactions between the positive charges of S4 and the negatively charged amino acids of the S1 and S3 segments (Fig. 1.3A).

The structure of the cytoplasmic region of the protein was solved by X-ray crystallography by Matsuda et al., 2011 and Liu et al., 2012 (Fig. 1.3B). It consists of two domains, the phosphatase domain and the carboxyl-terminus domain, C2. The phosphatase domain contains the protein-tyrosine phosphatases (PTP) signature motif, HCX₅R (with X being any residue) located within a loop called the P (phosphatase binding)-loop. The P-loop along with two other elements, the TI (threonine/isoleucine)-loop and the WPD (tryprophane/proline/aspartic acid)-loop form the active site pocket of the phosphoinositide phosphatase. The C2 domain creates a hydrogen bond network with the phosphatase domain via its CBR3 (calcium binding region 3)-loop, although it does not appear to be actively involved in the catalysis.

The linker domain plays a pivotal role in the VSP activity. It is considered responsible for the electrochemical coupling between the voltage sensor and the phosphatase domain. It consists of approximately 18 amino acids including several positive charged

residues that are suggested to facilitate the activation (Villalba-Galea et al., 2009; Liu et al., 2012; Hobiger et al., 2013). According to Hobiger's hypothesis the positive amino acids of the linker play two roles in the coupling process. First they interact electrostatically with the negatively charged PI headgroups of the plasma membrane recruiting the phosphatase domain closer to the membrane. Second they interact with the TI-loop of the active site and by neutralizing its negatively charged amino acids they facilitate the substrate binding.

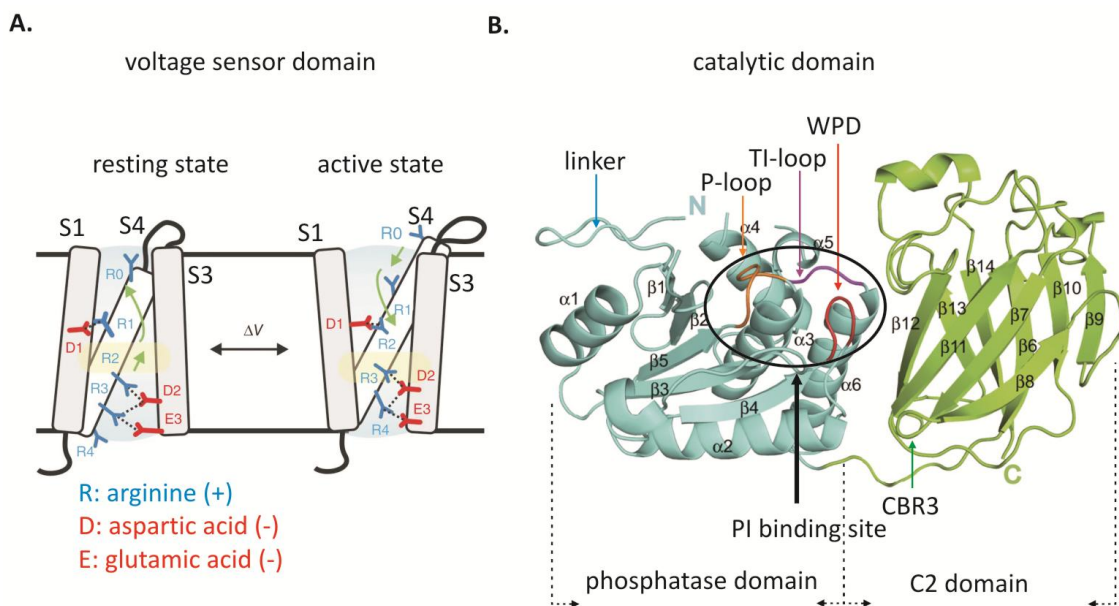


Figure 1.3: Structure of Ci-VSP. A: Mechanistic model of voltage sensing in Ci-VSP. During activation the S4 segment moves outwards and rotates by 60°. The arginines in S4 are stabilized by successive negative countercharges on S1 and S3. Modified from (Li et al., 2014). **B:** Schematic structure of the catalytic domain of Ci-VSP. The phosphatase domain consists of four β -strands surrounded by six α -helices. It contains the PI binding site which consists of three loop structures, the P-loop, the TI-loop and the WPD-loop. The C2 domain consists of nine β -strands and interacts with the phosphatase domain via its CBR3 loop. Image modified from (Matsuda et al., 2011).

1.5 Human VSPs

In the human genome, two genes encode for proteins homologous to voltage sensitive phosphatases and they are named hVSP1 (originally termed TPIP or TPTE2) and hVSP2 (originally termed TPTE) (Walker et al., 2001; Chen et al., 1999; Tapparel et al., 2003). hVSP1 which is expressed in testis, brain and stomach, presents phosphoinositide phosphatase activity *in vitro* (Walker et al., 2001). In contrast, hVSP2 that is found in testis lacks phosphatase activity probably due to amino acid exchanges in the catalytic motif of the P-loop (Chen et al., 1999). Various splice variants of hVSPs have been reported that mainly differ in the VSD (Fig. 1.4) (Tapparel et al., 2003). For hVSP1 there are four reported isoforms, all localizing at intracellular membranes, when tested in heterologous expression systems. hVSP2 also appears in four splice isoforms with three of them localized intracellularly and one isoform, hVSP2-3, localized at the plasma membrane. So far it has remained elusive whether these proteins are controlled via membrane depolarization.

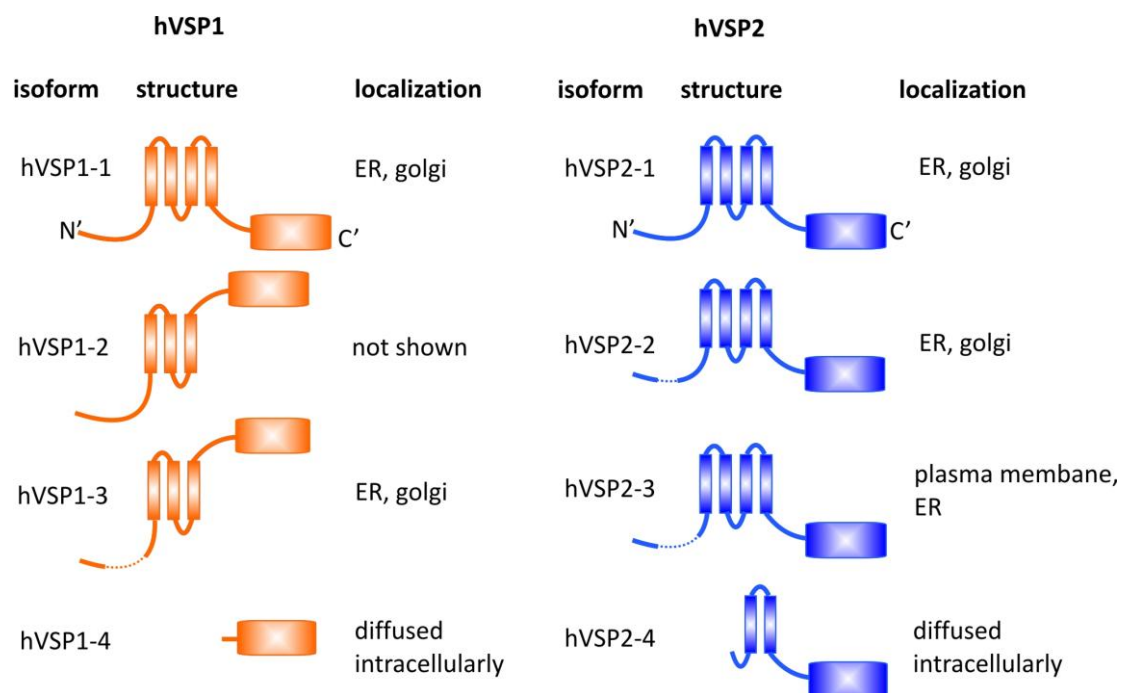


Figure 1.4: Human VSPs and their isoforms. Schematic representations of hVSP splice isoforms derived from computational predictions performed by Tapparel et al., 2003. Four different isoforms have been isolated for hVSP1 and hVSP2. The isoforms mainly differ in the VSDs, either by lacking parts of the N-terminal part or by lacking entire transmembrane

segments. The different isoforms are often located in different cellular compartments. The dashed lines in the N-terminal part represent missing amino acids.

1.6 Physiological role of VSPs

The function of VSPs *in vivo* remains largely unknown but some hypotheses have been proposed concerning their role in physiological processes and possible mechanisms of their activation. As demonstrated in Table 1 VSPs are expressed not only in neuronal tissue, where regulation by voltage may be straightforward, but are also detected in non-neuronal tissue such as sperm, blood and kidney.

In adult *Ciona intestinalis* for example, Ci-VSP is found in blood cells (Ogasawara et al., 2011). Notably, in blood cells NADPH oxidase activity leads to cell membrane depolarization that could potentially activate Ci-VSP.

In *Xenopus*, mRNA was found in several tissues predominantly in oocytes and sperm (Ratzan et al., 2011). Interestingly, the membrane potential of *Xenopus* eggs changes during fertilization from -20 to +20 mV, to block polyspermy. This voltage range is similar to the voltage range for activation of XI-VSP1. The authors therefore hypothesise that the PI(4,5)P₂ depletion by XI-VSP inhibits cell membrane fusion, preventing this way the merging of an additional sperm to the oocyte.

The chick ortholog Gg-VSP is expressed exclusively in the mesonephros during embryonic development and might be activated by transepithelial membrane potential (Neuhaus and Hollemann, 2009). Gg-VSP has also been suggested to regulate cell structure through the production of PI(3,4)P₂ (Yamaguchi et al., 2014).

The mammalian VSPs remain the most elusive. They are found in different tissues including sperm, brain, kidney, etc. (Table 1) but their physiological role is entirely unknown. Moreover it is unclear if they are voltage regulated and their substrate specificity has been only studied *in vitro*.

1.7 PTEN

1.7.1 PTEN and disease

PTEN is one of the most frequently mutated tumor suppressor proteins resulting in human cancer and other pathological conditions. Somatic PTEN mutations result in multiple sporadic tumor types, most frequently in the endometrium, central nervous system, skin and prostate (Chalhoub and Baker, 2009). Germline dominant mutations are related to hamartoma tumor syndromes, benign malformations predisposing for cancer (Hollander et al., 2011). More recently, the involvement of PTEN in neuronal activity and development has also been demonstrated, with PTEN germline mutations associated with autistic spectrum disorders (ASDs) (Garcia-Junco-Clemente and Golshani, 2014; Varga et al., 2009).

PTEN exerts its tumor suppressor activity via direct antagonism of the phosphatidylinositol 3-kinase (PI3K) signaling pathway which regulates cell growth, survival, and proliferation. More specifically, by being a 3-phosphatase of PI(3,4,5)P₃, PTEN counteracts the PI(3,4,5)P₃ production via PI3K (Fig. 1.5).

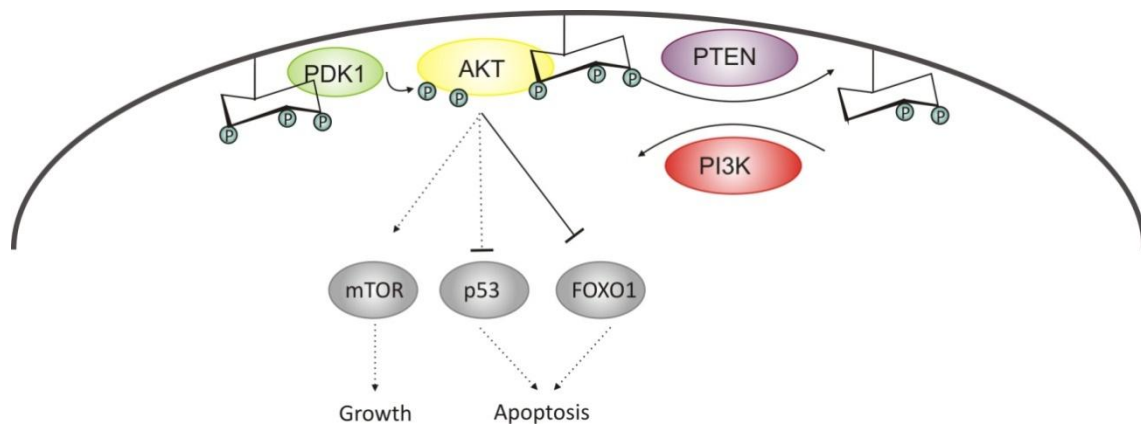


Figure 1.5: Simplified phosphatidylinositol 3-kinase (PI3K) signaling pathway. PI3K phosphorylates PI(4,5)P₂ to PI(3,4,5)P₃. PI(3,4,5)P₃ recruits AKT and its activator PDK1 to the membrane, where AKT will be activated by phosphorylation. AKT will then activate or deactivate several targets by phosphorylation, promoting cellular growth, survival and proliferation by various mechanisms. For simplicity, only some of the key players of the pathway are demonstrated. PTEN is the negative regulator of the PI3K signaling pathway since it directly antagonizes PI(3,4,5)P₃ production by PI3K. Dashed lines represent indirect

interaction of AKT with protein targets. PI3K, phosphatidylinositol 3-kinase; AKT, protein kinase B; PDK1, phosphoinositide dependent kinase 1; mTOR, mammalian target of rapamycin; FOXO1, forkhead box 1. Schematic modified from (Chalhoub and Baker, 2009).

The effect of mutations on PTEN activity has been assessed so far *in vitro* with phosphatase assays or *in vivo* with a yeast survival model. More specifically, in *in vitro* phosphatase assays, PTEN reacts with soluble or vesicle placed PIs, and the produced orthophosphate is measure using radioactivity or colorimetric assays (Lee et al., 1999; Maehama and Dixon, 1998). The yeast survival system is a non mammalian model, where PI3K and PTEN are coexpressed in *S. Cerevisiae* (Cid et al., 2008). PTEN phosphatase activity is assessed by its ability to counteract the toxic effect of a hyperactive form of PI3K, leading to cell survival.

However, effects of PTEN mutations, in particular with respect to catalytic activity, cannot be addressed in the mammalian cell with the above techniques. The creation of the chimeric protein PTEN_{CIV}, previously from our laboratory, allowed for the first time examination of PTEN's catalytic activity in living mammalian cells (Lacroix et al., 2011). PTEN_{CIV} will be presented in detail in the following section.

1.7.2 PTEN structure and PTEN_{CIV}

VSPs are homologues of the tumor suppressor protein PTEN and their catalytic domains share substantial sequence similarity (Fig. 1.6A). As both, PTEN and the VSPs belong to the protein-tyrosine-phosphatase (PTP) super-family, they share the hallmark of the family, the HCX₅R active site motif (Liu and Bankaitis, 2010). The active site HCX₅R motifs within the P-loop of PTEN and Ci-VSPs are virtually identical apart from the fact that an alanine in PTEN is replaced by a glycine in the VSPs (Fig. 1.6B). Functionally, however, the two proteins are strikingly distinct: PTEN acts as a 3-phosphatase of PI(3,4)P₂/PI(3,4,5)P₃. In contrast Ci-VSP mainly acts as a 5-phosphatase of PI(4,5)P₂/PI(3,4,5)P₃ (Fig. 1.6C).

The crystal structures of the catalytic domain of Ci-VSP and PTEN also revealed a high degree of structural similarity with both proteins presenting the same architecture of phosphatase and C2 domains (Matsuda et al., 2011; Lee et al., 1999). The linker (or PBM) domain, although not included in the crystals, is also similar by sequence homology. There are only two main structural differences between PTEN and Ci-VSP. The first involves the position of TI-loop and the second the position of CBR3-loop (Matsuda et al., 2011). In particular, it is suggested that the TI-loop is located towards the active site pocket in Ci-VSP but not in PTEN, which may result in a bigger active site pocket in PTEN required for the accommodation PI(3,4,5)P₃, PTEN's predominate substrate. The second difference occurs in the CBR3-loop, which in Ci-VSP makes a contact with the WPD-loop whereas in PTEN it is considered to be involved in PTEN's membrane association.

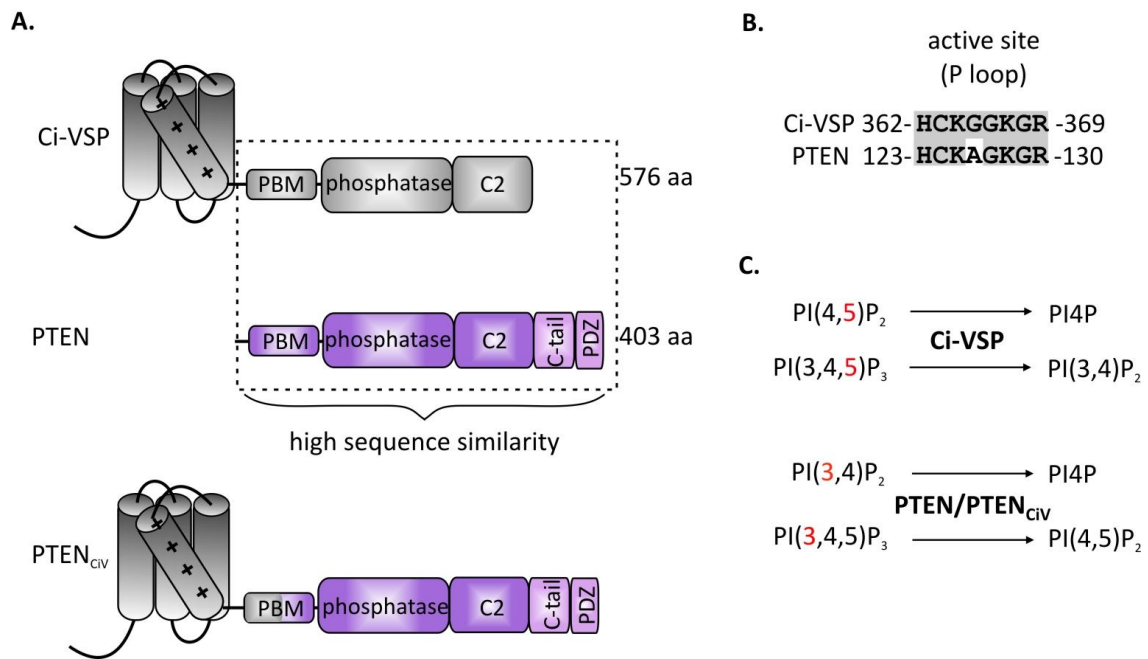


Figure 1.6: Ci-VSP, PTEN and PTEN_{CiV}. **A:** Ci-VSP and PTEN demonstrate high sequence and structural similarity in their enzymatic domain. Fusion of PTEN with the VSD of Ci-VSP generated a chimeric protein that is activated by membrane depolarization while retaining the enzymatic properties of PTEN. PBM, PIP₂ binding module; C-tail, the carboxyl-terminus domain; PDZ, domain binding motif, postsynaptic density protein–*Drosophila* disc large tumor suppressor–zonula occludens 1 protein. **B:** Part of the catalytic active site, called the P-loop, presents high sequence similarity between Ci-VSP and PTEN. **C:** Diagrammatic representation of the enzymatic specificity of Ci-VSP, PTEN and PTEN_{CiV}.

PTEN has a complex, not fully understood, mechanism of activation. Its N-terminal PBM site plays a role in membrane recruitment, in a similar manner as in Ci-VSP. However, the C-terminal part of PTEN, comprising the C-tail and the PDZ domain-binding-motif (domains that are absent from Ci-VSP, Fig1.6A), is also involved in the regulation of the protein. Phosphorylation of the C-tail domain at several sites promotes an intramolecular interaction with the remainder of the molecule that regulates the membrane association and activity of PTEN (Rahdar et al., 2009). Moreover PDZ domain-containing proteins bind to PTEN's PDZ domain-binding-motif and target it to the plasma membrane (Das et al., 2003).

Recently, a chimeric protein was created by fusing the VSD of Ci-VSP with the entire PTEN protein. In that way, a membrane-localized, voltage-regulated PTEN, termed PTEN_{CiV} (Lacroix et al., 2011) was generated. This chimera displayed enzymatic activity in a strictly depolarization-dependent manner and fully recapitulated the catalytic activity of the wild type protein in being a 3-phosphatase of PI(3,4)P₂/PI(3,4,5)P₃ (Fig. 1.6C). With its ability to switch enzymatic activity rapidly and reversibly in living mammalian cells, PTEN_{CiV} provided a novel approach for studying this important tumor suppressor.

1.8 Experimental approaches to study VSPs

The study of VSPs in living cells requires first a method to control them by using voltage and second a method to record their activity. For this reason, VSPs are primarily studied using electrophysiological methods on cell systems heterologously expressing the VSP of interest. For big host cells, such as *Xenopus laevis* oocytes, the two electrode voltage clamp is used while for smaller, mammalian cells the patch clamping approach is required. These electrophysiological methods allow for precise temporal control of the membrane potential and accordingly activation of VSPs. To record the activity of VSPs the experimenter can either directly monitor the electrical properties of the voltage sensor or monitor the phosphatase activity of the catalytic

domain as an effect of membrane depolarization. The following sections provide a detailed description of these two monitoring techniques.

1.8.1 Measurement of sensing current

The voltage sensing mechanism of VSPs closely resembles that of voltage gated channels (Villalba-Galea et al., 2008; Bezanilla, 2008). Changes in the membrane potential lead to movement of the positively charged S4 segment of the voltage sensor domain (Fig. 1.2). The fast movement of these charges within the membrane electrical field produces transient currents called sensing currents, as depicted in figure 1.7. Similar transient currents are generated also by voltage gated channels and are called gating currents since they regulate the opening of the channel's pore. When the voltage sensor moves to its active state, at depolarizing potentials, an outward transient current occurs called the “On” sensing current, while an inward transient current, the “Off” sensing current, occurs when the sensor returns to the resting position.

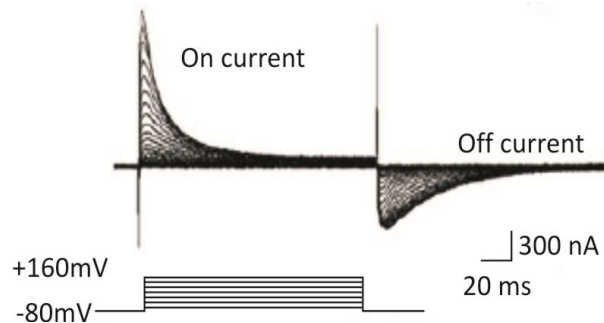


Figure 1.7: VSPs' sensing currents. Sensing currents are produced as a result of membrane depolarization and represent the movement of the S4 segment within the membrane electric field. Outward currents, called the “On” sensing currents, occur at depolarizing potentials, in cells kept at a holding potential of -80 mV. Return to the holding potential results in an inward, “Off”, current representing the returning of the sensor to its resting position. Modified from (Murata et al., 2005).

The characteristics of sensing currents provide important information about the VSPs. For example the charge movement of the voltage sensor can be calculated by the time

integral of the sensing current. These sensing charges can be used to assess the expression levels of VSP in expression systems (Villalba-Galea et al., 2009). In addition, by measurement of the sensing charges over a range of voltages, with voltage step protocols as shown in figure 1.7, it is possible to derive the voltage dependence of the activation of VSD. Lastly, kinetic analysis of the decay rate of the “Off” currents can be used to assess the coupling of the voltage sensor to the phosphatase domain (Hobiger et al., 2012).

1.8.2 Measurement of catalytic activity

The enzymatic activity of VSPs can be studied dynamically in living cells by directly monitoring the changes of PIs levels as a result of VSPs activation. Two different approaches have been used to monitor PI level changes; PI(4,5)P₂ sensitive K⁺ channels and PI sensors.

The use of K⁺ channels, such as KCNQ2/3 and Kir2.1, as reporters of the phosphatase activity is well established (Murata et al., 2005; Hossain et al., 2008; Liu et al., 2012; Sakata et al., 2011). These channels require PI(4,5)P₂ for their function, therefore depletion of this phospholipid via VSPs results in decrease of the ionic current (Fig. 1.8A,B).

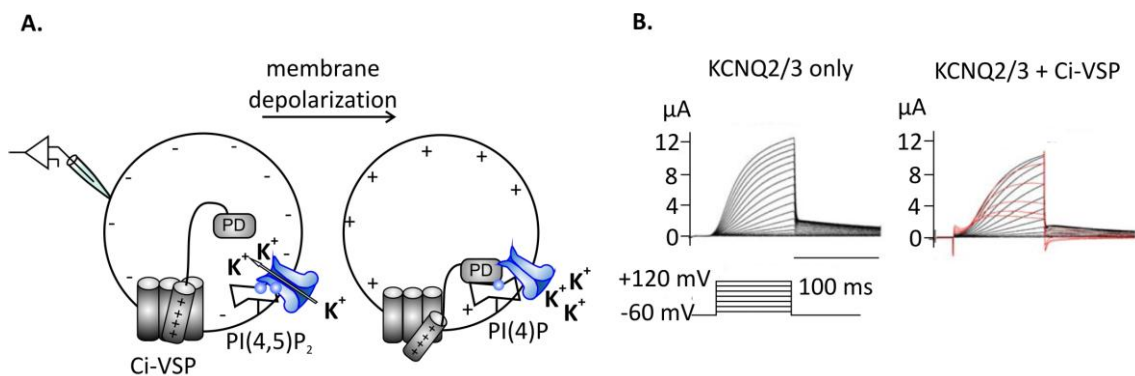


Figure 1.8: K⁺ channels for monitoring the catalytic activity of VSPs. **A:** Schematic representation of a cell expressing Ci-VSP and a PI(4,5)P₂ sensitive K⁺ channel. Since these channels require PI(4,5)P₂ for their activity, depletion of PI(4,5)P₂ by Ci-VSP results in inhibition of the ionic current. **B:** In cells heterologously expressing KCNQ2/3 increasing voltage steps result in increasing ionic currents. In contrast, in cells coexpressing KCNQ2/3 and Ci-VSP the

ionic current decays at high potentials (red traces), indicating decreased PI(4,5)P₂ levels. Modified from (Murata and Okamura, 2007).

An alternative way to monitor VSPs enzymatic activity is by genetically encoded PI sensors and fluorescence microscopy (Várnai and Balla, 2006). PI sensors derive from proteins that physiologically bind to different phosphoinositides headgroups. One of the most extensively used are the pleckstrin homology (PH) domains isolated from several proteins and depending on the protein of origin, PH domains can specifically bind to certain PI species. Fusion of such domains with fluorescent proteins generates sensors that are able to report about concentration and localization of specific PI species. Table 2 lists the biosensors used in this work.

Name	PI specificity	Reference
Akt-PH	PI(3,4)P ₂ /PI(3,4,5)P ₃	Servant et al., 2000
Btk-PH	PI(3,4,5)P ₃	Salim et al., 1996
GRP-PH	PI(3,4,5)P ₃	Klarlund et al., 1997
OSBP-PH	PI(4)P	Levine and Munro, 1998
PLCδ ₁ -PH	PI(4,5)P ₂	Várnai and Balla, 1998
TAPP1-PH	PI(3,4)P ₂	Kimber et al., 2002
tubby	PI(4,5)P ₂	Santagata et al., 2001

Table 3: Biosensors used in this work.

The use of these biosensors for assessing the catalytic activity of VSPs has been well established (Murata and Okamura, 2007; Halaszovich et al., 2009; Ratzan et al., 2011). As an example, we consider cells coexpressing Ci-VSP and a PI(4,5)P₂ specific sensor (Fig.1.9A). At hyperpolarizing potentials Ci-VSP is inactive and the sensor is located mainly in the membrane where the PI(4,5)P₂ concentration is high. Activation of Ci-VSP with membrane depolarization would result in PI(4,5)P₂ depletion and therefore translocation of the sensor to the cytoplasm. This change in the membrane fluorescence can be recorded using confocal microscopy or more elegantly with total internal reflection fluorescence (TIRF) microscopy that specifically allows for

measurement of the plasma membrane fluorescence. An example of a patch clamping experiment, using Ci-VSP, PLC δ_1 -PH-GFP and TIRF microscopy is presented in figure 1.9B.

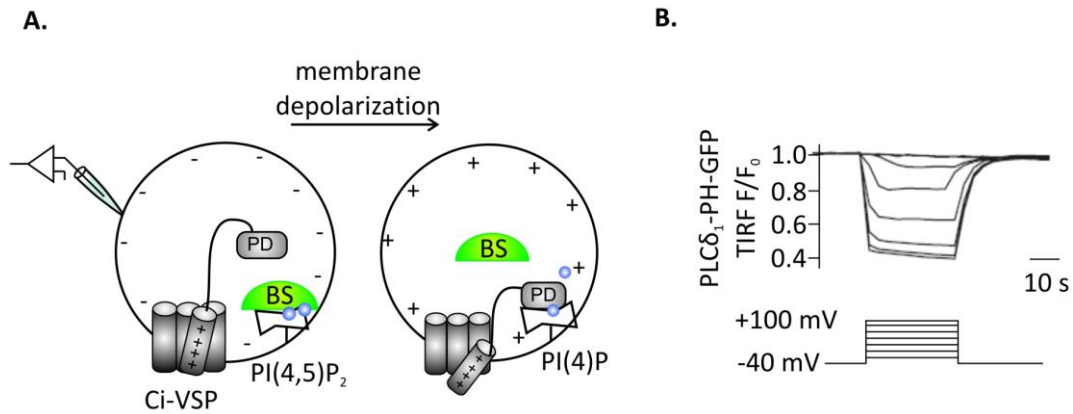


Figure 1.9: PI sensors for monitoring the catalytic activity of VSPs. **A:** Schematic representation of a cell expressing Ci-VSP and a PI(4,5)P₂ specific sensor under whole cell patch clamp condition. Membrane depolarization results in activation of Ci-VSP, PI(4,5)P₂ depletion and translocation of the biosensor (BS) to the cytosol. **B:** Time course graph of the TIRF microscopy signal from cells transfected with Ci-VSP and PLC δ_1 -PH-GFP, a PI(4,5)P₂ specific biosensor. Activation of Ci-VSP at different depolarizing membrane potentials, causes depletion of PI(4,5)P₂, translocation PLC δ_1 -PH-GFP to the cytosol and therefore decrease of the membrane fluorescence intensity. Modified from (Halaszovich et al., 2009).

1.9 Aims of this work

This work expands in two directions: first, to further our understanding of VSP function and second, to develop a simplified method for using VSPs as tool for experimental manipulation of PI concentrations.

In the first section, we studied different aspects of VSPs and PTEN_{CIV} function and regulation that remained until now unknown, including substrate specificity, localization and dependence on intracellular conditions. More specifically, first we aimed at examining the substrate specificity of hVSP1, that was never been shown in living cells. Given the lack of plasma membrane localization of this protein, we initially focused on targeting it to the membrane by exchanging parts of it with VSPs that show strong plasma membrane localization, such as Ci-VSP and hVSP2. Second we focused

on characterizing a novel PTEN patient specific mutation by using the PTEN_{CiV} chimera. Interestingly this mutation, A126G, occurs in the highly conserved P-loop, part of the phosphatase's active site (Fig. 1.6B). The existence of a glycine in this position is however characteristic of 5-phosphatases such as Ci-VSP. Therefore, here we studied the effect of mutations in this position on the phosphatase activity and substrate specificity of PTEN_{CiV}. Third we investigated different modulators of VSPs' activity such as intracellular pH and redox state. pH changes are known to occur in processes such as sperm physiology, cell growth and migration. Although their exact physiological role is not yet fully understood, VSPs have been also suggested to be involved in the above mentioned processes. Here we compared the PIs' depletion rates caused by VSP activation under different intracellular pH values. We then assessed the effect of pH on the sensing of VSPs and in the kinetics of PI(4,5)P₂ resynthesis. In addition we attempted to identify the amino acid that could act as the pH sensor by site directed mutagenesis of histidine residues of Dr-VSP. Lastly in this section, we systematically tested the effect of oxidation on Ci-VSP.

All the above work was conducted by using whole-cell patch clamp technique for the control of the membrane potential and the subsequent activation of VSPs. This technique requires electrophysiological instrumentation and expertise as well as laborious single cell recordings. Thus, in the second section we aimed to simplify the manipulation of VSPs activation by developing a broadly applicable and electrophysiology-free approach. Such an approach could not only facilitate the study of VSPs but could also expand their use as phosphoinositide manipulation tools.

To avoid electrophysiological methods we employed cation channels to induce membrane depolarization in a population of living cells. We compared different cation channels, i.e. constitutive open, ligand or light activated channels, for their ability to evoke VSPs activation. Different ways of monitoring VSPs activity by using fluorescence-tagged PI biosensors combined with standard microscopy or FRET (Förster Resonance Energy Transfer) were also studied. At last, having established the optimal conditions, we aimed at demonstrating the usefulness of this approach by

employing the PTEN_{CIV} chimera in order to study PTEN tumorigenic mutations and inhibitors, in a technically easy way, in a population of living cells.

2 Materials and Methods

2.1 Molecular Biology

Introduction of mutations into our expressing vectors was performed using the Quickchange II XL, Site-Directed mutagenesis kit (Agilent Technologies, Santa Clara, CA). Briefly, the technique was based on a polymerase chain reaction (PCR) using primers containing the desired mutation (biomers.net, Ulm, Germany). Template DNA was discarded by digestion (Dpn1, Thermo Scientific, Dreieich, Germany) and the PCR product was transformed in competent cells for DNA replication and purification.

The general strategy for the creation of chimeric proteins was as follows; restriction sites were created with mutagenesis at the point of interest on the plasmids encoding for the two proteins. The plasmids were then digested with the appropriate enzymes (Thermo Scientific) and separated with electrophoresis based on their size. The selected DNA fragments were then fused using ligase (Thermo Scientific) and transformed in competent cells. For the final construct the restriction site was removed from the fusion site by mutagenesis. Lastly, the complete coding sequence of the construct was verified by sequencing (Seqlab, Gottingen, Germany).

Specifically, the hVSP1_{hV2-3N} chimera was constructed from amino acids 1-50 from hVSP2-3 and amino acids 71-522 from hVSP1. A *KpnI* restriction site was added at the site of fusion on the original plasmids. The hVSP1_{hV2-3V} chimera was created by site-directed mutagenesis on the hVSP1_{hV2-3N}. That required substitution of eight amino acids located on the VSD of hVSP1_{hV2-3N}. The hVSP1_{CiN} was constructed from amino acids 1-123 from Ci-VSP and amino acids 82-522 from hVSP1. A schematic representation of these constructs can be found in the results part in figure 3.1. The hVSP1_{CiV} and PTEN_{CiV} chimeras were created previously from colleagues as described in (Halaszovich et al., 2012) and (Lacroix et al., 2011) respectively.

The Frubby construct was created by Dr. D. Schneider, from the Pippi-PI(4,5)P₂ sensor (kindly provided from Dr. M. Matsuda, Japan (Yoshizaki et al., 2007)), by replacing the PLC δ_1 -PH domain with Tubby-Cterm protein. The AktAR construct was kindly provided from Dr. J. Zhang, Baltimore, USA (Gao and Zhang, 2008).

2.2 Cell culture and transfection

The experiments were performed with human embryonic kidney 293 (HEK) cells and Chinese hamster ovary (CHO) cells. HEK cells were cultured in MEM Alpha medium containing 10% standard FBS, 1% penicillin-streptomycin 10.000 U/ml, 1% NEAA (100x) and 1% Na-Pyruvate (100x) (all chemicals were purchased from Gibco, Life Technologies). CHO cells were cultured in MEM Alpha medium containing 10% standard FBS, 1% penicillin-streptomycin 10.000 U/ml. For splitting and plating, the cells that had reached 80-90% confluency, were washed with PBS (1x) (Life Technologies) and incubated with Trypsin (1x) (Life Technologies) for 1-4 minutes for separation. The cells were then suspended in MEM Alpha medium for termination of the trypsinization process and then centrifuged for 2 min at 1200 rpm (Megafuge 2OR, Heraeus Instruments, Hanau, Germany). The pellet was then resuspended with 1 ml of fresh medium and distributed either in flasks for the continuation of the cell line or on glass cover slips (Thermo Scientific) and glass bottom dishes (WillCo Wells B.V., Amsterdam, The Netherlands) for experimental usage. A HERAcCell 150i (Thermo Scientific) incubator was used to keep the cells at 37°C and at 5% CO₂.

24-48 hours after plating, the cells were transfected with expression vectors (cf. table 4) using JetPEI (Polyplus Transfection, Illkirch, France), a linear polyethylenimine derivative, according to the manufacturer's instructions. PI(4,5)P₂-3-kinase p110 α (K227E) was cotransfected with PTEN_{CIV} to increase PI(3,4,5)P₃ levels (Rodriguez-Viciana et al., 1996). Before the start of the AktAR experiments, PI(3,4,5)P₃ levels were elevated by incubating the cells with 0.4 ng/ μ l Insulin-like growth factor-1 for 15 minutes (Halaszovich et al., 2009). HEK cells were preferred for confocal imaging, since they present a stronger membrane localization of PI markers. CHO cells were primarily used for patch clamp experiments. For patch clamping, single cells, with no contact to neighbor cells, are preferred. Since CHO cells form loose connections with each other, it is easy to remove neighbor cells by applying gentle suction through the patch clamping pipette. Experiments were performed 24-48 hours after transfection at room temperature.

Name	UniProt accession No.	Amino acids	Vector	Citation
Biosensors				
AktAR	Chimeric construct		pcDNA3	1
Akt1-PH	P31749	1-164	pEGFP-N, pECFP-N, pEYFP-N	2
Btk-PH	Q06187	1-177	pEGFP-N	3
Frubby	Chimeric construct		pCAGGS	Dr. D. Schneider
GRP1-PH	O43739_2	261-381	pEGFP-C	4
OSBP-PH	P22059	88-188	pEGFP-N	5
PLC δ_1 -PH	P51178	1-170	pEGFP-N, pEYFP-C, pECFP-C	6
Tapp1-PH	Q9HB21	182-303	pEYFP-C	7
Tubby-Cterm	P50586_2	243-505	pEGFP-C, pERFP-C	8
Channels				
Chr2(H134R)	B4Y105	Full length	pEYFP	9
KCNQ4	P56696	Full length	pcDNA3.1	10
Kir2.1	P35561	Full length	pBK-CMV	11
TASK3	Q9NPC2	Full length	pcDNA3.1	12
TRPV1	Q35433	Full length	pEYFP-N (stop codon before YFP)	13
Enzymes				
Ci-VSP	Q4W8A1	Full length	pRFP-C, pECFP-C	14
Dr-VSP	B3IUN7	Full length	pIRES-eGFP, pIRES- Δ eGFP	15
XI-VSP1	Q4KLP3	Full length	pRFP-C	16
hVSP1	Q6XP53-3	Full length	pRFP-C, pRFP-N	17
hVSP2	P56180-3	Full length	pEGFP-C	18

hVSP1 _{Clv}	Chimeric construct		pRFP-C	O. Ebers
PTEN _{Clv}	Chimeric construct		pRFP-C	19
PI3-kinase p110 α (K227E)	P32871	Full length	pcDNA3.1	20

Table 4: List of the plasmids used in this study. References: 1, (Gao and Zhang, 2008); 2, (Servant et al., 2000); 3, (Salim et al., 1996); 4, (Klarlund et al., 1997); 5, (Levine and Munro, 1998); 6, (Várnai and Balla, 1998); 7, (Kimber et al., 2002); 8, (Santagata et al., 2001); 9, (Nagel et al., 2003); 10, (Chambard and Ashmore, 2005); 11, (Raab-Graham et al., 1994); 12, (Enyedi and Czirják, 2010); 13, (Caterina et al., 1997); 14, (Murata et al., 2005); 15, (Hossain et al., 2008); 16, (Ratzan et al., 2011); 17, (Walker et al., 2001); 18, (Chen et al., 1999); 19, (Lacroix et al., 2011); 20, (Rodriguez-Viciano et al., 1996).

2.3 Patch clamping

2.3.1 Background

Patch clamping is an electrophysiological method developed in 1976 by Neher and Sackmann (Neher and Sakmann, 1976) which enabled for the first time the measurement of single channel ionic currents. Since then, a number of different recording configurations have developed, allowing for the electrophysiological investigation of the behavior of single cells or whole cellular networks in the nervous system (Hamill et al., 1981).

Here, we used the whole-cell configuration, which allows the electrophysiological study of intact cells. Since our primary aim here was to control the membrane potential, we used the voltage clamp mode in which, the membrane potential is controlled by the experimenter and the changes in the ionic current are recorded. As shown in figure 2.1A a glass pipette of a diameter not exceeding 5 μm , was filled with a conducting salt solution, resembling the ionic composition of the intracellular solution. The pipette approaches the cell and with application of gentle suction the pipette tip will create a high resistance seal known as gigaseal, since it is usually in the range of Gigaohms. Application of a voltage pulse or/and suction will break the membrane patch and create a low-resistance access into the cell (Liem et al., 1995).

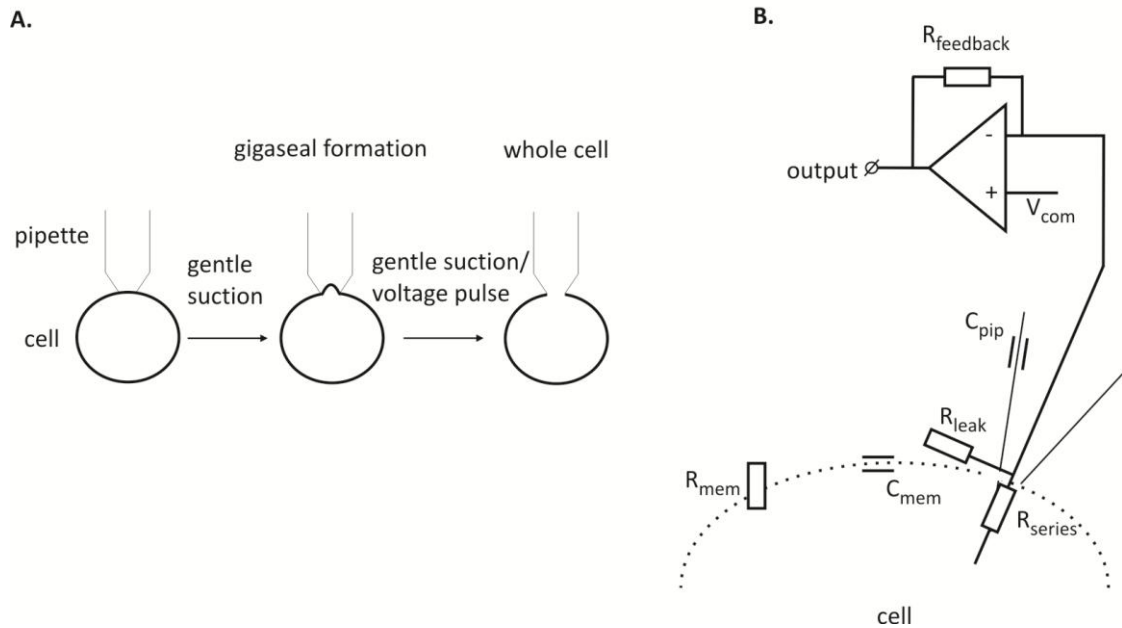


Figure 2.1: The whole-cell patch clamping technique. **A:** Schematic representation of the whole-cell configuration. A pipette of small diameter needs to create a high resistance seal, gigaseal, with the cell membrane. Disruption of the seal with gentle suction or a voltage pulse opens the cell and provides access to the intracellular space. **B:** Simplified equivalent circuit for the whole-cell patch clamp configuration. A chlorided silver wire connects the cell interior to a feedback amplifier. Such an amplifier operates by calculating the difference between the command and the measured voltage and converting it to current. V_{com} , command voltage; $R_{feedback}$, feedback resistance; C_{pip} , pipette capacitance; R_{leak} , leak resistance; R_{series} , series resistance; C_{mem} , membrane capacitance; R_{mem} , membrane resistance. Figures modified from (Liem et al., 1995; Molleman, 2003).

Figure 2.1B depicts a simplified equivalent circuit of the whole-cell patch clamp configuration. A single chlorided silver electrode connects the intracellular compartment to a high resistance amplifier. Patch clamping amplifiers operate through a feedback system. The voltage set by the experimenter, V_{com} , is compared to the measured membrane voltage. The difference between the set and measured membrane voltage is instantly corrected by current injection. This current, but of opposite sign, is the actual ionic current of the cell membrane. Several properties of the cell should be considered to acquire a precise patch clamp measurement. For example, the pipette and membrane capacitance, C_{pip} and C_{mem} , are compensated by internal electronic systems to prevent the appearance of capacitance currents. Another factor to be considered is the leak resistance, R_{leak} , introduced from the

membrane damage caused by the patching pipette. The R_{leak} needs to be high to increase cell viability and decrease voltage clamp errors. The series resistance, R_{series} , represents the pipette and access resistance and also needs to be compensated to avoid voltage clamp errors.

2.3.2 Patch clamping protocols

Whole cell patch clamping was performed in CHO cells using an EPC-10 amplifier and PatchMaster software (both HEKA). Patch pipettes' resistance was typically 1.5-4.0 M Ω , recordings were sampled at 20 kHz and low-pass-filtered at 5 kHz.

Sensing currents were recorded in response to test pulses between +40 mV and +180 mV, from a holding potential of -70 mV. The increment of the voltage was 20 mV and the duration of the pulse was 200 ms. Linear leak and capacitive currents were subtracted using a P/N (positive/negative) protocol.

In TIRF experiments hVSP1_{CIV} was activated with membrane depolarization at +80 mV for 1 minute from a holding potential of -100 mV. PTEN_{CIV} was activated at + 80 mV for 30 seconds from a holding potential of -60 mV. Ci-VSP, Dr-VSP and XI-VSP1 were activated at different voltages, as indicated in the results part, for 30 seconds from a holding potential of -60 mV.

In the experiments where Kir2.1 channels were coexpressed with Dr-VSP, Kir2.1 currents were evoked by a 300 ms test pulse to -100 mV from a holding potential of -60 mV (Fig.2.2A). During the experiment, Dr-VSP was activated by membrane depolarization at different membrane potentials (Fig.2.2B red trace), resulting in depletion of PI(4,5)P₂. Since Kir2.1 requires PI(4,5)P₂ for its activity, activation of Dr-VSP causes inhibition of the Kir2.1 currents as shown in the representative pulse traces (dashed boxes in figure 2.2B). To create the current-to-time trace (Fig.2.2B black trace), one Kir2.1 current measurement was recorded every 6 seconds. The data were next normalized to the baseline current prior to the activation of Dr-VSP (Fig.2.2C).

For current clamp recordings of cells expressing ChR2, cells were held at 0 pA and changes of membrane voltage were recorded upon 1 second blue light exposure.

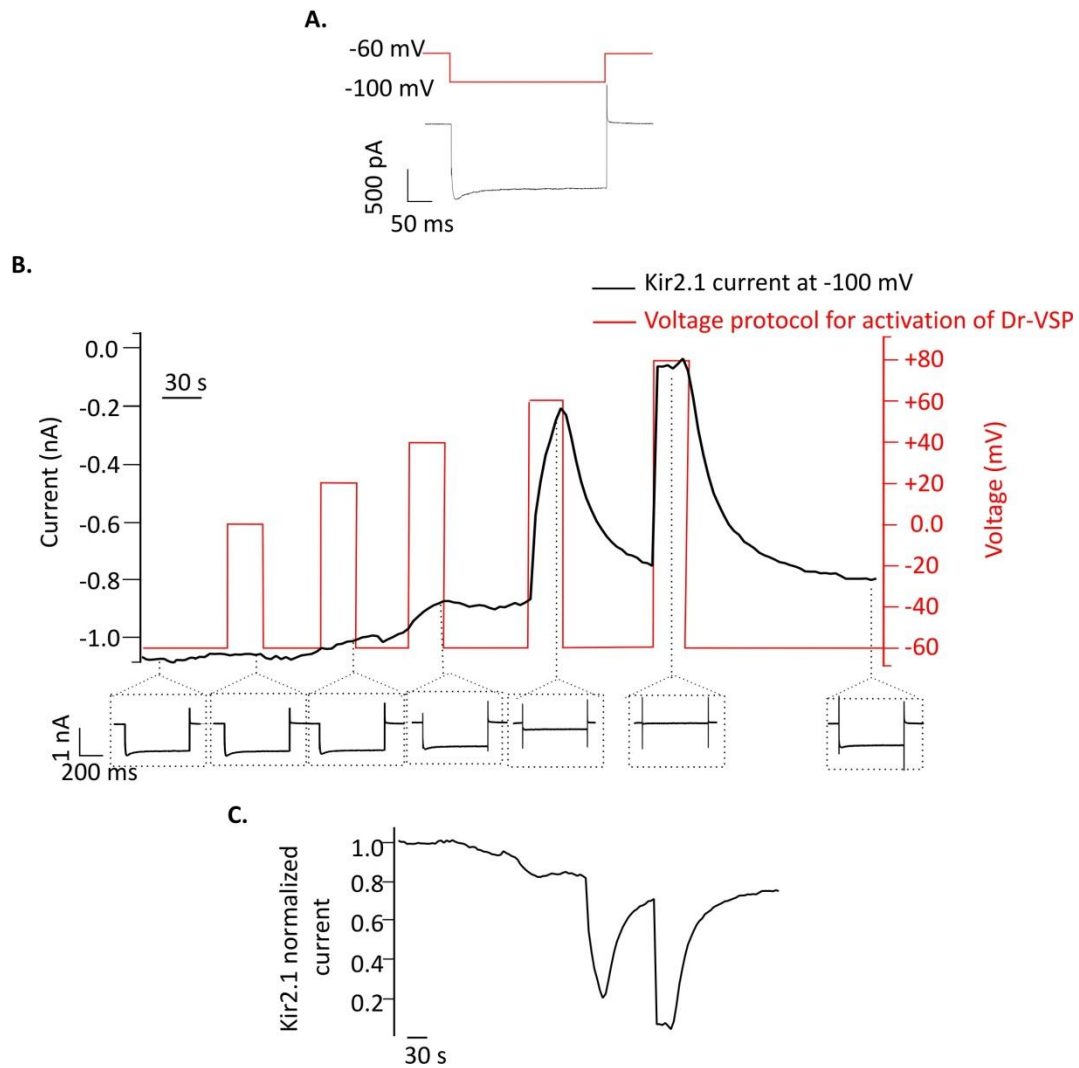


Figure 2.2: Protocol for Kir2.1/Dr-VSP measurements. **A:** Current recorded from a CHO cell expressing Kir2.1 channel. Recordings were made at +100 mV from a holding potential of -60 mV. **B:** Graph showing the current-to-time trace from a CHO cell coexpressing Kir2.1 channel with Dr-VSP. The current trace (black trace) was created from the Kir2.1 current value, recorded every 6 seconds. Since Kir2.1 is PI(4,5)P₂ sensitive, activation of Dr-VSP at positive potentials inhibits the channel's activity, as shown in the representative Kir2.1 currents in the dashed boxes. The voltage protocol used for activation of Dr-VSP is shown in the red trace. **C:** For presentation, the current was normalized to the average current before the activation of Dr-VSP.

2.4 Total Internal Reflection Fluorescence (TIRF) Microscopy

TIRF microscopy (Axelrod, 1981; Fish, 2009) allows for recording fluorescence signals from the cell membrane and it is an ideally suited tool to monitor the spatial and temporal dynamics of fluorescent PI markers. Briefly, the excitation field of the TIRF

decreases exponentially with distance from the coverslip on which the sample is placed. Because of this decrease in the intensity the excitation field is also termed evanescent field (Fig. 2.3A). This allows for the excitation of fluorophores within approximately 100 nm from the coverslip-sample interface, minimizing therefore the detection of intracellular signals.

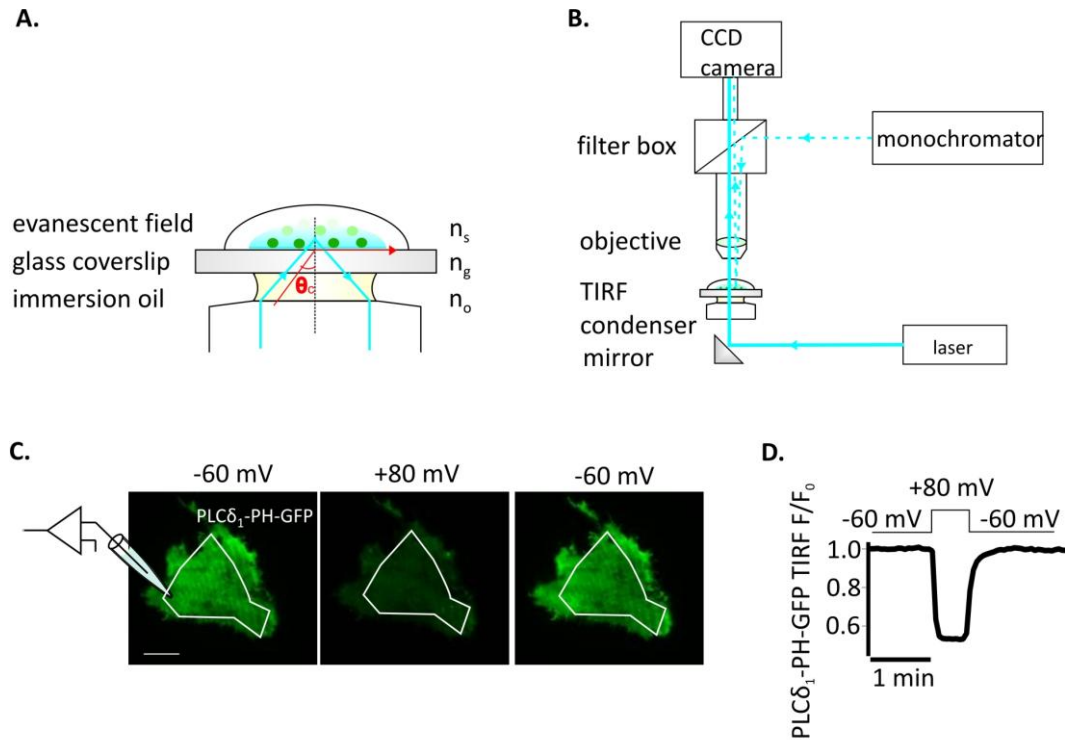


Figure 2.3: TIRF microscopy function and measurements. **A:** The laser light passes first through immersion oil and then into a glass coverslip with equal refractive indexes, $n_o = n_g$. Then the light exits the glass and encounters the interface with the sample. It changes direction because of the different refractive index of the sample, $n_s > n_g$. If the angle of incidence is greater than the “critical” angle θ_c the light will not penetrate through the sample but it will be reflected. As a result an evanescent field is generated that allows for excitation of the fluorophores close to the plasma membrane. **B:** Laser light is guided through a mirror to the TIRF condenser which allows an easy adjustment of the laser beam to the correct illumination angle. The excitation light is then collected by a CCD (charged couple device) camera. A monochromator allows for simultaneous recordings of the epifluorescence signal from the sample. Modified from <http://www.olympusmicro.com/primer/techniques/fluorescence/tirf/tirfintro.html>. **C:** TIRF images of a CHO cell expressing Ci-VSP and the PI(4,5)P₂ marker PLC δ_1 -PH-GFP. A voltage jump from -60 to +80 mV leads to a decrease in the TIRF signal. Scale bar 10 μ m. **D:** Representative time course graph of the TIRF signal, deriving from an experiment as in panel C.

TIRF imaging was performed by using a Bx51WI upright microscope with a TIRF-condenser (Olympus, Hamburg, Germany) and a 488 nm laser (Picarro, Sunnyvale, CA). The setup was equipped with a LUMPlan FI/IR 40x/0.8- numerical aperture water immersion objective (Olympus), an IMAGO-QE cooled CCD camera (TILL Photonics GmbH, Grafelfing, Germany) and a monochromator (Polychrome IV, TILL Photonics). A schematic representation of the setup is demonstrated in figure 2.3B.

TIRF microscopy is an excellent tool for studying the PIs dynamics in living cells. Using fluorescent tagged PI biosensors, TIRF microscopy allows for monitoring changes of the PI levels at the plasma membrane, following VSP activation. Our setup combines TIRF microscopy with patch clamping instrumentation and facilitates simultaneous control of VSP activity and monitoring PI dynamics from the plasma membrane.

As shown in figure 2.3C, a cell coexpressing a VSP and a PI(4,5)P₂ specific biosensor is depolarized via the whole cell patch clamp method. This results in activation of the VSP, PI(4,5)P₂ depletion and translocation of the biosensor from the plasma membrane to the cytosol and therefore decrease of the membrane fluorescence. The fluorescence was recorded from the “footprint”, of the cell, avoiding the cell edges, (Fig. 2.3C) and underwent background correction using TILLvision software. For the time course TIRF traces, fluorescent signal (F) was normalized to the baseline fluorescence prior to stimulation (F₀), (Fig. 2.3D).

2.5 Confocal Laser Scanning Microscopy

The confocal laser scanning microscope allows for acquisition of high contrast and high resolution single plane fluorescent images. It is a powerful tool to investigate the localization and dynamics of fluorescently tagged molecules. A laser is used as light source providing a high power light beam able to be focused on a tight spot of the sample. The resolution of confocal microscopy is however limited due to diffraction of light. Depending on the excitation wavelength and the numerical aperture of the objective, the resolution can be in the range of hundreds of nanometers. The scanning ability of the microscope is achieved by scanning mirrors that change the angle of the laser beam allowing for a pixel-by-pixel image acquisition. The light emitted from the

sample passes through a pinhole, where the out of focus light is obstructed, creating therefore a single plane image (Fig. 2.4A).

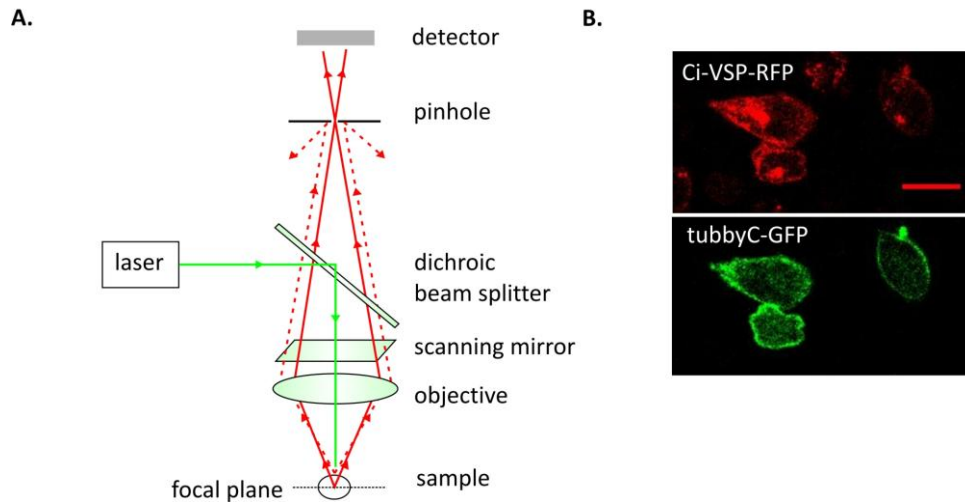


Figure 2.4: Confocal microscopy. A: Schematic diagram of the confocal microscope principle. A light beam generated by a laser is guided via a dichroic beam splitter to scanning mirrors. The scanning mirrors change the angle of the laser beam allowing for a pixel-by-pixel image acquisition. In the next step the light emitted from the sample passes through a pinhole, where only the in focus light is allowed to pass, creating therefore a single plane image. In the last step, the light intensity is detected by a photodetection device which transforms the light signal into an electrical signal. **B:** Representative confocal images of CHO cells expressing Ci-VSP-RFP and the PI(4,5)P₂ biosensor tubbyC-GFP both located at the plasma membrane under resting conditions. Schematic in panel A modified from: <http://www.zeiss.com/microscopy/ende/products/confocal-microscopes/confocal-microscopy-lsm-710.html>

Our setup consists of a Zeiss LSM710 Examiner upright microscope (Carl Zeiss AG; Jena; Germany) equipped with an argon multiline laser for excitation of YFP at 514 nm and GFP at 488 nm. A DPSS 561 nm laser line was used for RFP excitation and a 405 nm laser Diode was used for CFP excitation. For detection, wavelength ranges were 582-754 nm for RFP and 493-582 nm for GFP. The objective used was a W-Plan-Apochromat 20x1.0 DIC M27. The microscope is equipped with an HBO lamp with excitation bandpass filters 470/40 nm (blue) and 436/20 nm (violet). Confocal microscopy data acquisition was performed using ZEN2009 (Zeiss) software.

We used confocal microscopy to determine the cellular localization of the different VSPs (Fig. 2.4B) or to acquire time series recordings of the biosensor's translocation

following activation of VSP. For the time series recordings, the fluorescence was averaged for regions in the cytosol (F_{cyt}) and normalized to the baseline fluorescence prior to stimulation (F_0).

2.6 Förster Resonance Energy Transfer (FRET)

The phenomenon of FRET is based on the energy transfer between two fluorophores in close proximity to each other. Such an interaction occurs when the distance between the two molecules is smaller than ~ 20 nm. The use of FRET in microscopy involves a donor fluorophore, in our case CFP, that when excited can transfer its energy to the nearby acceptor fluorophore, here YFP, resulting in the acceptors excitation (Fig.2.5A). This can occur since the emission spectrum of CFP overlaps with the excitation spectrum of YFP (Fig. 2.5B).

Here, widefield illumination FRET measurements were performed using a Nikon Eclipse TE2000-U inverted microscope equipped with a 40x0.55 LWD objective and coupled with an Oligochrome (TILL Photonics) light source. CFP and YFP were excited using a 430/24 nm (F49-430, AHF Analysentechnik, Tübingen, Germany) filter and a 500/20 nm (F49-500, AHF) filter respectively. Emission signal passed first through a tripleband beamsplitter CFP/YFP/mCherry (F68-017, AHF) and next detection area was selected using a viewfinder and a uEye camera (TILL Photonics). For CFP and YFP/FRET emission detection, a 470/23 nm (F49, AHF) and a 535/30 nm filter respectively, were placed in front of the photodiodes (TILL Photonics). Photodiode output signals were amplified by Oligochrome Imaging Control Unit (ICU). Next, these analog signals were acquired via the digital-analog converter integrated in the EPC-10 amplifier (HEKA electronics, Lambrecht, Germany). A simplified schematic representation of our setup is shown in figure 2.5C. Fluorescence intensity from a wide area including several cells -except for AktAR experiments, where fluorescence was collected from a single cell- was acquired and processed with PatchMaster software. FRET ratios, calculated as $f\text{FRET}/f\text{CFP}$, were normalized to the baseline before stimulation. $f\text{CFP}$ and $f\text{FRET}$ were the signals from the CFP and FRET emission channels, corrected for the dark current recorded without illumination.

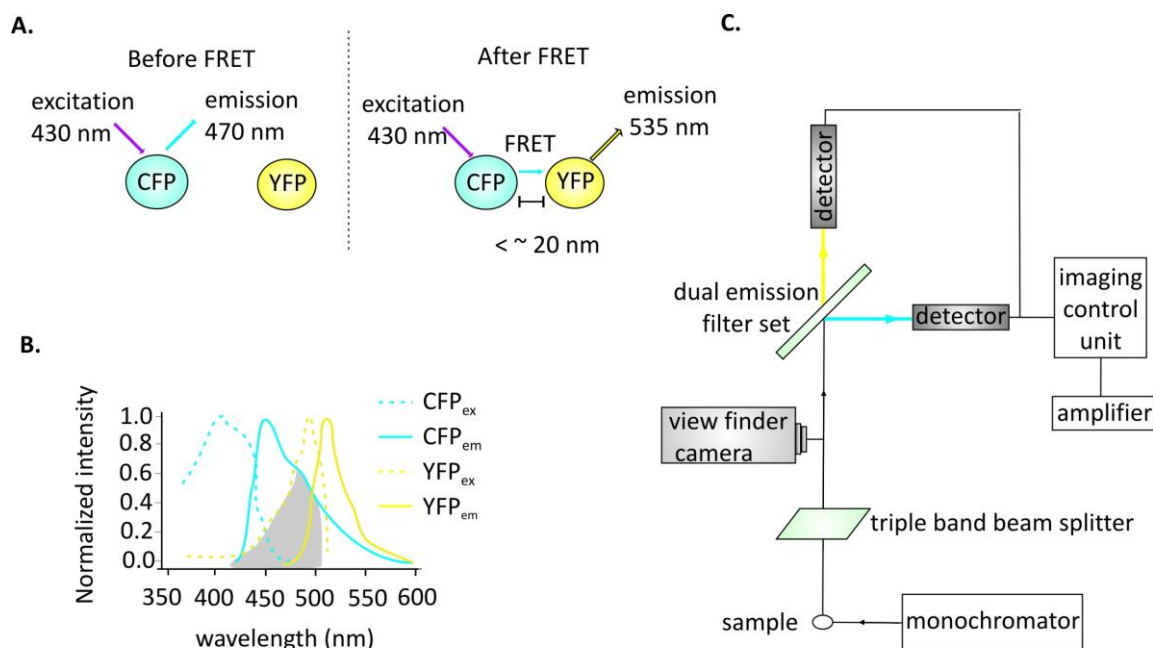


Figure 2.5: The FRET approach. **A:** When the two fluorophores are in distance from each other CFP excitation leads to normal 470 nm emission. Energy transfer between CFP and YFP only occurs when the fluorophores are in close proximity. At this case the energy from CFP emission is transferred to the YFP which emits at 535 nm. **B:** Excitation and emission spectra for CFP and YFP. The gray area represents the overlap between the CFP emission and the YFP excitation, which explains the phenomenon of energy transfer. **C:** Schematic representation of the FRET microscope setup used in this work. A filter based light source (Oligochrome) was used for sample excitation. The emission light first passed through a triple band beam splitter and then through a view finder camera for cell selection. To achieve dual emission detection, CFP/YFP beam splitter was placed before the detectors. Lastly, the signal was delivered to an imaging control unit (ICU) for conditioning and to an amplifier for analysis and storage.

2.7 Solutions and chemicals

In most experiments, cells were kept in extracellular solution containing (mM) 144 NaCl, 5.8 KCl, 0.9 MgCl₂, 1.3 CaCl₂, 0.7 NaH₂PO₄, 5.6 D-glucose, and 10 HEPES, pH 7.4 (with NaOH) 305-310 mosm/kg (standard extracellular solution). Solutions with increased K⁺ concentration were made by replacing NaCl with KCl. For maximal depolarization, a 150 mM K⁺ solution was required prepared as follows (mM): 150 KCl, 0.9 MgCl₂, 1.3 CaCl₂, 0.7 NaH₂PO₄, 5.6 D-glucose, and 10 HEPES, pH 7.4 (with KOH). For the TRPV1 and Chr2(H134R) experiments Ca²⁺ was omitted from the standard extracellular solution to prevent the Ca²⁺ dependent activation of phospholipases (PLC) (Ca²⁺-free extracellular solution) (Rebecchi and Pentylala, 2000).

For experiments combining patch clamping and TIRF imaging cells were kept in standard extracellular solution while the intracellular solution in the patch pipette contained (mM) 135 KCl, 2.41 CaCl₂, 2.5 MgCl₂, 5 EGTA, 5 HEPES and 3 Na₂-ATP, pH 7.3 (with KOH), 290-295 mosm/kg.

For experiments where the sensing currents were measured, we used solutions lacking K⁺ and Na⁺ to minimize the ionic currents. The extracellular solution contained (mM): 75 NMDG, 80 HEPES, 1 CaCl₂, 1 MgCl₂ and glucose 10mM, pH 7.5 (with methanesulfonic acid), 305-310 mosm/kg. For the intracellular solution we used (mM): 65 NMDG, 3 MgCl₂, 1 EGTA, 100 HEPES, pH 7.5 (with methanesulfonic acid), 290-295 mosm/kg.

Capsaicin, IGF1 and glutathione disulfide (GSSG) were purchased from Sigma-Aldrich (St.Louis, Missouri), the Bisperoxovanadate compounds from Santa Cruz Biotechnology (Dallas,TX), DTT from Fermentas (St. Leon-Rot, Germany) and H₂O₂ from Calbiochem (Billerica, Massachusetts).

2.8 Data analysis

To determine the kinetics of the sensing currents' decay and of the PI(4,5)P₂ recovery, we calculated the time constants τ by fitting the acquired data to the exponential function described in figure 2.6A. The charge movement Q was calculated by time integration of the sensing current (Fig.2.6B). For the voltage dependence of Kir2.1 currents, the data were fitted to the Boltzmann equation to calculate the voltage for half maximal current inhibition ($V_{1/2}$) (Fig.2.6C). For the capsaicin concentration-response curve, data were fitted to the Hill equation to calculate the half maximal effective concentration (EC₅₀) (Fig.2.6D).

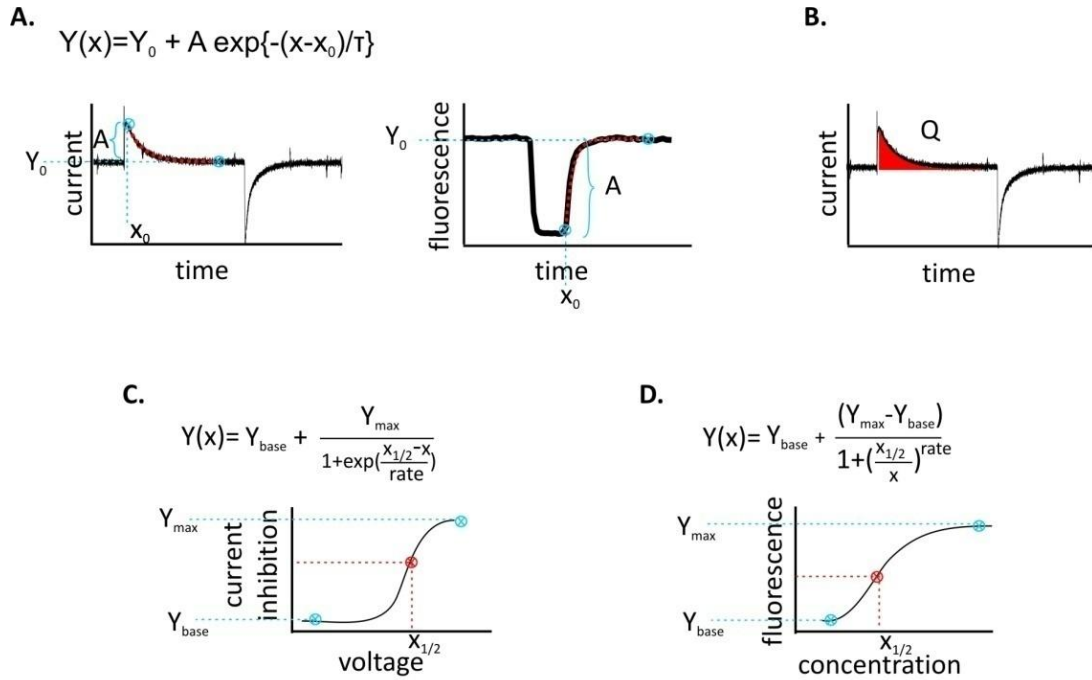


Figure 2.6: Data calculation and curve fitting. **A:** To calculate the time constant of the sensing current decay or the time constant of the PI(4,5)P₂ resynthesis the curves were fitted to a single exponential equation. **B:** The charge movement was calculated by time integration of the “On” sensing current. **C:** To calculate the V_{1/2} (x_{1/2} in the figure) of Kir2.1 channels inhibition the curve was fitted to the Boltzmann (Sigmoid) equation. **D:** To estimate the EC₅₀ (x_{1/2} in the figure) of the capsaicin induced activation we fitted the curve to the Hill equation.

To calculate the maximal response to K⁺ or capsaicin, values acquired during the last 30 seconds of the application were averaged. For ChR2-mediated Ci-VSP activation, the maximal response represents the first value acquired after the blue light exposure. To estimate which cation channel led to the fastest response we calculated the time required to reach 50% of the maximal response (t_{1/2} initiation), for each individual cell. For ChR2 analysis, we utilized the blue light exposure time curve (Fig. 3.12I) to calculate the time required for fluorescence intensity to reach 50% of its maximal value. For recovery kinetics, the time required to reach 50% of the baseline after the end of the application was calculated (t_{1/2} recovery). Only cells that demonstrated a fluorescence intensity change greater than 4% upon application of the substance were used for the analysis.

Error bars show the S.E.M, n represents the number of cells and e represents the number of experiments. For statistical analysis, a two-tailed Dunnett's test was performed to compare the control to different experimental groups, a Student's T-test was used to compare two groups and a Scheffe's test for multiple comparisons. Statistical significance was assigned at $P < 0.05$ and is marked as * for the Dunnett's and Scheffe's test and as # for the Student's T-test. IgorPro (Wavemetrics, Lake Oswego,OR) software was used for data analysis and presentation.

3 Results

3.1 Functional characterization of VSPs

The first part of the results involves the study of several aspects of VSP function such as substrate specificity, subcellular localization and dependence on pH and redox state. VSPs were activated via whole-cell patch clamping and the phosphatase activity was monitored using TIRF microscopy of fluorescent-tagged PI biosensors.

3.1.1 Generation of a functional human VSP chimera targeted to the plasma membrane

Although VSPs have been isolated from the human genome several years ago (Chen et al., 1999; Tapparel et al., 2003; Walker et al., 2001), the mechanism of their activation remains up to now elusive. *In vitro* phosphatase assays suggested that hVSP1 acts as a 3-phosphatase of PI(3,4,5)P₃, while hVSP2 lacks phosphatase activity. However, regulation of hVSP1 by membrane voltage has not been demonstrated so far because all the splice variants (Fig.1.4) are localized in intracellular membranes, when expressed in heterologous expression systems. On the other hand, splice variants of the catalytically inactive hVSP2 show distinct cellular localization, with the hVSP2-3 isoform located in the plasma membrane. The different splice variants of hVSP1 and hVSP2 mainly differ in the length of the cytoplasmic N-terminus.

Here we attempted to target hVSP1 to the plasma membrane and examine whether its enzymatic activity is controlled by the voltage sensor domain. Overexpression of mRFP tagged hVSP1-1 in CHO cells was restricted to intracellular compartments, as revealed by confocal microscopy, consistent with previous observations (Walker et al., 2001; Tapparel et al., 2003). This subcellular localization was independent of the position of the mRFP tag (Fig. 3.1A, B).

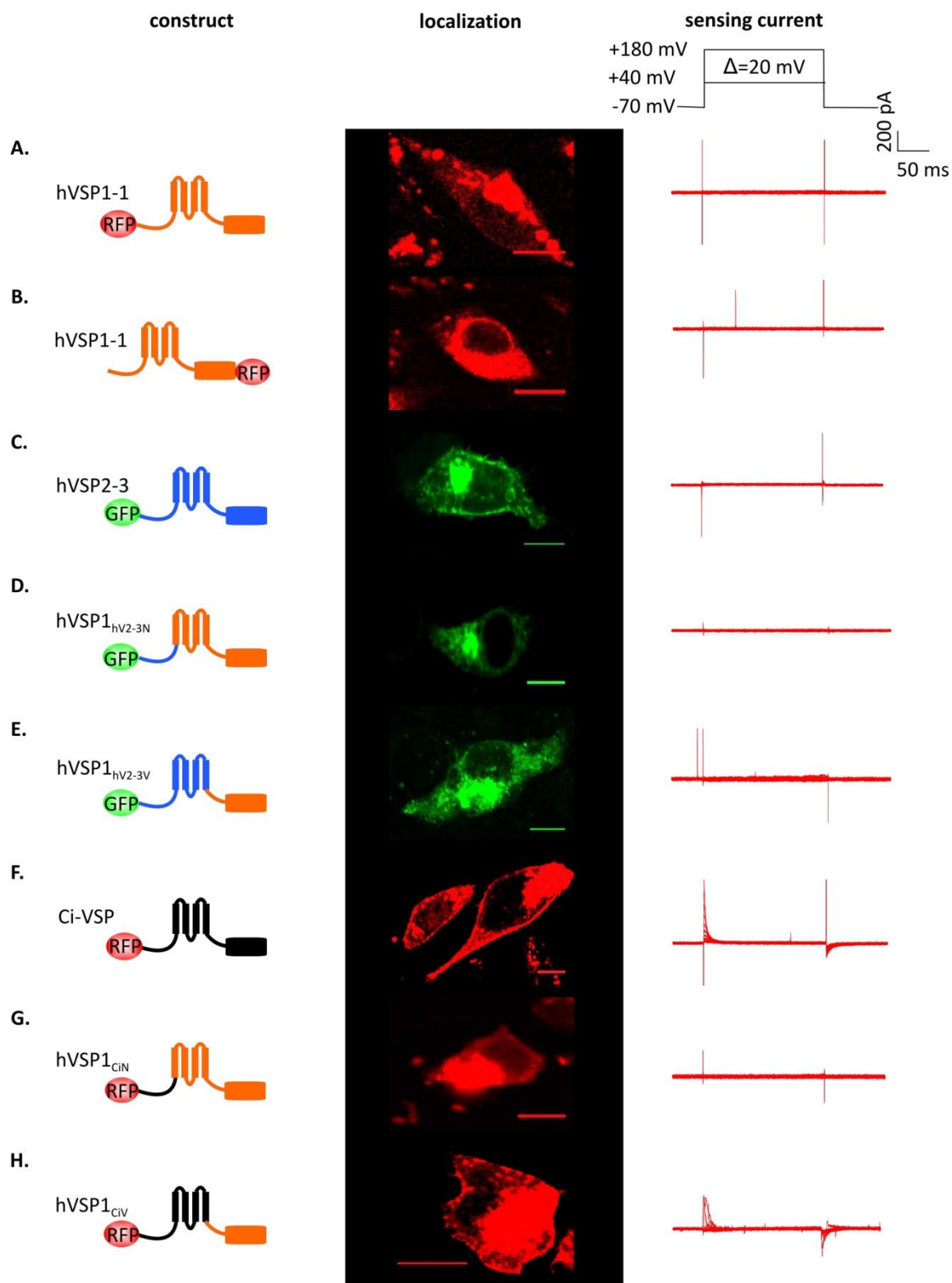


Figure 3.1: Cellular localization and sensing currents of wild type and chimeric VSPs. A and B: hVSP1 is located in intracellular compartments. C: hVSP2-3 is the only hVSP2 isoform localizing at the plasma membrane. D and E: Chimeric proteins fusing the N-terminus (D) or the VSD (E) of hVSP2-3 with hVSP1 demonstrated no plasma membrane localization and no sensing

currents. **F:** Membrane localization of Ci-VSP. **G:** The chimeric protein hVSP1_{CIN} presenting intracellular localization and no sensing currents. **H:** hVSP1_{CIV} demonstrated membrane localization and sensing currents. Scale bar 10 μ m.

Given the fact that hVSP2-3 splice variant is located at the plasma membrane (Fig.3.1C) we considered a possible role of the cytoplasmic N-terminus in membrane targeting. Therefore, we first created a chimeric protein substituting the N-terminus of hVSP1 with the N-terminus of hVSP2-3, named hVSP1_{hV2-3N} (Fig. 3.1D). hVSP1_{hV2-3N} did not succeed in reaching the plasma membrane and presented no electrical activity in the form of sensing currents.

The second chimeric protein created, named hVSP1_{hV2-3V}, consists of the entire voltage sensor of hVSP2-3 and the phosphatase domain of hVSP1 (Fig. 3.1E). This construct also presented no detectable plasma membrane localization and no sensing currents.

Next we thought of utilizing the Ci-VSP N-terminus and VSD since this VSP is strongly localized to the plasma membrane and generates robust sensing currents easily detected with patch clamping (Fig. 3.1F). We followed the same approach as previously and exchanged the N-terminus of hVSP1 with the N-terminus of Ci-VSP, creating a chimeric protein named hVSP1_{CIN} (Fig. 3.1G). This chimera also failed to reach the plasma membrane. The only hVSP1 chimera that reached the membrane and generated sensing currents was created by exchanging the entire voltage sensor domain of hVSP1 with the voltage sensor of Ci-VSP, named hVSP1_{CIV} (the specific construct was created by O. Ebers)(Fig. 3.1H).

Since hVSP1_{CIV} was the only chimera targeted to the membrane, we proceeded by testing its lipid phosphatase activity in living cells, using patch clamping combined with TIRF microscopy. In CHO cells coexpressing hVSP1_{CIV} and the PI(4,5)P₂ sensor PLC δ ₁-PH-GFP (Várnai and Balla, 1998) depolarization of the membrane potential resulted in decrease of the fluorescent signal signifying PI(4,5)P₂ depletion (Fig. 3.2A). As a control experiment, we transfected the catalytic inactive (dead) hVSP1 mutant C363S, in order to show that the fluorescence decrease really results from the phosphatase activity of the protein. The specific mutation is known to inactivate all VSP homologues because it disables the catalytic mechanism of the phosphatase. Indeed, cells transfected with the catalytically “dead” hVSP1 demonstrated no decrease in the fluorescence intensity

(Fig. 3.2A). To assess if the dephosphorylation occurs at the 4- or 5-phosphate of $\text{PI}(4,5)\text{P}_2$, $\text{hVSP1}_{\text{CIV}}$ was cotransfected with the $\text{PI}(4)\text{P}$ sensor OSBP-PH-GFP (Levine and Munro, 1998). Activation of $\text{hVSP1}_{\text{CIV}}$ by depolarization resulted in an increase of the membrane fluorescence indicating increase of the $\text{PI}(4)\text{P}$ concentration. This finding suggests that the $\text{hVSP1}_{\text{CIV}}$ acts as a 5-phosphatase of $\text{PI}(4,5)\text{P}_2$ (Fig. 3.2B). Lastly, when the $\text{PI}(3,4)\text{P}_2$ sensor TAPP1 (Kimber et al., 2002) was used, an increase of the fluorescence was observed, suggesting that $\text{hVSP1}_{\text{CIV}}$ acts also as a 5-phosphatase of $\text{PI}(3,4,5)\text{P}_3$ (Fig. 3.2C).

As a conclusion, our results suggest that hVSP1 is a functional phosphatase that can be activated via an N-terminal voltage sensor and despite of what was previously believed, hVSP1 acts as a 5-phosphatase of $\text{PI}(4,5)\text{P}_2$ and $\text{PI}(3,4,5)\text{P}_3$.

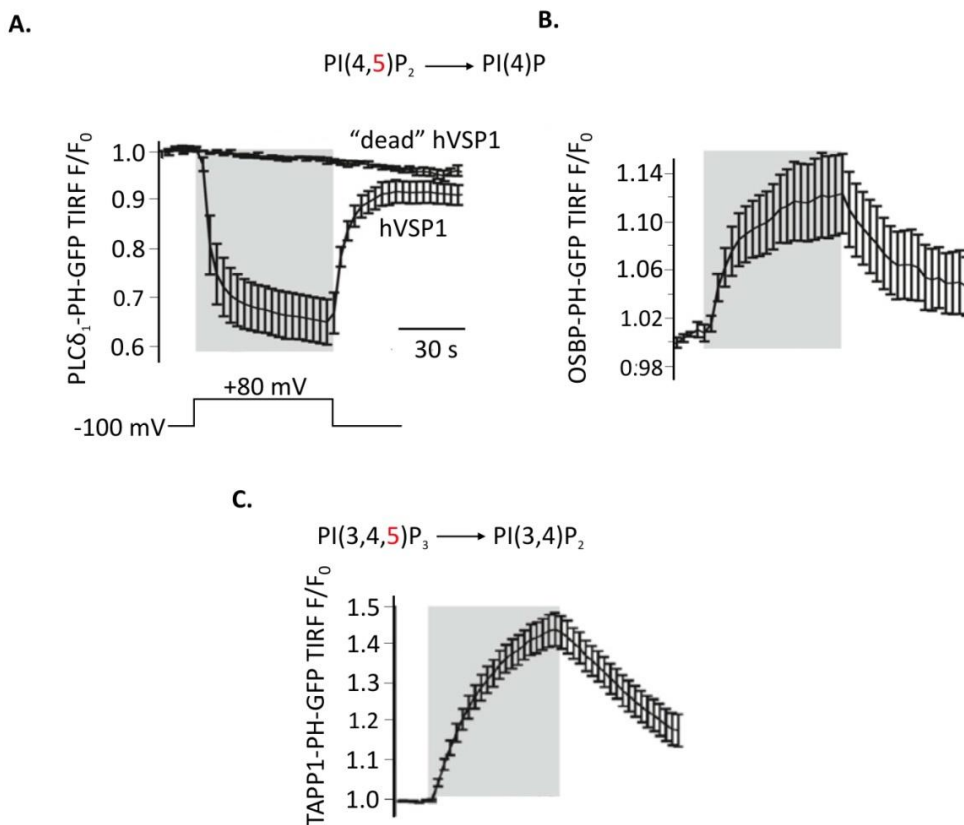


Figure 3.2: Enzymatic activity of $\text{hVSP1}_{\text{CIV}}$. **A:** TIRF signals of CHO cells expressing $\text{hVSP1}_{\text{CIV}}$ and the $\text{PI}(4,5)\text{P}_2$ sensor $\text{PLC}\delta_1\text{-PH-GFP}$. Membrane depolarization leads to activation of the phosphatase, $\text{PI}(4,5)\text{P}_2$ depletion and $\text{PLC}\delta_1\text{-PH-GFP}$ translocation ($n=7$). No decrease in the fluorescent signal is observed with the catalytically dead mutant C363S ($n=4$). **B:** TIRF signal of cells expressing $\text{hVSP1}_{\text{CIV}}$ and the $\text{PI}(4)\text{P}$ sensor OSBP-PH-GFP . Activation of the phosphatase

leads to an increase of the fluorescent signal indicating PI(4)P production. **C:** When the PI(3,4)P₂ sensor TAPP1 was coexpressed with hVSP1_{CiV}, an increase of the fluorescence was observed, suggesting that hVSP1_{CiV} dephosphorylates PI(3,4,5)P₃ in the 5 position. The image is modified from (Halaszovich et al., 2012) and experiments were performed by Dr. Michael Leitner.

3.1.2 Functional characterization of a novel PTEN oncogenic mutation

PTEN is one of the most frequently mutated tumor suppressors in human cancer and other pathological conditions. It exerts its tumor suppressor activity via direct antagonism of the phosphatidylinositol 3-kinase (PI3K) signaling pathway by counteracting the PI(3,4,5)P₃ production via PI3K (Fig. 1.5). PTEN displays remarkable structural and functional similarity with VSPs. This enabled the development of the chimeric protein PTEN_{CiV}, which fully reproduced the substrate specificity of wild-type PTEN and could be activated by membrane depolarization, provided a novel approach for controlling the activity of PTEN and studying this important tumor suppressor (Lacroix et al., 2011).

Here we use this approach to characterize the enzymatic activity of a novel PTEN mutation identified from a prostate cancer sample (Costa et al., 2015). The mutation occurred at position 126 where the original alanine was mutated to a glycine. Alanine 126 is located within the highly conserved HCX₅R motif, in the catalytic P-loop site of PTEN. Interestingly, this A126G mutation produces an amino acid sequence identical to VSP family proteins. Functionally, PTEN is a 3-phosphatase, whereas Ci-VSP primarily acts as a 5-phosphatase of PI(4,5)P₂/PI(3,4,5)P₃ (Fig. 3.3A). We therefore hypothesized that the A126G mutant could convert the substrate specificity of PTEN from a 3- to a 5-phosphatase.

We used whole-cell patch clamping for activation of PTEN_{CiV} and TIRF microscopy to investigate the effect of this oncogenic mutation on the phosphatase activity of PTEN. When A126G PTEN_{CiV} was coexpressed with the PI(3,4,5)P₃ specific domain Btk-PH-GFP (Salim et al., 1996), activation of A126G PTEN_{CiV} resulted in a decrease of the membrane fluorescence, indicating that the mutant retains phosphatase activity against PI(3,4,5)P₃ (Fig. 3.3B). The WT PTEN_{CiV} showed also a decrease in the fluorescence signal, signifying the PI(3,4,5)P₃ depletion.

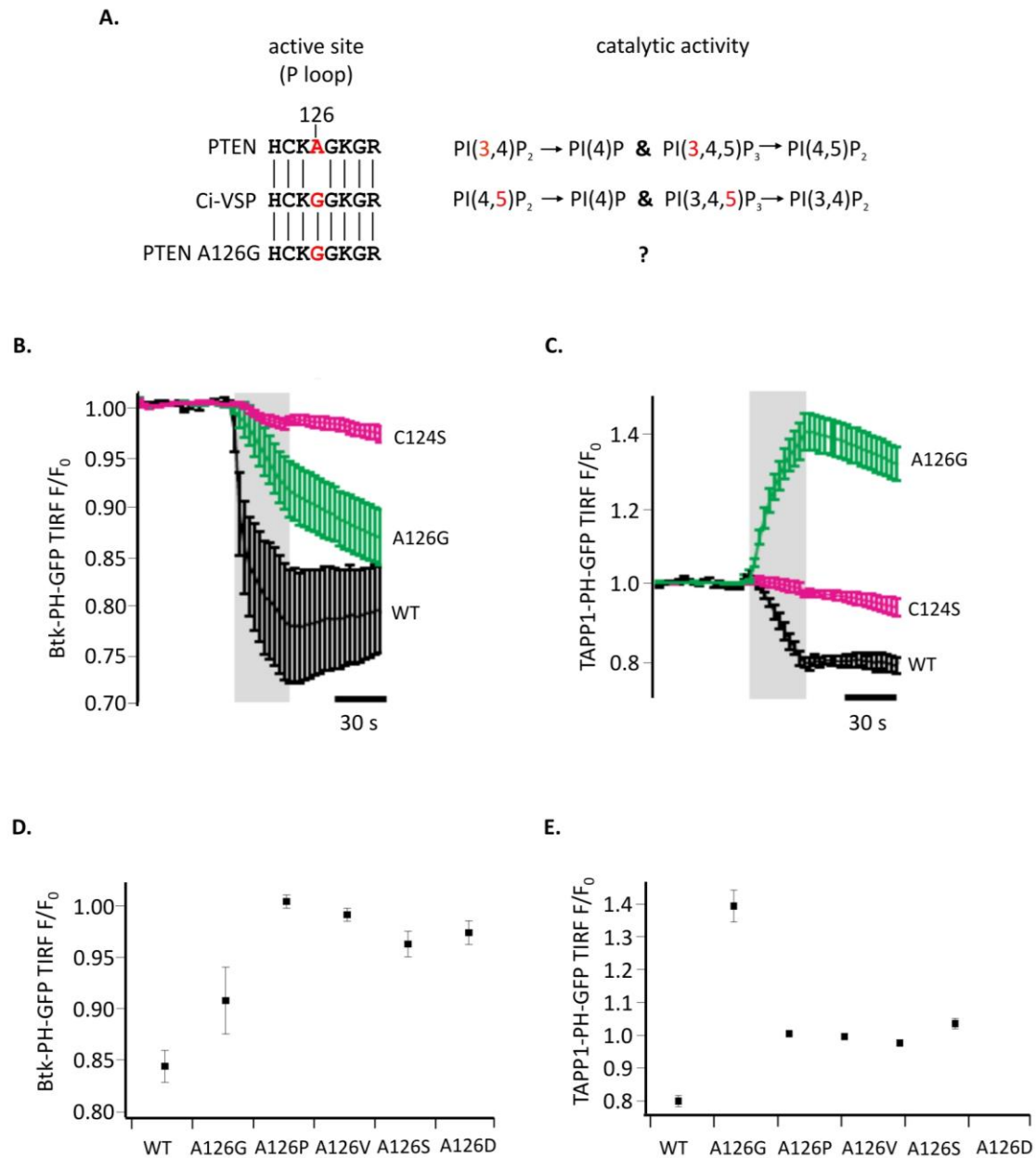


Figure 3.3: The PTEN A126G oncogenic mutant is causing a gain of function. **A:** Amino acid sequence comparison of the HCK₅R motif, in the active site region of PTEN and Ci-VSP. Within the P-loop the only amino acid that differs is the alanine 126. **B:** Time course of TIRF signals from cells coexpressing the PI(3,4,5)P₃ specific domain Btk-PH-GFP with WT, A126G, or the catalytically inactive C124S PTEN_{CIV}. PTEN_{CIV} was activated at +80 mV for 30 seconds from a holding potential of -60 mV. The decrease of the fluorescent signal represents the depletion of PI(3,4,5)P₃. **C:** Time course of TIRF signals from cells coexpressing the PI(3,4)P₂ specific domain TAPP1-PH with WT, A126G, or the catalytically inactive C124S PTEN_{CIV}. WT PTEN_{CIV} results in a decrease in the TIRF signal meaning depletion of PI(3,4)P₂. In contrast the A126G mutant demonstrates an increase of fluorescence signal indicating an increase in the PI(3,4)P₂ concentration. **D and E:** Summary data of phosphatase activity of several PTEN oncogenic

mutants at the position A126. Experiments were performed as in panels B and C with fluorescence being measured at the end of the depolarization step. In D, the oncogenic mutants A126P and A126V demonstrate complete loss of enzymatic activity while the mutants A126G, A126S and A126D demonstrate decreased activity compared to the WT PTEN_{CIV}. In panel E, only the A126G mutation causes an increase of fluorescence signal. At least 7 cells per mutant were measured. Graphs B-E were modified from (Costa et al., 2015). TIRF measurements for A126G, A126P and A126V were performed by Dr. M. Leitner.

For control, we transfected with the catalytically inactive (dead) mutant C124S. The specific mutation is known to inhibit the catalytic mechanism of PTEN and of VSPs, resulting in inactive phosphatases. As shown in Figure 3.3B, no decrease in the fluorescence intensity was observed for C124S PTEN_{CIV}. However, when the PI(3,4)P₂ specific domain TAPP1-PH was coexpressed with A126G PTEN_{CIV}, a robust increase in the fluorescent signal was observed (Fig. 3.3C). This increase in PI(3,4)P₂ levels suggests that A126G PTEN_{CIV} indeed acts as a 5-phosphatase of PI(3,4,5)P₃, consistent with our original speculation.

Moreover, to examine if this switch in the phosphatase specificity is an exclusive feature of the A126G mutant, we extended this approach to further oncogenic somatic mutations reported in COSMIC (Catalogue of Somatic Mutations in Cancer (<http://cancer.sanger.ac.uk/cancergenome/projects/cosmic/>)). We mutated alanine in position 126 to proline, valine, aspartic acid and serine and performed experiments as described in panels B and C. Coexpression of the mutants with the PI(3,4,5)P₃ specific domain Btk-PH- GFP (Fig. 3.3D), revealed no or decreased phosphatase activity. When the PI(3,4)P₂ specific domain TAPP1-PH was used, none of the mutants presented an increase of fluorescence signal (Fig. 3.3E) and therefore no switch in the specificity.

In conclusion, we showed that alanine to glycine exchange at the position 126 in the HCX₅R motif, converted the specificity of PTEN from a 3-phosphatase to a 5-phosphatase of PI(3,4,5)P₃.

3.1.3 The effect of intracellular pH and redox state on VSPs

Although little is known about the physiological role of VSPs, it has been hypothesized that they have a function in sperm physiology and fertilization, cell morphology, growth and development, (Murata et al., 2005; Ratzan et al., 2011; Yamaguchi et al.,

2014; Neuhaus and Hollemann, 2009). However, it is not really clear, if the voltage changes that occur in these cells types are sufficient for activating VSPs, given their relatively positive range of activation. Therefore it was an obvious undertaking to search for additional activating stimuli and conditions.

Sperm physiology and fertilization are known to be influenced by intracellular pH and redox state changes (Nishigaki et al., 2014; Zeng et al., 1996; Baltz et al., 1995; Aitken et al., 1995; de Lamirande and O’Flaherty, 2008). In addition, changes in the intracellular pH are shown to be important in cell polarity and migration (Casey et al., 2010). Thus, in this part we are investigating the effect of intracellular pH and redox state on VSPs activity.

3.1.3.1 Acidic intracellular pH increases the PI(4,5)P₂ but not the PI(3,4,5)P₃ depletion by VSPs

To study the effect of pH, we performed whole-cell patch clamp experiments with intracellular solutions of different pH values (pH_{int}). CHO cells were transfected with the VSP isolated from zebrafish, named Dr-VSP, and the PI(4,5)P₂ sensor PLC δ_1 -PH-GFP. We found that at acidic pH_{int} , the PI(4,5)P₂ depletion was more pronounced compared to neutral or alkaline pH_{int} (Fig. 3.4A). To exclude that this pH effect resulted as an artifact from pH sensitivity of GFP or the binding affinity of the biosensor, we chose an additional, independent method to monitor Dr-VSP activity. The inward rectifier K⁺ channel Kir2.1 has already been used as a readout of VSP activity as it is highly sensitive to PI(4,5)P₂ depletion (Liu et al., 2012; Sakata et al., 2011). Moreover Kir2.1 is insensitive to pH changes in the range used here (Qu et al., 2000). Activity of Kir2.1 was monitored as the inward current during a step voltage pulse to -100 mV from a holding potential of -60 mV. Activation of Dr-VSP with membrane depolarization inhibited the Kir2.1 currents as shown in figure 3.4B. The degree of current inhibition was higher when pH_{int} 6.4 was used compared to pH_{int} 7.3, indicating that the PI(4,5)P₂ depletion was stronger under acidic intracellular conditions. The voltage dependence of the current inhibition – and hence activity of Dr-VSP - was shifted towards more negative potentials when pH_{int} 6.4 was used (Fig. 3.4C). Specifically, the $V_{1/2}$ for pH_{int} 6.4 was

estimated 44 ± 4.3 mV while for $\text{pH}_{\text{int}} 7.3$ the $V_{1/2}$ was 59 ± 15 mV as calculated from fitting the Boltzmann equation to the measurements.

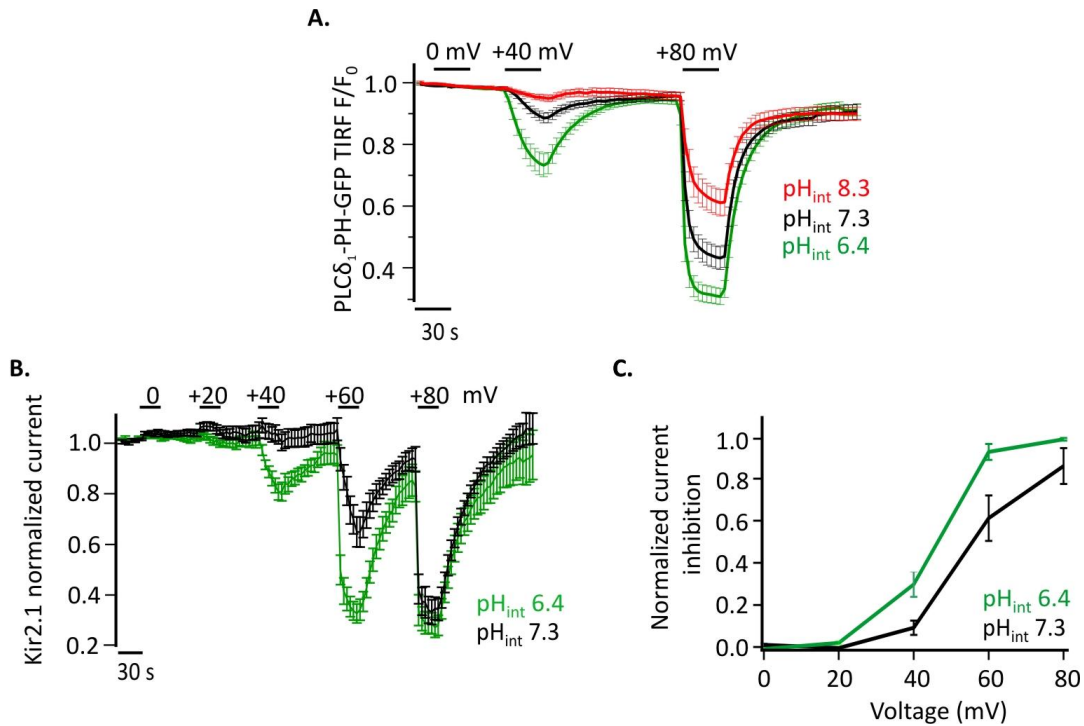


Figure 3.4: Increased PI(4,5)P₂ depletion at acidic pH with Dr-VSP. **A:** TIRF signals from cells expressing Dr-VSP and the PI(4,5)P₂ sensor PLC δ_1 -PH-GFP. Increased PI(4,5)P₂ depletion is observed at acidic pH_{int} ($e=18$ for $\text{pH}_{\text{int}} 8.3$, $e=19$ for $\text{pH}_{\text{int}} 7.3$ and $e=20$ for $\text{pH}_{\text{int}} 6.4$). **B:** Normalized currents in cells coexpressing the K⁺ channel Kir2.1 and the Dr-VSP. Here, the inward currents at -100 mV from a holding potential of -60 mV were measured. Kir2.1 channels were inhibited by Dr-VSP mediated PI(4,5)P₂ depletion. Dr-VSP was activated by depolarizing voltage pulses to 0, +20, +40, +60 and +80 mV. Stronger inhibition is observed under acid intracellular conditions, indicating potential increased Dr-VSP activity ($e=7$ for $\text{pH}_{\text{int}} 7.3$ and $e=8$ for $\text{pH}_{\text{int}} 6.4$). **C:** Voltage-current inhibition curve for Kir2.1 estimated by plotting the current value at the end of each voltage application from graph B. The use of $\text{pH}_{\text{int}} 6.4$ caused a shift of the curve towards more negative potentials.

The pH sensitivity observed above is not restricted to Dr-VSP but was also apparent in VSP from other species, such as in Ci-VSP and the *Xenopus laevis* VSP, XI-VSP1. TIRF experiments as in figure 3.4A were performed for Ci-VSP and XI-VSP1 and similar results were obtained, with acidic pH to increase the degree of PI(4,5)P₂ depletion. To present the data, the fluorescence time course traces were normalized to the fluorescence value prior to VSP activation and then plotted against voltage (Fig. 3.5).

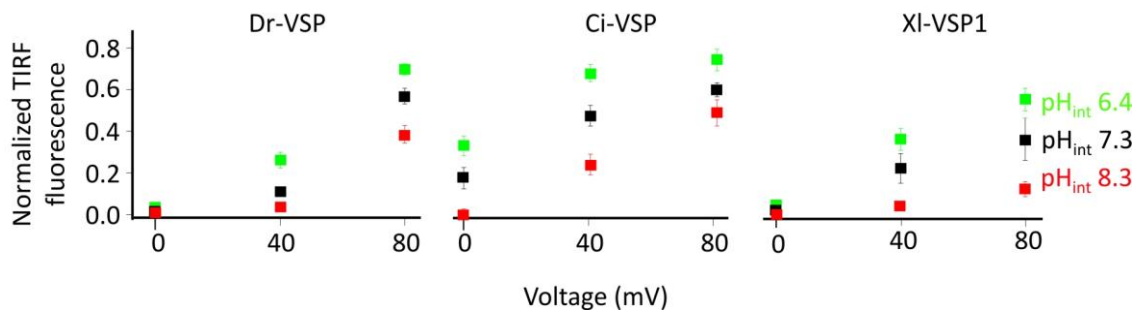


Figure 3.5: Other VSPs present similar sensitivity to pH. Graphs representing the TIRF signals from cells expressing Dr-VSP, Ci-VSP or XI-VSP1 with the PI(4,5)P₂ sensor PLCδ₁-PH-GFP. The values for these graphs derive from time series experiments as in figure 3.4A, plotted against voltage. For Dr-VSP the values derive from graph 3.4A. At least 7 cells for each pH value were measured.

To study if this pH sensitivity is also apparent with PI(3,4,5)P₃ as a VSP substrate, Dr-VSP was coexpressed with the Btk-PH-GFP domain, a PI(3,4,5)P₃ specific sensor. In contrast to dephosphorylation of PI(4,5)P₂, TIRF experiments revealed no pH sensitivity of PI(3,4,5)P₃ depletion by Dr-VSP (Fig. 3.6).

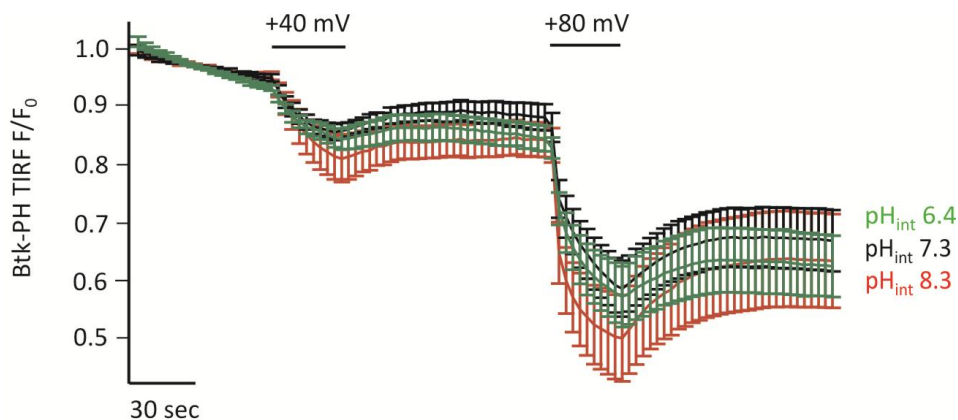


Figure 3.6: Intracellular pH does not affect the PI(3,4,5)₃ depletion via Dr-VSP. Here the Btk-PH-GFP sensor was used to monitor PI(3,4,5)₃ levels. Different intracellular pH values did not change the degree of PI(3,4,5)P₃ depletion after activation of Dr-VSP at +40 and +80 mV. e=8 at pH_{int} 6.4, e=8 at pH_{int} 7.3, e=8 at pH_{int} 8.3.

3.1.3.2 pH does not affect the voltage dependence of VSP sensing

Since VSPs consist of two distinct domains, the voltage sensor domain and the catalytic domain, we asked if the increased PI(4,5)P₂ depletion observed at acidic intracellular pH can be explained by a shift in the voltage dependence of the sensing (gating).

According to this hypothesis, at acidic pH more VSDs would be at the “On” conformation at a certain voltage. This could potentially be the explanation for the increased PI(4,5)P₂ depletion at acidic pH. To test this hypothesis we calculated the charge movement from the “On” sensing current of Dr-VSP, during a stepwise increase of the membrane potential (Fig. 3.7A, B). We observed no significant differences in the voltage dependence of the sensing currents under different intracellular pH values. In particular the $V_{1/2}$ at pH_{int} 6.5 was 98.15 ± 4.9 mV, for pH_{int} 7.5 was 106.64 ± 4.2 mV and for pH_{int} 8.5 107 ± 5.8 mV. For statistical testing, a Scheffe’s test was performed for multiple comparisons between the three groups, revealing however no significant differences.

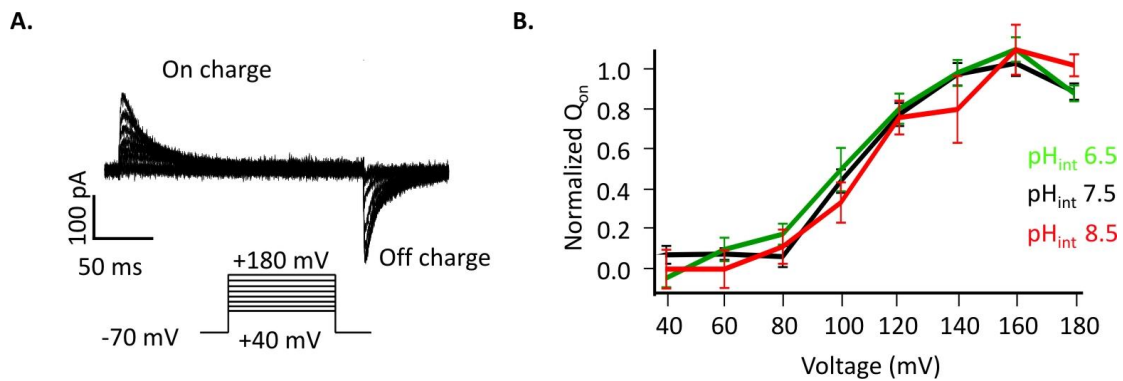


Figure 3.7: The sensing of Dr-VSP was not affected by the different pH_{int}. **A:** Representative recording of sensing (gating) currents of Dr-VSP. The voltage sensor moves outwards in response to increasing membrane potential. **B:** No significant shift in the Q-V curve between the different intracellular pH values. $e=14$ for pH_{int} 6.5, $e=14$ for pH_{int} 7.5, $e=9$ for pH_{int} 8.5.

3.1.3.3 pH does not affect the kinetics of PI(4,5)P₂ resynthesis

PI(4,5)P₂ levels depend on the simultaneous activity of PI(4)P 5-kinases and VSP (Fig. 3.8A). Here we considered the possibility that the increased PI(4,5)P₂ depletion observed under acidic conditions results from impairment of the kinase activity. To test this hypothesis we estimated the rate of PI(4,5)P₂ resynthesis from time course TIRF experiments as demonstrated in figure 3.8A, which represents the kinase activity. Specifically we calculated the time constant τ by fitting the data to the exponential function. The rates of PI(4,5)P₂ resynthesis were not significantly different between

different intracellular pH values for all three tested VSPs (Fig. 3.8B), indicating that the kinetics of the PI(4,5)P₂ resynthesis remain stable. Hence, this finding further supports the hypothesis that the observed differences result from changes in VSP activity.

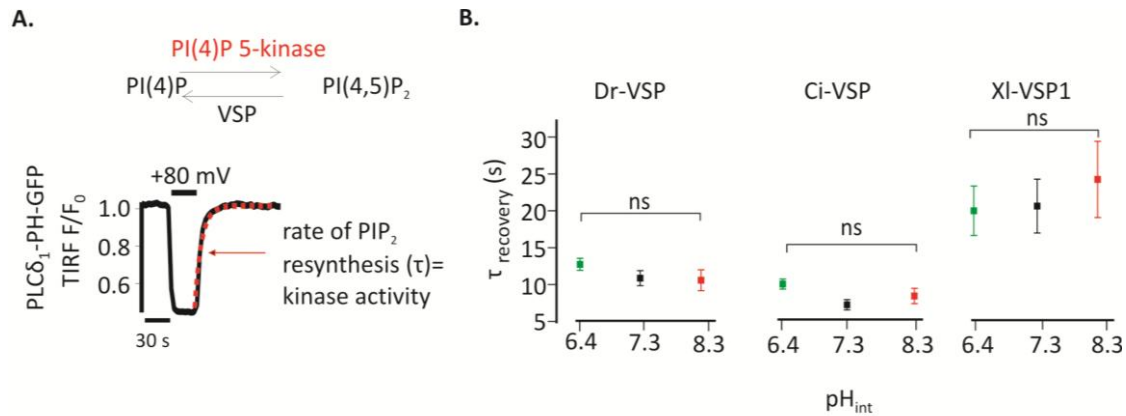


Figure 3.8: The kinetics of PI(4,5)P₂ resynthesis are not affected by the pH_{int}. **A:** Decreased PI(4,5)P₂ levels can occur either because of increased VSP activity or because of decreased PI(4)P 5-kinase activity. By estimating the rate of PI(4,5)P₂ resynthesis it is possible to evaluate the kinetics of the kinase activity. Red dotted line represents the fitting of the curve to the exponential function in order to estimate the τ value. **B:** PI(4,5)P₂ recovery rates for Dr-VSPs, Ci-VSP and XI-VSP1 under different intracellular pH conditions. No statistically significant differences between pH_{int} 6.4 and pH_{int} 8.3 were observed by performing a Student's T-test.

3.1.3.4 The pH sensitivity is not mediated by the pH buffer

In a study on the regulation of connexin channels by pH (Bevans and Harris, 1999) it was shown that the observed pH sensitivity was not due to the protonation of the channel but resulted from protonation state of the pH buffer used. Specifically, protonated aminosulfonate compounds, commonly used as pH buffers, directly inhibited connexin channel activity in a pKa related manner.

Similar to the connexin example, we considered that the protonated form of HEPES, (pKa value of 7.5 at 25°C), could potentially affect VSP activity and thereby account for the pH sensitivity of PI(4,5)P₂ depletion. Moreover, we wanted to test if the pH buffering of HEPES at extreme pH values was efficient, since this buffer is considered useful at pH range 6.8-8.2. We therefore compared HEPES with TAPS, a buffer with pKa value of 8.5 at 25°C and useful pH range 7.7-9.1 (Fig. 3.9A). Because of the different pKa values of these two buffers the protonation of HEPES would be substantially lower

than that of TAPS at pH 8.3. TIRF experiments in cells expressing Dr-VSP and PLC δ_1 -PH-GFP were performed at pH_{int} 8.3 using HEPES or TAPS (Fig. 3.9B). The responses observed with the two pH buffers were indistinguishable, suggesting that the differences in the PI(4,5)P₂ depletion could not be explained by an interaction of the buffer with the Dr-VSP. In addition, the finding suggested that pH buffering of HEPES was sufficient at pH 8.3.

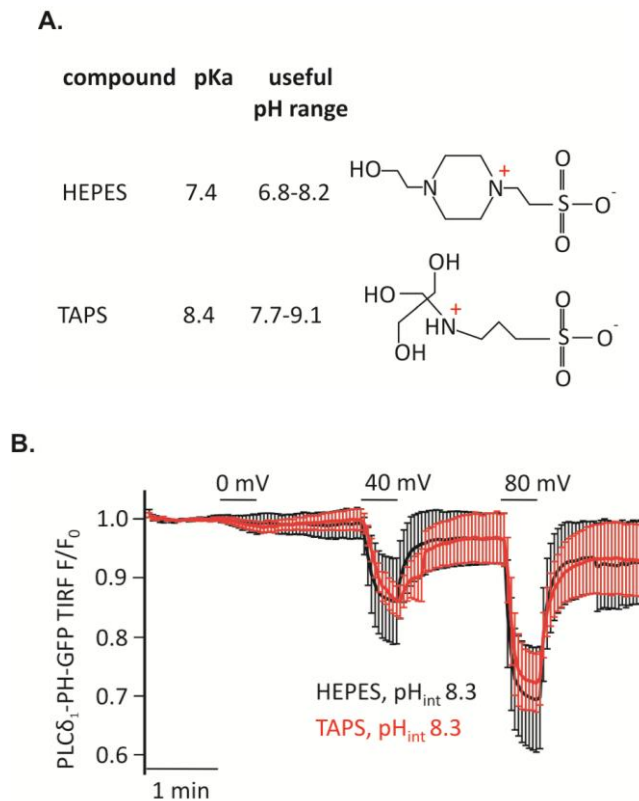


Figure 3.9: pH sensitivity of PI(4,5)P₂ depletion is independent of the buffer. **A:** Chemical structures of HEPES and TAPS. They share a common structural motif of the protonatable amine but present different pKa values and pH ranges. **B:** No difference in the PI(4,5)P₂ depletion between HEPES (e=5) and TAPS (e=7) at pH_{int} 8.3.

3.1.3.5 Testing the involvement of single histidines in the pH sensitivity

As reviewed in (Srivastava et al., 2007) several proteins have been found to be regulated by intracellular pH changes by means of alternation of their conformation or by changes of their interactions with other molecules. A key role in these processes is played by the protonation state of titratable residues and particularly histidine that has a pKa value of 6.1 (Fig. 3.10A). At acidic pH, protons bind to histidines changing the

electrostatic forces and consequently the protein structure (Lukin and Ho, 2004) or increasing the affinity of the protein to its ligands (Miura et al., 1999).

Similarly, it is possible that protons directly interact with VSPs increasing their catalytic activity. To test this hypothesis, we investigated the possible existence of pH-sensing histidines in VSPs, which could account for the observed pH dependence of PI(4,5)P₂ depletion. Single site mutations were performed at the positions H239, H271, H301 and H490 of the phosphatase domain of Dr-VSP. These histidines were chosen since they are conserved among the three VSPs that demonstrated pH sensitivity (Fig. 3.10B). Histidines were substituted by the positively charged arginine, mimicking the protonated state of histidine. Since protonation state of arginine (pK_a=12) is predicted to remain constant at the pH range used in these experiments, it was anticipated that substitution of putative pH-sensing histidines with arginines would abrogate the pH sensitivity of Dr-VSP.

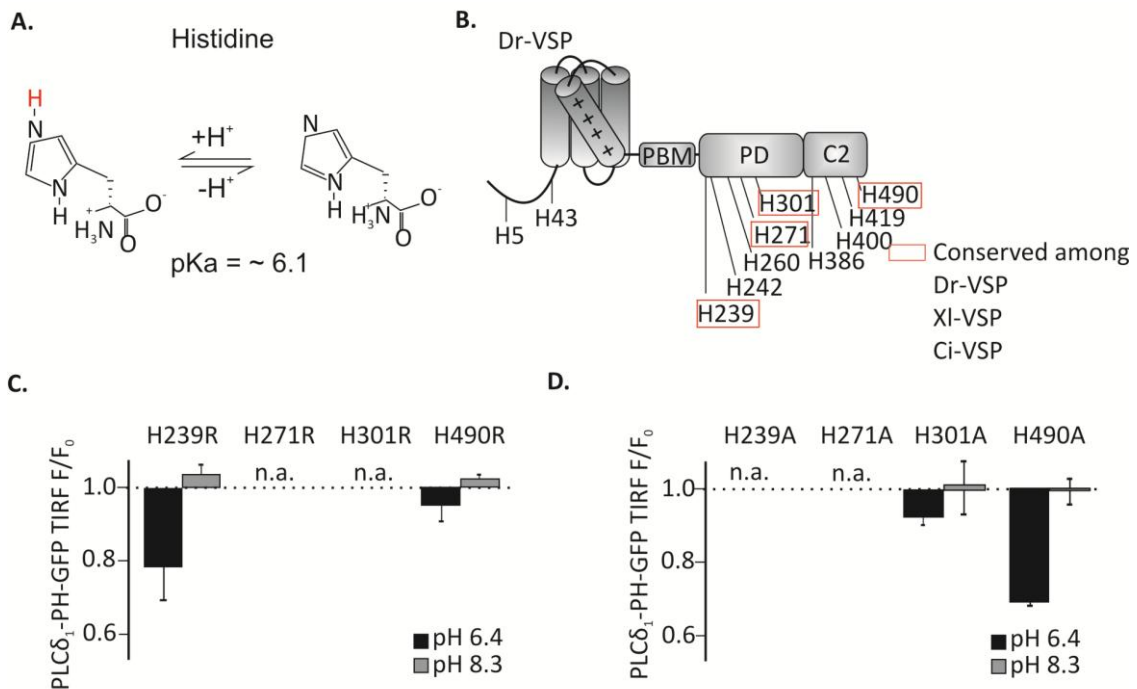


Figure 3.10: Mutagenesis of histidines does not abolish the pH sensitivity of Dr-VSP. **A:** Under acidic conditions histidine exists in its protonated form. **B:** Dr-VSP contains eleven histidines within its cytoplasmic region. Four of these histidines are conserved among the Dr-VSP, Ci-VSP and XI-VSP (all three VSPs present similar pH dependent activity Fig.3.5). **C:** Substitution H239R

and H271R resulted in proteins demonstrating no activity (n.a.) while the H301R and H490R mutants retained the pH sensitivity, seen here as increased PI(4,5)P₂ depletion. **D:** Substitution of H239A and H301A resulted in a catalytically inactive protein while substitutions H271A and H490A still demonstrated increased PI(4,5)P₂ depletion under acidic conditions. A minimum of 4 cells per experiment was obtained.

We performed TIRF experiments in cells coexpressing Dr-VSP mutants with PLC δ_1 -PH-GFP and compared the phosphatase activity between pH_{int} 6.4 and 8.3. For the mutants H239R and H490R the pH sensitivity persisted, indicating no involvement of these histidines in the pH sensing (Fig. 3.10C). The remaining two mutants, H271R and H301R, resulted in a catalytically inactive protein, providing therefore no information about the involvement of these histidines in the pH dependence. We considered that the larger size of the arginine could account for the loss of protein function by interfering with the original protein conformation. Therefore to further examine these positions, we mutated histidine to the small and neutral amino acid alanine, to achieve minimal disturbance of the protein. This time, mutation in the position H301 resulted in an active but pH sensitive response while the H271A mutant remained inactive (Fig. 3.10D). In summary, identification of a single histidine accounting for the observed pH dependence was not possible.

3.1.3.6 Oxidation inhibits the phosphatase activity of Ci-VSP

Reactive oxygen species (ROS) at low and controlled levels can play a role in various signaling pathways, including cell survival and growth pathways, by affecting the activity of target proteins, such as transcription factors, growth factor receptors and phosphatases (Holmström and Finkel, 2014). ROS are also known to regulate sperm capacitation via the regulation of tyrosine phosphorylation (de Lamirande and O'Flaherty, 2008). The most frequent targets of ROS are cysteine residues that under oxidizing conditions form disulfide bonds with proximal intramolecular cysteines, changing thus the conformation of the protein (Fig. 3.11.A).

Ci-VSP and PTEN have also been suggested to be regulated by oxidation (Lee et al., 2002; Matsuda et al., 2011). In the work of Matsuda et al., the crystal structure of Ci-VSP's cytoplasmic region revealed that the protein can exist in two forms: the first

form presented a disulfide bond between C363 and C310, while the second form lacked such bond. These cysteines are conserved in PTEN where they interact under oxidative conditions, inhibiting phosphatase activity (Lee et al., 2002). However, so far only *in vitro* assays were used to assess the effect of oxidation on Ci-VSP and PTEN phosphatase activity. Given the possible involvement of Ci-VSP in cell growth and sperm physiology, here we systematically studied the effect of different redox agents on Ci-VSP in living cells.

CHO cells expressing Ci-VSP and the PI(4,5)P₂ sensor PLCδ₁-PH-GFP were treated with the oxidizing agents hydrogen peroxide (H₂O₂) or glutathione disulfide (GSSG), or with the reducing agent dithiothreitol (DTT). In a representative recording shown in figure 3.11B, a cell initially responding to a +80 mV pulse, demonstrated no phosphatase activity after application of 5 mM H₂O₂ for 5 minutes, indicating inhibition of Ci-VSP, while lower concentrations of peroxide only partially inhibited the protein (Fig. 3.11C). Application of peroxide did not influence the sensing currents of Ci-VSP suggesting that only the phosphatase domain of the protein is affected by oxidation (Fig.3.11D). The mild oxidant GSSG and the reducing agent DTT had no effect on the phosphatase activity (Fig. 3.11F). Based on the crystal structure of Ci-VSP the disulfide bond between the C310 and C363 may account for oxidative inhibition (Matsuda et al., 2011)(Fig. 3.11E). To examine the involvement of the C310 in the inhibition we mutated this amino acid to serine, which is similar to cysteine but lacks the sulfur and is therefore unable to form disulfide bridges. Indeed the C310S mutant was less sensitive to inhibition by H₂O₂ compared to the WT Ci-VSP (Fig. 3.11F).

In conclusion, VSPs can be regulated, in addition to voltage, by intracellular pH or oxidation. While structural and functional data strongly suggest disulfide bridge formation between C310 and C363 as the mechanism for inhibition via oxidation, it remains unknown whether pH changes can directly affect the phosphatase activity of VSPs.

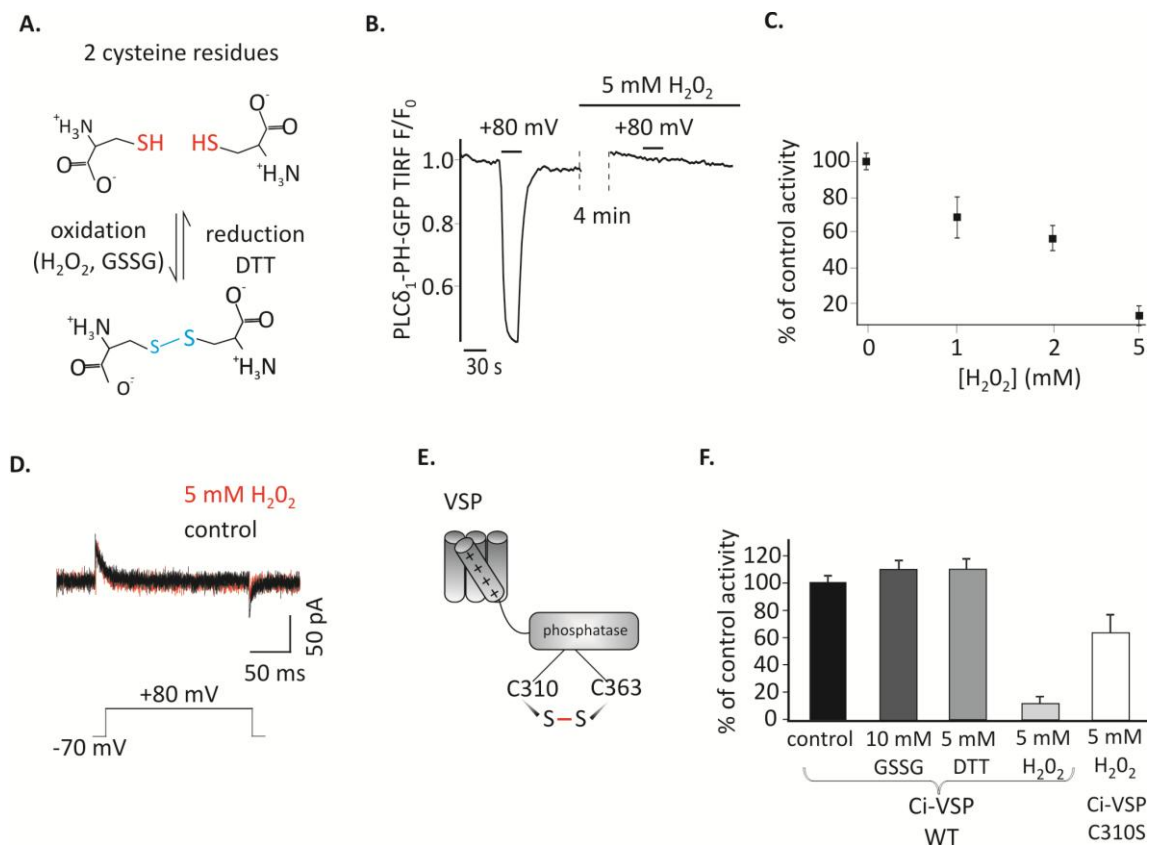


Figure 3.11: The effect of oxidation on the phosphatase activity of Ci-VSP. **A:** Under oxidizing conditions cysteine residues form disulfide bonds altering thus the conformation of the protein. **B:** Incubation with 5 mM H₂O₂ for 5 minutes in cells coexpressing Ci-VSP and PLCδ₁-PH-GFP completely inhibited the phosphatase activity of the protein. **C:** H₂O₂ concentration curve deriving from experiments as in panel B. **D:** The gating of Ci-VSP is not affected by application of 5 mM H₂O₂ for 5 minutes. **E:** Schematic of Ci-VSP showing the position of the cysteines that are involved in the inhibition by oxidation. **F:** Graphs comparing the effect of redox agents on WT Ci-VSP as well as the effect of 5 mM H₂O₂ on Ci-VSP C310S mutant (white bar).

3.2 Development of an experimentally simple method for manipulation of cellular PI concentrations and for analysis of PTEN

All experiments described above were performed using the patch-clamp technique to control VSPs activity by membrane potential. This laborious technique requires electrophysiological instrumentation and time consuming, single cell measurements, which clearly limit the accessibility and popularity of VSPs as tools for manipulating PI levels in living cells. In the second part of this thesis we aimed at developing an

approach where membrane depolarization is achieved by activation of cation channels, to allow for a technically simple way to control VSPs activity in populations of living cells.

3.2.1 Activation of Ci-VSP in intact cells by membrane depolarization via cation channels

To activate VSPs without electrophysiology we developed the experimental strategy depicted in figure 3.12A, where overexpressed cation channels are used to depolarize the cell membrane, thereby activating the VSP. To monitor VSPs activity we used the same basic detection strategy as before, which involves fluorescence-tagged biosensors specific for the VSP's substrates (Várnai and Balla, 2006).

We started by exploring cation channel based strategies to activate the prototypical Ci-VSP. First, the K^+ channels TASK-3 or KCNQ4 (Kv7.4) were used to depolarize the cells. These channels have substantial open probability under basal conditions, since TASK-3 is a constitutively open "leak" channel (Enyedi and Czirják, 2010), whereas KCNQ4 is a voltage gated channel open at potentials above -50mV, when expressed in CHO cells (Chambard and Ashmore, 2005). Given that both channels provide a substantial K^+ conductance, cell depolarization can be simply achieved by increasing the extracellular K^+ concentration.

Indeed, we observed PI(4,5)P₂ depletion as reported by translocation of the PI(4,5)P₂ biosensor tubbyC-GFP (Santagata et al., 2001) when 150 mM K^+ was applied to cells co-expressing Ci-VSP and either KCNQ4 or TASK-3 (Fig. 3.12B and C). Strong and rapid activation of Ci-VSP was achieved with either channel. Slightly more cells cotransfected with KNCQ4 (92%) than cells cotransfected with TASK-3 (80%) responded to application of K^+ . Therefore KCNQ4 was used for further experiments. When co-expression of channels was omitted, only 50% of the cells responded to application of K^+ and changes in PI(4,5)P₂ concentration were weak (Fig. 3.12C), indicating that, at least in CHO cells, endogenous K^+ channels were not sufficient to strongly drive Ci-VSP activity. The translocation of tubbyC-GFP was completely absent when catalytically

dead Ci-VSP C363S was used (Fig. 3.12C), confirming that sensor translocation resulted from Ci-VSP mediated PI(4,5)P₂ depletion.

VSPs can be used to deplete PIs in a gradual fashion by imposing graded membrane depolarization (Halaszovich et al., 2009). Membrane potential has a roughly logarithmic dependence on extracellular K⁺ when membrane properties are dominated by the K⁺ conductance, suggesting that membrane potential and consequently Ci-VSP activity can be gradually increased by elevating extracellular [K⁺]. In fact, when various K⁺ concentrations were washed in, Ci-VSP activity, measured as the degree of translocation of the biosensor, was also graded (Fig. 3.12D). Maximum activity occurred at 150 mM K⁺, which was the maximum concentration we could achieve while keeping physiological osmolarity.

As an alternative approach to achieve membrane depolarization we utilized the capsaicin-activated TRPV1 channel (Fig. 3.12E), a non-selective cation channel that depolarizes the membrane when active (Caterina et al., 1997). Because TRPV1 is also Ca²⁺ permeable and Ca²⁺ influx could potentially activate PLC (Rebecchi and Pentylala, 2000) to cause PI(4,5)P₂ cleavage, we used Ca²⁺-free extracellular solutions in these experiments. Application of capsaicin to HEK cells coexpressing TRPV1, Ci-VSP and tubbyC-GFP resulted in robust PI(4,5)P₂ depletion, whereas no effect was observed in the absence of TRPV1 or Ci-VSP (Fig. 3.12E). 100 nM of capsaicin was sufficient to induce the full response, as demonstrated by the capsaicin concentration-response curve (Fig. 3.12F).

Over the last years, light-activated prokaryotic ion channels have been established as optogenetic tools for manipulation of the membrane potential (Lin, 2011). Among these channels, Channelrhodopsin-2 (ChR2), has been studied extensively and used widely to depolarize cells. ChR2 is a non-selective cation channel activated by visible light with a response spectral peak at around 450 nm (Nagel et al., 2003; Lin et al., 2009). Since activation by light may enable enhanced spatiotemporal control and facilitate experimentation, we also attempted to use ChR2 to activate VSPs.

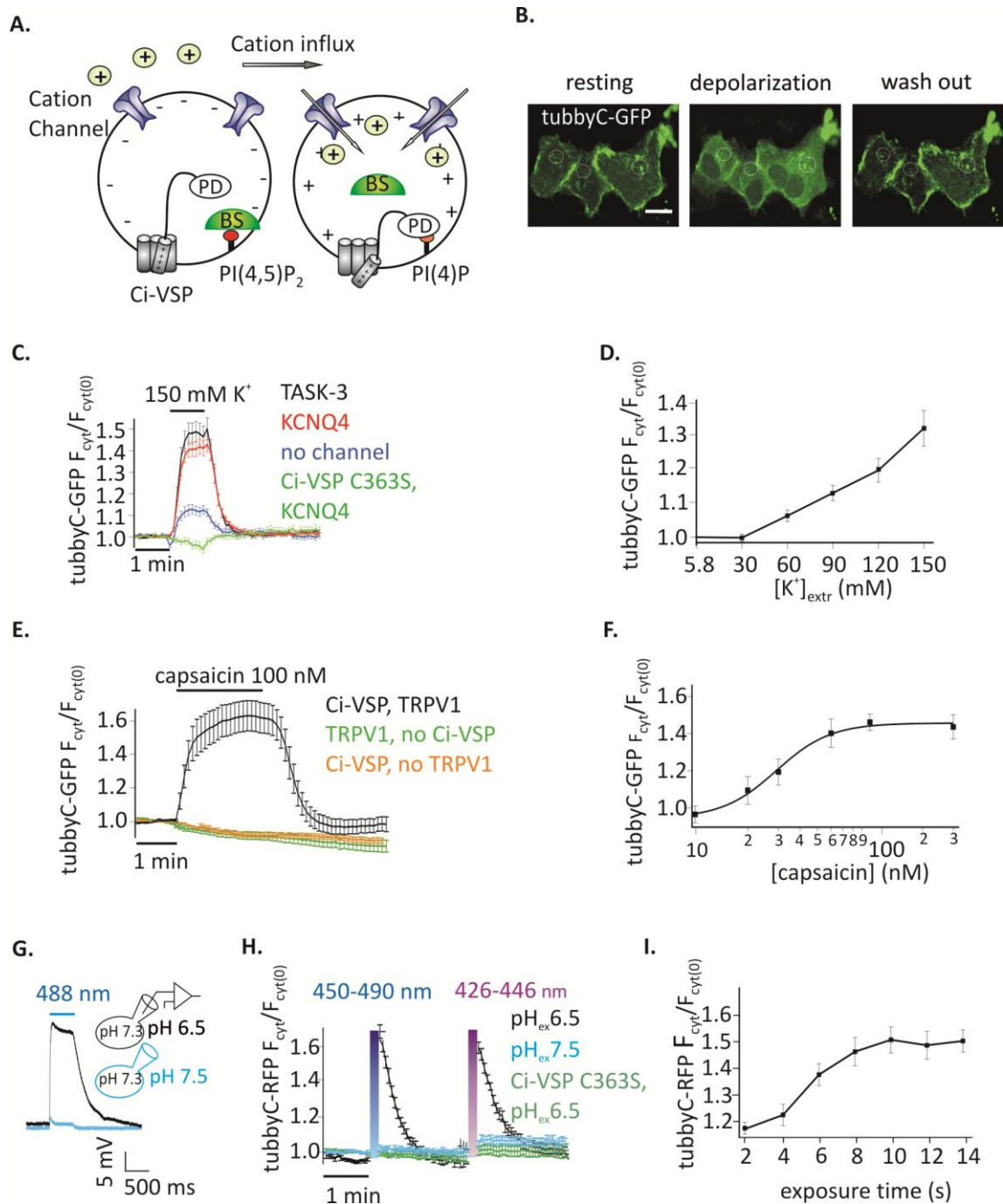


Figure 3.12: Activation of Ci-VSP by membrane depolarization through overexpressed cation channels. **A:** Scheme representing the general strategy used to activate Ci-VSP. Cells coexpress Ci-VSP, a PI biosensor and a cation channel. Cation influx into the cell results in membrane depolarization, activation of Ci-VSP, depletion of PI(4,5)P₂ and lastly translocation of the sensor to the cytoplasm. BS, biosensor; PD, phosphatase domain. **B:** Confocal images of HEK cells coexpressing Ci-VSP, KCNQ4 and tubbyC-GFP acquired before, during and after application of 150 mM K⁺. Fluorescence signal was recorded from cytoplasmic regions. Scale bar 20 μm. **C:** Time series of relative increase of cytoplasmic fluorescence calculated from CHO cells

expressing Ci-VSP, tubbyC-GFP and the K⁺ permeable channels TASK-3 (n=48, e=16), KCNQ4 (n=82, e=16) or no channel (n=28, e=9). The catalytically dead mutant Ci-VSP C363S (n=23, e=8) was used as negative control. TubbyC translocates to the cytoplasm upon 150mM K⁺ application for 1 minute. **D:** K⁺ concentration-response curve from HEK cells coexpressing Ci-VSP, tubbyC-GFP, and KCNQ4 (n=15, e=6). **E:** Application of 100 nM capsaicin in HEK cells coexpressing TRPV1 channel, Ci-VSP and tubbyC-GFP resulted in Ci-VSP activation and tubbyC translocation (n=25, e=8). No effect was observed in the absence of Ci-VSP (n=19, e=7) or TRPV1 (n=16, e=6). **F:** Capsaicin concentration-response curve ($EC_{50} = 29 \pm 3\text{nM}$; at least 10 cells per concentration). **G:** ChR2-mediated membrane depolarization. Representative current clamp recording from a CHO cell expressing ChR2, without current injection ($I_{\text{hold}}=0\text{pA}$). Membrane depolarization increased under low pH extracellular conditions. **H:** Activation of ChR2 with violet (426 – 446 nm) or blue (450 – 490 nm) light exposure for 10 seconds in HEK cells coexpressing tubbyC-RFP and Ci-VSP. tubbyC translocation was observed only at extracellular pH 6.5 (n=12, e=4), but not at pH 7.5 (n=11, e=4) or with the catalytically dead Ci-VSP C363S mutant (n=23, e=4). **I:** Exposure time-response curve showing that 10 seconds of exposure with blue light resulted in maximal tubbyC translocation.

We first explored conditions for sufficient depolarization by ChR2. Extracellular acidification (pH 6.5) turned out to strongly increase the depolarization of cells expressing ChR2 when stimulated with blue light (Fig. 3.12G), most likely due to the high H⁺ permeability of ChR2 (Nagel et al., 2003). This finding suggested low extracellular pH as the optimal condition to activate Ci-VSP via ChR2. Indeed, Ci-VSP was successfully activated only when extracellular solution of pH 6.5 was used but not at the standard extracellular pH 7.4 (Fig. 3.12H). As in the case of TRPV1, we used Ca²⁺-free solution to prevent activation of PLC by Ca²⁺ influx. 10 seconds of blue or violet light exposure were sufficient for maximal stimulation of Ci-VSP, measured via translocation of tubbyC-RFP to the cytoplasm (Fig. 3.12I). An RFP-tagged sensor was used in these experiments, because GFP excitation interferes with ChR2 activation.

To compare the performance of the above methods of Ci-VSP activation, we evaluated the maximal response to each stimulus as well as the time required for PI(4,5)P₂ depletion (i.e. sensor translocation) and the time required for PI(4,5)P₂ recovery after cessation of the stimulus. Activation of all three channel types resulted in robust PI(4,5)P₂ depletion. Specifically, Ci-VSP activation induced by TRPV1 and ChR2 was slightly, but not significantly, stronger (sensor translocation 1.63 ± 0.09 and 1.65 ± 0.064 fold, respectively), compared to the KCNQ4-mediated response (1.51 ± 0.04 fold

increase; Fig. 3.13A). The fastest response (Fig. 3.13B) was observed using Chr2 ($t_{1/2} = 4.35 \pm 0.42s$, followed by KCNQ4 ($t_{1/2} = 18.2 \pm 1.75s$) and TRPV1 ($t_{1/2} = 25.02 \pm 3.73s$). For the recovery after stimulation, $t_{1/2}$ was $12.37 \pm 1.24s$ for Chr2, $19.92 \pm 2.73s$ for KCNQ4 and $27.89 \pm 3.05s$ for TRPV1 (Fig. 3.13C).

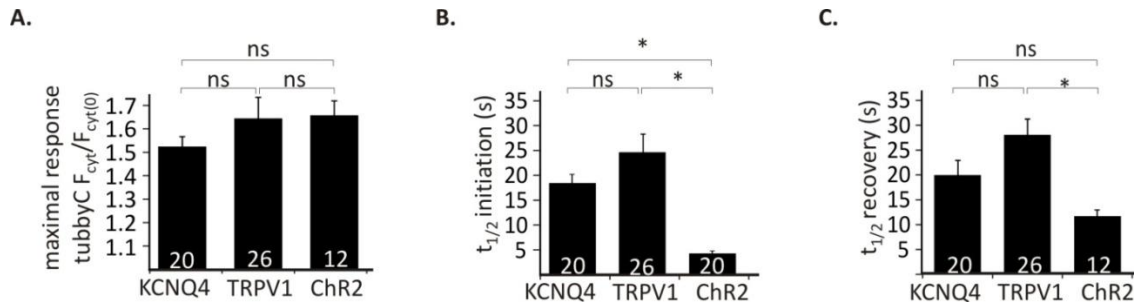


Figure 3.13: Comparison of the three depolarization methods in HEK cells cotransfected with Ci-VSP, tubbyC and one of the different channels. **A:** Bars representing the maximal response observed by overexpression of KCNQ4, TRPV1 and Chr2. For KCNQ4 we used the tubbyC translocation value from experiments as in graph Fig. 3.12C, for TRPV1 from graph Fig. 3.12E and for Chr2 the maximal value from the blue light activation in graph Fig. 3.12H. **B:** Bars representing $t_{1/2}$ of initiation, meaning the time required to reach 50% of the maximal response, for the three channels, calculated from data summarized in Fig. 3.12C, Fig.3.12E, and Fig.3.12I respectively. **C:** Bars showing $t_{1/2}$ of recovery, the time required for 50% recovery to baseline. Numbers in columns represent the number of cells.

3.2.2 Monitoring Ci-VSP activity without imaging

The above method for monitoring PI depletion is based on the translocation of PI sensors between cytosol and plasma membrane. Detection of translocation requires imaging-based experiments with subcellular resolution, usually involving confocal microscopy (Murata and Okamura, 2007) or advanced microscopy techniques such as TIRF microscopy (Halaszovich et al., 2009). Such approaches may not be optimal in many experimental settings including high-throughput assays, because experiments and analysis are based on single-cell data and thus are time-consuming, may be difficult to automatize, and involve costly and complex equipment (e.g., confocal microscope, laser, TIRF-lenses). One way to circumvent these disadvantages is to employ PI sensors based on Förster resonance energy transfer (FRET).

Previously, pleckstrin homology (PH) domains of phospholipase C δ_1 (PLC δ_1 -PH) fused to CFP and YFP have been used as FRET probes to detect PI(4,5)P₂ concentration dynamics (Várnai and Balla, 1998; Falkenburger et al., 2010b; Hertel et al., 2011); dissociation of the domains into the cytosol increases their distance, thus reducing FRET between both fluorophores (Fig. 3.14A). As shown in figure 3.14B and C, activation of Ci-VSP with capsaicin in cells coexpressing TRPV1, PLC δ_1 -PH-CFP and PLC δ_1 -PH-YFP induced synchronous increase in CFP signal and a decrease in the FRET efficiency. Here, we used photodiodes to measure both CFP and YFP fluorescence emission, demonstrating that the FRET-based approach eliminates the need for microscopic spatial separation of membrane-bound and cytosolic fluorescence.

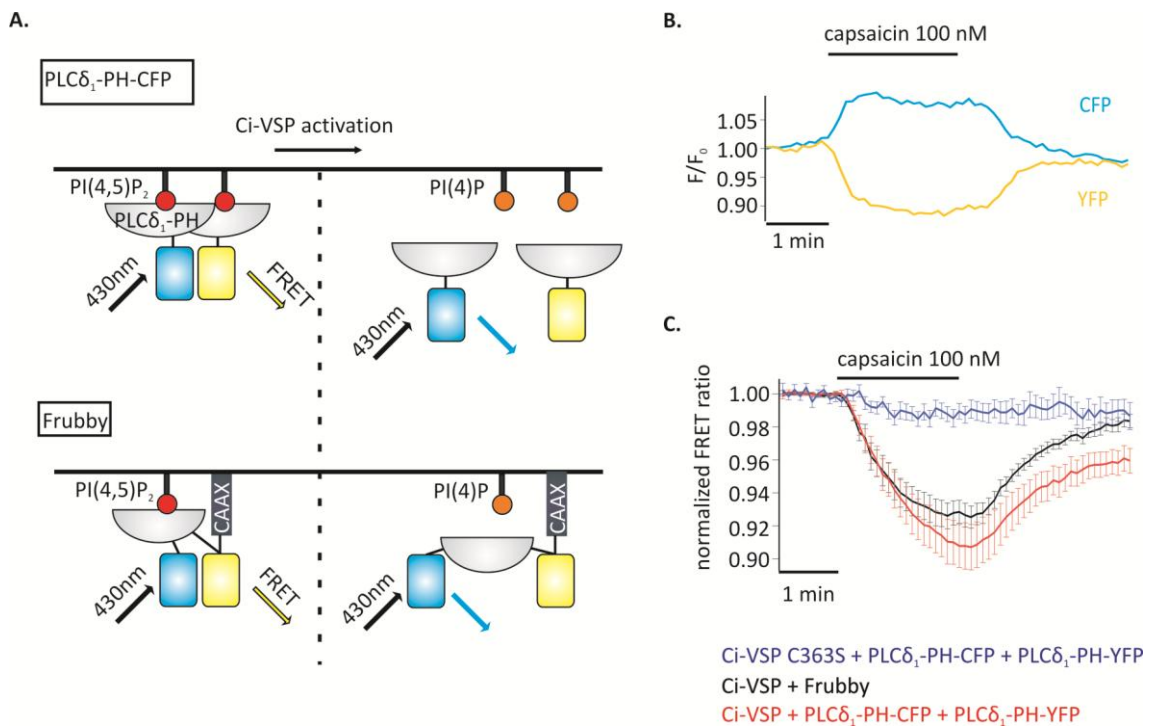


Figure 3.14: FRET sensors to monitor Ci-VSP activation. **A:** Schematic representation of two different FRET sensors used to monitor Ci-VSP activity using photometry. PLC δ_1 -PH-CFP and PLC δ_1 -PH-YFP are located at the membrane before Ci-VSP activation and act as FRET donor and acceptor, respectively. FRET is disturbed when the sensors translocate to the cytoplasm after activation of Ci-VSP. Frubby is a construct that allows for intramolecular FRET and as shown in the schema it is held at the plasma membrane via a CaaX motif. **B:** Representative trace of fluorescence signal from a cell expressing Ci-VSP, TRPV1 channel, PLC δ_1 -PH-CFP and PLC δ_1 -PH-YFP. Treatment with capsaicin results in an increase of CFP and a decrease of FRET signal. **C:** FRET ratio traces of the two FRET sensor systems. Both the PLC δ_1 -PH-CFP and PLC δ_1 -PH-YFP

system ($e=15$) and frubby ($e=13$) show a robust decrease of FRET ratio. No decrease in FRET is observed when the catalytically dead mutant Ci-VSP C363S ($e=6$) is used.

We further sought to improve this approach, because consistency and reliability of this method may suffer from variable expression stoichiometry of both PH domains and from changes in fluorescence intensity resulting from sensor translocation. We therefore additionally used an intramolecular FRET sensor where CFP and YFP coexist in a single molecule. Such a sensor, based on PLC δ_1 -PH and anchored to the PM via a CAAX-box has been developed previously and termed Pippi-PI(4,5)P $_2$ (Yoshizaki et al., 2007). However, dual sensitivity of the PLC δ_1 -PH sensor domain to both PI(4,5)P $_2$ and IP $_3$ may be a problem under some experimental conditions (Várnai and Balla, 2006; Szentpetery et al., 2009). In contrast, tubbyC combines insensitivity to IP $_3$ release (Quinn et al., 2008) with suitable sensitivity to changes in PI(4,5)P $_2$ levels as shown previously (Halaszovich et al., 2009) and in figure 3.12. Thus, our laboratory colleague Dr. Daniela Schreiber designed and constructed the “frubby” sensor (Fig. 3.14A). In frubby the PLC δ_1 -PH domain of the original Pippi-PI(4,5)P $_2$ sensor (Yoshizaki et al., 2007) was replaced by tubbyC as the PI(4,5)P $_2$ -binding domain. We went on to combine detection of PI(4,5)P $_2$ changes using frubby with activation of Ci-VSP by TRPV1. As shown in figure 3.14C, application of capsaicin to cells coexpressing frubby, Ci-VSP and TRPV1 induced a strong FRET ratio change. Notably, signal amplitude was similar, but signal variability was smaller and reversibility was more complete compared to the bi-molecular FRET sensor (Fig. 3.14C).

In conclusion, the combination of ligand-controlled activation of Ci-VSP together with FRET detection using the frubby sensor allowed for the temporally precise depletion of PI(4,5)P $_2$ in intact cells and concomitant monitoring of PI(4,5)P $_2$ changes without the need for single-cell imaging.

3.2.3 PTEN_{CIV} chimera for functional analysis of the tumor suppressor

PTEN

Similarly to the approach we used for Ci-VSP, we attempted to activate PTEN_{CIV} without electrophysiological methods and compare the phosphatase activity of different PTEN mutants.

First we aimed to optimize the method by selecting the appropriate channel and sensor that would provide the most robust responses. We selected TRPV1 for activation of PTEN_{CIV} for three reasons. First, it presented a more robust response compared to the KCNQ4 as shown in figure 3.15A and 3.15B. Second, application of high extracellular K⁺ concentrations interfered with some GFP-tagged biosensors, leading to a decrease in the fluorescent signal (Fig. 3.15B). This decrease does not represent translocation of the sensors, as fluorescence decrease was even observed when free GFP was cotransfected, instead of a sensor (Fig. 3.15C). As shown in figure 3.15D, the PI(4,5)P₂ sensor tubbyC-GFP showed stronger membrane association compared to PI(3,4,5)P₃ sensors Akt-PH-GFP, Btk-PH-GFP, and GRP1-PH-GFP. Since we recorded the fluorescence signal from the interior of the cell, it is possible that the fluorescence decrease observed in panels B and C would be more pronounced with those domains that show higher cytosolic fluorescence under basal conditions. Vice-versa, in previous experiments using tubbyC (Fig. 3.12C), a sensor that is strongly localized at the membrane, this fluorescence decrease was not observed. The third reason to select TRPV1 for these experiments was that we could not use ChR2 because activation of ChR2 with blue light is incompatible with GFP-tagged sensors for PI(3,4,5)P₃.

Since PTEN is a PI(3,4)P₂/PI(3,4,5)P₃ 3-phosphatase, we also tested various sensor domains that specifically bind to these 3-phosphorylated PIs for their suitability to quantitatively assess activity of PTEN_{CIV}. Akt-PH-GFP and Btk-PH-GFP showed larger responses than GRP1-PH-GFP, as shown in figure 3.15A. Because response kinetics were faster for Akt-PH than for Btk-PH we chose Akt-PH as the most suitable sensor for subsequent experiments.

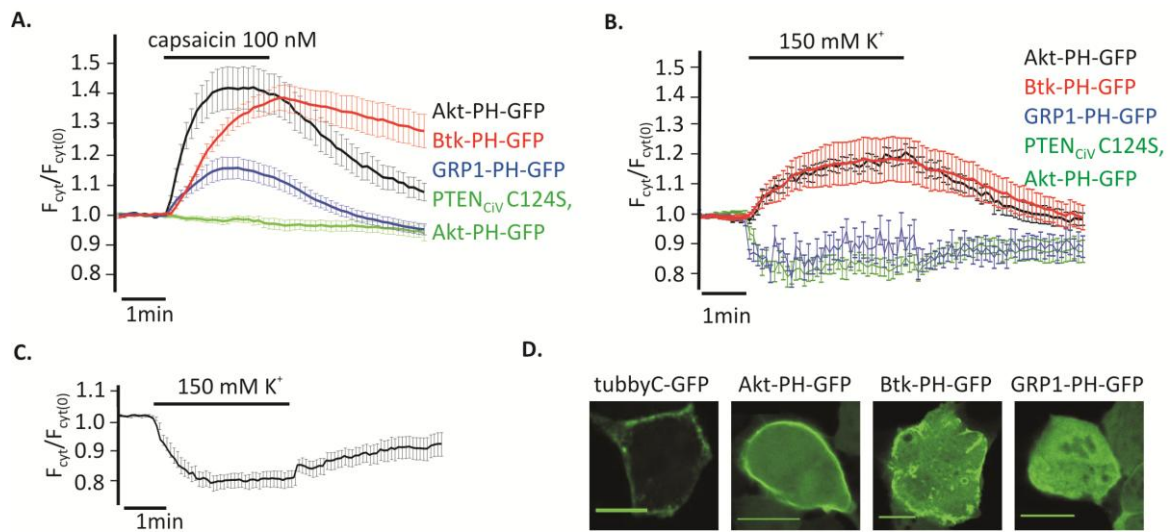


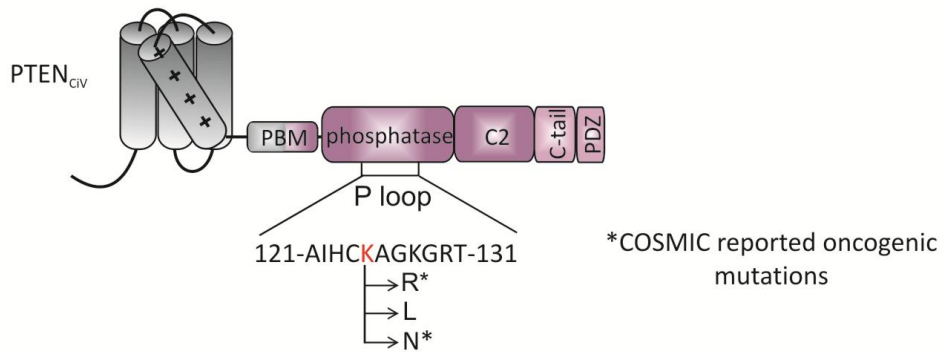
Figure 3.15: Selection of a suitable channel and sensor for studying PTEN_{CIV}. **A:** Fluorescence traces resulting from TRPV1-mediated membrane depolarization. Cells expressing PTEN_{CIV} and TRPV1 channel were used to compare the different PI(3,4,5)P₃ sensors Btk-PH-GFP (n=36, e=26), Akt-PH-GFP (n=31, e=16) and GRP1-PH-GFP (n=19, e=14). Akt-PH and Btk-PH presented the biggest responses. The green trace represents cells coexpressing the catalytically dead PTEN_{CIV} C124S, TRPV1 and Akt-PH-GFP. No effect was observed with the PTEN_{CIV} C124S mutant (n=14, e=7). **B:** Fluorescence traces resulting from KCNQ4-mediated membrane depolarization. Cells cotransfected with KCNQ4, PTEN_{CIV} and Akt-PH (n=34, e=12) or Btk-PH (n=15, e=12) present an increase of the fluorescence signal upon application of 150 mM K⁺. In contrast, application of K⁺ caused a decrease in the signal in control experiments with cells cotransfected with KCNQ4, PTEN_{CIV} C124S, Akt-PH (n=15, e=15), or in cells cotransfected with KCNQ4, PTEN_{CIV} and GRP1-PH-GFP, a PI(3,4,5)P₃ sensor with low membrane affinity (n=14, e=8). **C:** Control experiment where free GFP was coexpressed with PTEN_{CIV} and KCNQ4. The cytoplasmic fluorescence signal also decreased upon K⁺ application. This implies that the decreases seen in panel B is most likely not due to an actual sensor translocation (n=22, e=11). **D:** Confocal images of HEK cells expressing different PI sensors. The PI(4,5)P₂ sensor tubbyC-GFP is strongly located to the membrane compared to PI(3,4,5)P₃ sensors Akt-PH-GFP, Btk-PH-GFP, and GRP1-PH-GFP. Scale bar 15 μm.

Having optimized the method in terms of channel and PI sensor, we then assessed its usefulness by examining the effect of mutations on the catalytic activity of PTEN. To this end, we focused on Lysine 125, located in the catalytic pocket of the protein (Fig. 3.16A). PTEN mutations at this position are frequently found in cancer, according to COSMIC.

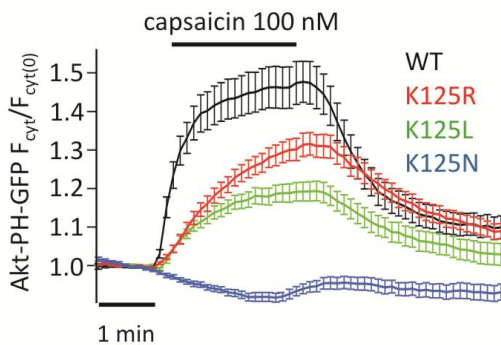
In addition to oncogenic K125R and K125N, we also analyzed K125L because all three PTEN mutants were previously examined with a yeast survival model (Rodríguez-Escudero et al., 2011), thus allowing for direct comparison of methods. When challenged with capsaicin-triggered depolarization, all three mutants showed impaired phosphatase activity compared to “wildtype”, PTEN_{CIV} (Fig. 3.16B). K125R and K125L presented significantly reduced enzymatic activity, yielding maximum sensor translocation of $61.17 \pm 5.48 \%$ and $40.43 \pm 5.11 \%$, respectively, relative to “wildtype” PTEN_{CIV} activity, while the K125N mutation resulted in a complete loss of enzymatic function (Fig. 3.16C).

This approach expands and simplifies the study of PTEN mutations as presented in the section 3.1.2, where activation and thereby study of PTEN_{CIV} required patch clamping experiments.

A.



B.



C.

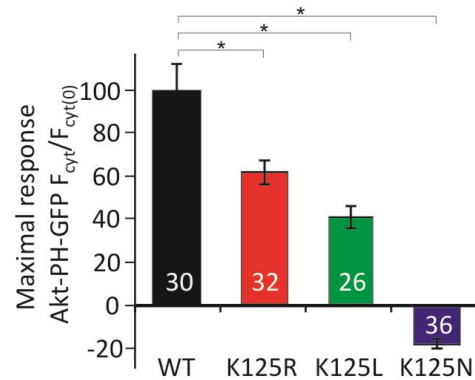


Figure 3.16: Analyzing PTEN mutations using PTEN_{CIV} and TRPV1 mediated membrane depolarization. A: Schematic representation of PTEN_{CIV}. Point mutations were introduced at K125 located in the P-loop of the catalytic domain. Asterisks mark oncogenic mutations as reported at COSMIC database (<http://cancer.sanger.ac.uk/cancergenome/projects/cosmic/>).

B: Time series traces of Akt-PH-GFP translocation upon activation with capsaicin in cells coexpressing TRPV1 channel and WT or mutated PTEN_{CIV}. **C:** Mean of Akt-PH-GFP translocation calculated for the last 30 seconds of capsaicin application, normalized to the average response measured with WT PTEN_{CIV}. Numbers in columns represent the number of cells. Statistically significant difference between WT and mutants is marked with *.

3.2.4 PTEN_{CIV} can be exploited to test PTEN inhibitors

Bisperoxovanadium (bpV) compounds are specific PTEN inhibitors and have been widely used to assess the role of PTEN in cellular processes (Schmid et al., 2004). They have been characterized using *in vitro* phosphatase assays and Western blot analyses of the phosphorylation of AKT, a downstream target of the PTEN pathway. We considered these compounds as a useful example for exploring the potency of the PTEN_{CIV}/live-cell approach in analyzing the effect of PTEN modulators on intact cells. We examined the effects of two compounds, bpV(HOpic) where bpV is attached to a polar functional group and bpV(phen) where bpV is attached to a neutral functional group.

TRPV1 was used to activate PTEN_{CIV} as described above. Here, we measured membrane association of the PTEN activity sensor Akt-PH-GFP by TIRF microscopy. TIRF microscopy provides stable imaging particularly in experiments where longer incubations are required.

First, cells were incubated with either bpV compound overnight and throughout the experiment. As shown in figure 3.17A, both compounds inhibited PTEN activity in a dose-dependent manner. Nearly complete inhibition was observed with 10 μ M of bpV(phen) or bpV(HOpic). Inhibition was partially reversible when cells that were incubated overnight with 10 μ M of bpV(phen) were washed and incubated with 5mM of the reducing agent DTT for 3 hours.

To investigate the time course of the inhibition, which is less easily addressed by conventional biochemical methods, we monitored the same cells before and after application of inhibitors. Cells responsive to a first stimulation by capsaicin were incubated for 30 minutes with 200 μ M bpV(phen). These cells did not respond to a second application of capsaicin indicating the inhibition of PTEN_{CIV} (Fig. 3.17B). Similarly, 30 minutes application of 200 μ M of bpV(HOpic) greatly decreased the

phosphatase activity (Fig. 3.17C). Control experiments were performed where no inhibitor was applied between subsequent capsaicin treatments (Fig. 3.17D). In that case, the second response -although decreased- remained pronounced. This decreased response might be explained by incomplete recovery of PI(3,4,5)P₃ levels.

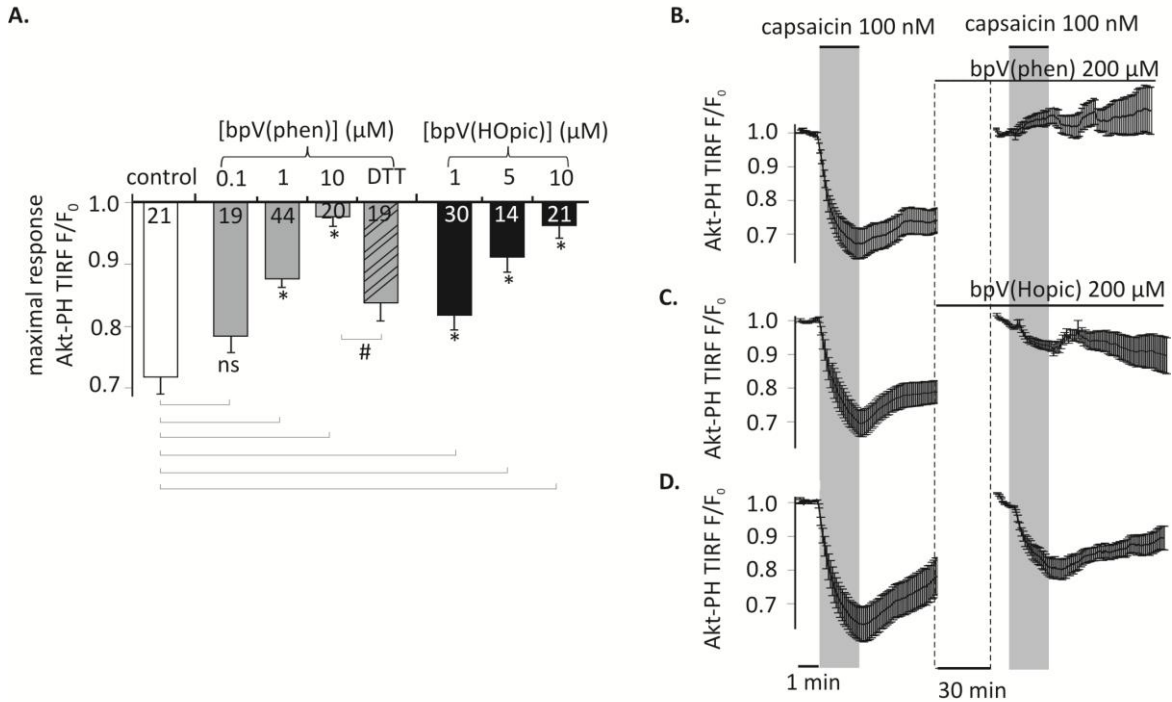


Figure 3.17: PTEN_{CIV} is inhibited by bisperoxovanadate compounds. **A:** Bars representing the effect of overnight incubation of bisperoxovanadate compounds on PTEN_{CIV} activity. Fluorescence intensity was acquired with TIRF microscopy from HEK cells expressing PTEN_{CIV}, TRPV1 channel and Akt-PH-GFP. Decrease in the fluorescence signal recorded from the membrane is observed upon capsaicin application. Cells were treated with different concentrations of the PTEN inhibitors bpV(phen) or bpV(Hopic). Cells that after an overnight incubation with 10 μM bpV(phen) were washed out and incubated for 3 hours with 5 mM of the reducing agent DTT showed a partial recovery of phosphatase activity. **B-D:** Graphs demonstrating the effect of the inhibitors in real time. **B:** HEK cells that had initially responded to a 100 nM capsaicin activation were incubated for 30 minutes with 200 μM of the inhibitors bpV(phen). After the 30 minutes incubation they presented no response to a second capsaicin application (n=11, e=4). **C:** Application of the inhibitor bpV(Hopic) also impairs PTEN_{CIV} activity (n=10, e=4). **D:** Graph showing a control experiment where no inhibitor was applied between the two capsaicin applications (n=9, e=3). Statistically significant difference between control and treated samples is marked with *, while the # sign indicates significant difference between the 10 μM bpV(phen) and the DTT treated samples. Numbers in columns represent the number of cells.

The much lower efficacy of bpV in acute application when compared to overnight incubation may indicate that permeation into the cell membrane is slow. To examine the inhibitors without the above limitation, we performed patch clamp experiments where bpV compounds were applied intracellularly through the patch pipette (Fig. 3.18A). PTEN_{CIV} was activated with a voltage jump from -60 mV to +80 mV for 30 seconds. Complete inhibition occurred at 10 μ M of bpV(phen) and bpV(Hopic) (Fig. 3.18C,D), similarly to our previous observations with overnight incubations. Patch clamp experiments also allowed us to record sensing currents of PTEN_{CIV}. We saw no change in the sensing currents, which confirms that the inhibitor acts specifically on the phosphatase domain and does not impair the VSD function (Fig. 3.18B). In conclusion, when the inhibitor was applied intracellularly, the inhibitory concentrations were similar to the concentrations required with overnight incubation, indicating that the peroxyvanadate compounds permeate slowly through the cell membrane.

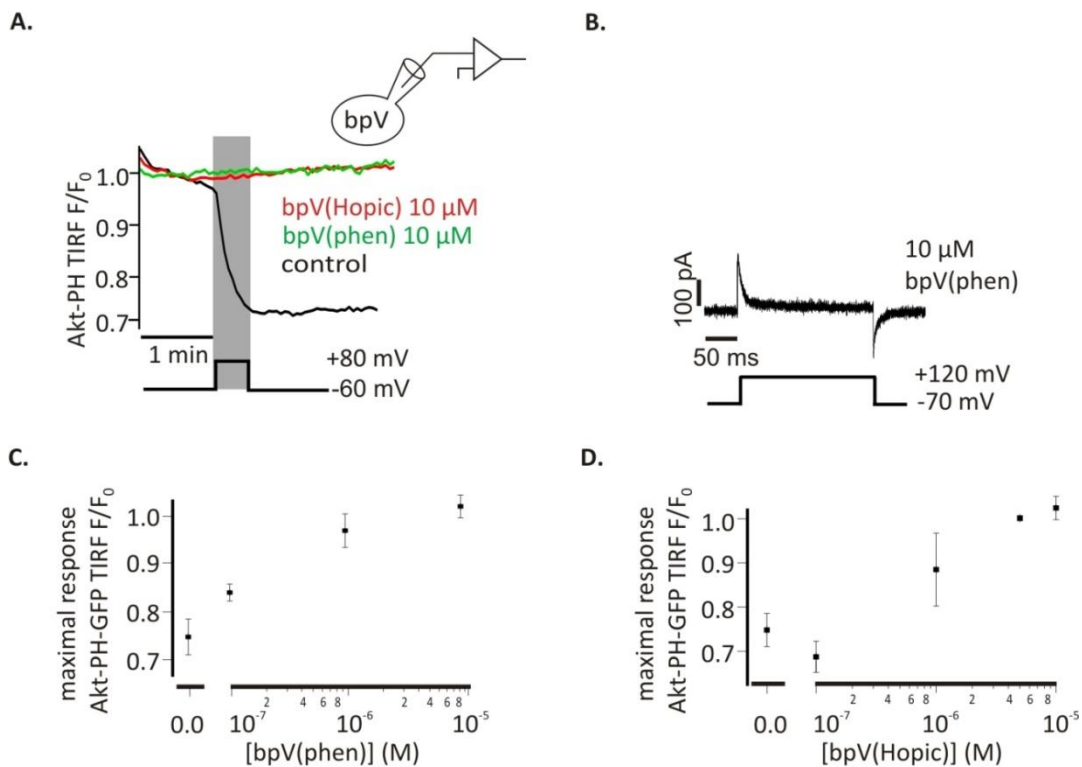


Figure 3.18: bpV(phen) and bpV(Hopic) abolish PTEN_{CIV} activity at micromolar concentrations when applied intracellularly. **A:** Representative recordings from patch clamped CHO cells expressing PTEN_{CIV} and Akt-PH-GFP. 10 μ M of inhibitor in the pipette completely abolish

PTEN_{CIV} phosphatase activity when PTEN_{CIV} was activated with a voltage jump from -60 mV to +80 mV for 30 seconds. **B**: Sensing current recorded at +120mV from a holding potential of -70 mV from a cell where 10 μM of bpV(phen) was applied through the patching pipette. **C and D**: Dose response curve for bpV(phen) and bpV(Hopic) derived from experiments as in panel A.

3.2.5 PTEN_{CIV} activation allows for rapid control of PI3K downstream pathways

The major role of PTEN is to antagonize the phosphatidylinositol 3-kinase (PI3K) signaling pathway. This pathway is controlled by the serine-threonine protein kinase AKT which is recruited and activated by plasma membrane PI(3,4,5)P₃ and in turn regulates a plethora of downstream targets through a cascade of protein kinases (Brazil et al., 2004). A simplified schematic of the PI3K signaling pathway is shown in figures 1.5 and 3.19A.

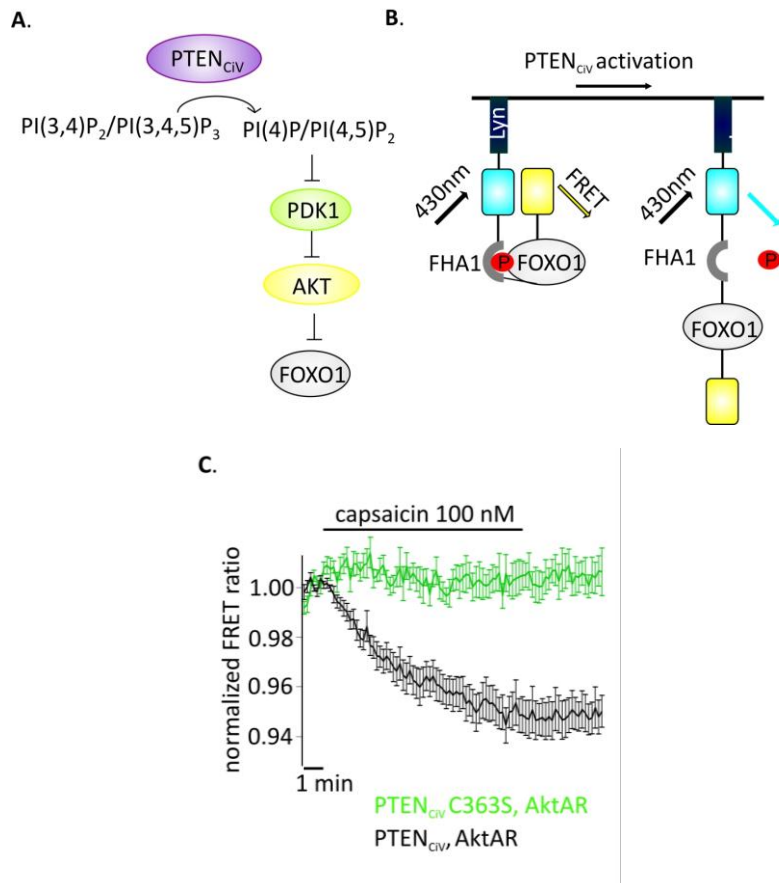


Figure 3.19: Activation of PTEN_{CIV} leads to rapid dephosphorylation of FOXO1. **A**: PTEN_{CIV} activation decreases PI(3,4)P₂/PI(3,4,5)P₃ levels which results in AKT's displacement from the

plasma membrane. This displacement prevents the phosphorylation and activation of AKT by PDK1. AKT is then unable to phosphorylate downstream targets like FOXO1. **B:** Schematic representation of the AKT activation reporter, AktAR. FOXO1 at the phosphorylated state dimerizes with the Forkhead associated (FHA) domain and results in approach of the fluorophores. Activation of PTEN_{CIV} should disrupt this interaction. **C:** FRET ratio traces of cells expressing TRPV1, PTEN_{CIV} and AktAR. Activation of PTEN_{CIV} with 100 nM of capsaicin for 10 minutes results in a decrease of the FRET signal, indicating the rapid dephosphorylation of FOXO1 (n=11, e=4 for PTEN_{CIV}; n=9, e=3 for PTEN_{CIV} C124S). FRET experiments performed by V. Thallmair.

We wondered if our method to rapidly change PTEN activity might have the potential to interrogate the dynamics of PI3K signaling. To assess the effect of PTEN_{CIV} on downstream targets of the AKT signaling pathway we utilized the AKT activity reporter, AktAR, described by (Gao and Zhang, 2008). AktAR is a membrane-anchored FRET sensor to monitor the kinase activity of AKT that is composed of part of the AKT-recognition sequence of FOXO1 and a forkhead-associated domain (FHA1). AKT-dependent phosphorylation of FOXO1 leads to dimerization of the two domains and an increase in the FRET signal, i.e. the FRET ratio directly correlates to the kinase activity of AKT (Fig. 3.19B). In cells coexpressing TRPV1, PTEN_{CIV} and AktAR, application of capsaicin for 10 minutes indeed led to a decrease of the FRET signal indicating decreased AKT activity. In contrast, no decrease was observed when catalytically-dead PTEN_{CIV} C124S was coexpressed (Fig. 3.19C). In conclusion ligand-induced activation of PTEN_{CIV} does not only allow to manipulate PI(3,4,5)P₃ at the plasma membrane but also to control and analyze the downstream signaling cascade including phosphorylation of AKT substrates in intact living cells.

4 Discussion

4.1 Functional characterization of VSPs

4.1.1 Generation of chimera for targeting hVSP1 to the membrane

Although our understanding about non-mammalian VSPs has substantially increased over the last decade, the function of the mammalian VSPs including their substrate specificity remained mostly unknown. The study of human VSPs has been proven particularly challenging because of specific characteristics of these proteins: in heterologous expression systems hVSP1 is shown to be catalytically active *in vitro* without being located at the plasma membrane, while hVSP2 (the isoform hVSP2-3) localizes at the membrane but demonstrates no phosphatase activity *in vitro* (Chen et al., 1999; Walker et al., 2001; Tapparel et al., 2003; Halaszovich et al., 2012).

This localization of hVSP1 in intracellular membranes in our expression system had restricted us so far from further electrophysiological investigation of this protein. Of note, in native tissue hVSP1 is found in spermatocytes, brain and stomach but its subcellular localization is unclear (Walker et al., 2001). It seems possible that hVSPs localize and operate in these compartments but in this case they might be activated by other mechanisms, speculatively pH, since voltage regulation in Golgi and ER is unlikely. It remains therefore ambiguous whether the lack of plasma membrane localization is an artifact of the heterologous expression or it resembles the natural location of the protein.

We sought for a way to target hVSP1 in the plasma membrane by maintaining its original structure as intact as possible. Exchange of the N-terminus or the entire voltage sensor of hVSP1 with the membrane targeted hVSP2-3 did not result in plasma membrane localization. Only replacement of the entire voltage sensor with the Ci-VSP resulted in plasma membrane localization and voltage activation. To further understand the mechanisms of membrane localization of VSPs, we truncated Ci-VSP, hVSP1 and hVSP2 right after the linker domain, generating therefore proteins that only consist of the voltage sensor domain. Interestingly, all truncated proteins presented

plasma membrane localization, with hVSP1-VSD being characterized by a clustered distribution in the membrane (data not shown). This finding indicates that all VSDs alone have the potential to reach the membrane but some putative ER or Golgi signal located within the phosphatase domain might restrain hVSP1 in these compartments. It is therefore possible that two opposing forces within hVSP1 decide the destination of the protein. This might explain why the hVSP1_{CIV} chimera presents membrane localization and activation but considerably weaker than Ci-VSP.

An interesting observation is that even with hVSPs that demonstrated membrane localization, such as hVSP2-3 and the truncated hVSP1, we detected no sensing currents. This raises the question why the voltage sensor of hVSPs, despite its high sequence similarity to non-mammalian VSPs, remains inactive. We performed a series of experiments to address this question without however succeeding so far. We sought for a residue in the hVSP1 voltage sensor that could potentially account for this loss of electrical activity. The strategy we followed was to exchange the charged residues (as they are shown to be crucial for the sensing) of the Dr-VSP's voltage sensor domain to the corresponding residues of hVSP2 and expect for a loss of the voltage sensor's activity. Nonetheless, all these mutated proteins retained their voltage sensitivity, suggesting that any other residue(s) could inhibit the voltage sensor activation. Therefore, further investigation is required to understand the cause of the loss of electrical activity in hVSPs.

An alternative suggestion about the role of hVSPs has been made by Sutton et al. (Sutton et al., 2012). In that work chimeric proteins were created by swapping the S3-S4 segments of the VSD of Dr-VSP with the corresponding segments of hVSP1 or hVSP2. These chimeras acted as voltage-sensitive proton channels, highlighting the possibility that mammalian VSPs evolved to have a surprisingly different function. However, we never detected any proton currents, even with constructs that strongly localize at the plasma membrane, such as hVSP2-3.

4.1.2 hVSP1 is a 5-phosphatase in living cells

The present data of the enzymatic activity of hVSP1_{CIV} chimera indicated that it acts as a 5-phosphatase which is inconsistent with previous *in vitro* phosphatase activity data that described the protein as a 3-phosphatase (Walker et al., 2001). Our data were acquired in living mammalian cells, and more closely represent the physiological environment of the native hVSP1 in comparison to the *in vitro* phosphatase data that were acquired using the isolated phosphatase domain and soluble substrates.

Moreover, it seems unlikely that the attachment of a heterologous voltage sensor domain could change the phosphatase specificity from the 3 to the 5 position. There is no obvious mechanism by which the VSD could interfere with the substrate specificity of the phosphatase. The creation of PTEN_{CIV} chimera further supports this idea; attachment of VSD in the PTEN did not alter its specificity as a 3- phosphatase.

Lastly, the P-loop of the catalytic center of hVSP1 containing a glycine in the HCX₅R motive (Fig. 1.6B) is identical to Ci-VSP, XI-VSP and Dr-VSP which are all 5-phosphatases. On the other hand PTEN which acts as a 3-phosphatase comprises an alanine at the same position. Latest discoveries, part of those were mentioned in this thesis, revealed the importance of this position in the determination of the substrate specificity. This finding provides further support to the data presenting hVSP1 as a 5-phosphatase.

4.1.3 Novel oncogenic gain-of-function PTEN mutant

Next we demonstrated the usefulness of the chimeric PTEN_{CIV} for the functional characterization of a patient specific somatic PTEN mutation. We showed that mutation of the alanine 126 to glycine located in the P-loop of catalytic center resulted in change of the substrate specificity of PTEN; A126G mutant acts as a 5-instead of 3-phosphatase of PI(3,4,5)P₃. Such a gain of function mutation would lead to generation of PI(3,4)P₂, a PI that is strongly involved in the regulation of cell migration and possibly tumor invasion (Oikawa and Takenawa, 2009). To show the relevance of A126G mutation in cell migration, our collaborators performed a scratch wound healing assay in a PTEN-null prostate cancer cell line heterologously expressing WT

PTEN, the catalytically dead mutant C124S or the A126G mutant. Indeed, they saw significantly increased cell migration at the A126G mutant compared to the catalytically dead mutant (Costa et al., 2015).

The above findings demonstrate that not all PTEN mutations lead to the same deficient phenotype and that PTEN can have a more complex impact on the PI3K signaling than it was previously assumed. This highlights the importance of the identification of the PTEN mutation in a patient-specific manner, since treatment might vary based on the patients genotype. PTEN_{CIV} proved to be a powerful tool for the study of PTEN mutants providing information about the enzymatic activity of the protein.

4.1.4 Does pH affect the catalytic activity of VSPs?

To explore additional signals that regulate VSPs, we tested the effect of pH on the VSP activity. We performed patch clamping experiments with Dr-VSP and the PI(4,5)P₂ sensor PLCδ₁-PH-GFP, using intracellular solution of different pH values (pH_{int}). We saw that acidic intracellular pH leads to an increased PI(4,5)P₂ depletion.

However, the pH dependence of the depletion is not necessarily due to a direct effect of the pH on the catalytic activity of Ci-VSP. pH can affect several other parameters, such as the sensing mechanism of VSPs, the kinetics of kinase activity, the binding affinity of the PI sensor or PIs themselves. In this part we discuss the possible involvement of each of them in the pH dependence of PI(4,5)P₂ depletion.

To estimate the effect of pH on the gating of VSPs we measured the “On” sensing currents. We observed an 8.48 mV leftward shift of the V_{1/2} at pH_{int} 6.5 compared to pH_{int} 7.5 and a 0.35 mV rightward shift of the V_{1/2} at pH_{int} 8.5 compared to pH_{int} 7.5. These differences however were not statistically significant. It is important to be mentioned that these sensing currents are relatively small in amplitude (in the range of hundreds of pA) and it is possible that small shifts in the voltage dependence can be difficult to detect.

Phosphoinositide levels in the living cell are rigidly regulated by the simultaneous action of phosphatases and kinases. Therefore the decrease in the PI(4,5)P₂ levels observed might be attributed to the slowdown of the kinases' activity. We were able to

exclude that 5-kinases' activity was affected by the changes in the intracellular pH, by estimating the time constant of the PI(4,5)P₂ resynthesis. These time constants were not significantly different among different intracellular pH, indicating that the kinetics of the PI(4,5)P₂ resynthesis remain stable.

An alternative explanation for the pH sensitivity observed is that acidic pH could decrease the binding affinity of our PI(4,5)P₂ sensor PLCδ₁-PH resulting therefore in a stronger dissociation from the plasma membrane. To our knowledge this has not been investigated previously. To exclude this possibility, we chose the pH insensible Kir2.1 channel as a PI(4,5)P₂ sensor to monitor Ci-VSP activity and observed that the pH sensitivity of the PI(4,5)P₂ depletion remained.

Alterations of intracellular pH would also change the protonation state and overall charge of the phosphoinositide itself. It was estimated that decrease of the pH value caused a decrease of the overall negative charge of the PIs (Kooijman et al., 2009). If we consider that electrostatic forces of the positively charged catalytic domain of Ci-VSP with the negatively charged PI contribute to their binding, then it is possible that decrease of PI's charge could affect this interaction. It is however difficult to estimate if this charge change would favor or hamper the catalysis. In any case, if changes in the protonation of PIs is the reason for the pH dependence, no amino acid residues within the VSP will be identifiable as causative for the pH dependence.

In conclusion, we showed for the first time that PI(4,5)P₂ depletion by VSPs is sensitive to pH changes. Until now, the molecular mechanism by which acidification results in increased PI(4,5)P₂ depletion remains unknown. Although a number of parameters have been excluded, it is an open question if the protonation of VSP itself is responsible for the effect.

4.1.5 Interaction between C363 and C310 possibly underlies the inhibition of Ci-VSP by oxidation.

Given the evidence that Ci-VSP and PTEN are regulated by oxidation (Matsuda et al., 2011; Lee et al., 2002), here we systematically studied the effect of different redox agents on Ci-VSP in living cells. We found that only the strong oxidant H₂O₂ inhibits the

protein's phosphatase activity. Moreover we examined the involvement of the amino acid C310 in the process, which based on structural data is considered to form a disulfide bond with the C363 inhibiting thereby the catalytic activity of Ci-VSP. Substitution of C310 to serine resulted in a protein that was less sensitive to inhibition by H_2O_2 . A potential explanation for this remaining degree of inhibition is that oxidation can affect proteins in several ways in addition to formation of disulfide bonds. For example, oxidation of cysteine can lead to thiyl radicals and mixed disulfides (e.g. with glutathione), while methionine residues can be oxidized to methionine sulfoxate (Shacter, 2000). These modifications could, theoretically, as well decrease the catalytic activity of Ci-VSP.

To summarize our findings regarding the regulation of VSPs by pH and redox state, we saw that acidification acts as a positive regulator of VSPs, increasing the PI(4,5)P₂ depletion, whereas strong oxidation and alkalization have a negative effect on the activity of VSPs (Fig. 4.1).

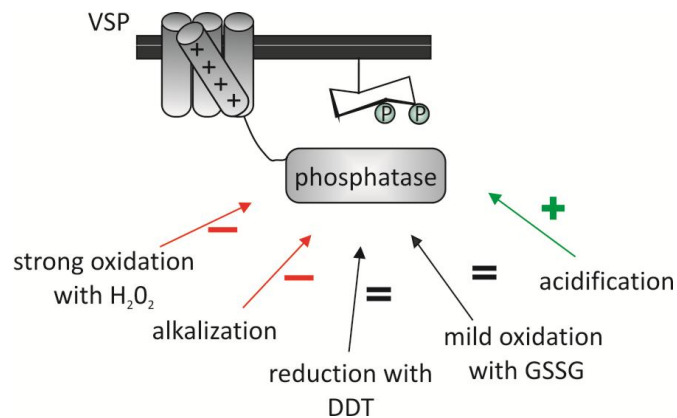


Figure 4.1: Summary of the regulation of VSPs by pH and oxidizing agents. Oxidation by H_2O_2 and alkalization negatively regulate the PI(4,5)P₂ depletion, in contrast to intracellular acidification which results in increased PI(4,5)P₂ depletion.

4.2 Controlling VSPs and PTEN_{CIV} without electrophysiology

As we have demonstrated so far, activation of VSPs in living cells requires the use of whole-cell patch clamping for the control of membrane potential. Since electrophysiological methods are not available to many laboratories, either because of

lack of equipment or electrophysiological expertise, we sought to find a simpler method for membrane depolarization.

We developed a fast, simple, reversible and scalable method that can be used not only as a tool to control PI levels in living cells, but also to study the tumor suppressor PTEN. The approach is based on the well characterized Ci-VSP and the engineered phosphatase PTEN_{CiV}. Our data demonstrate that activation of overexpressed cation channels is an easy and powerful method to activate Ci-VSP or chimeric VSPs and thereby manipulate PI(4,5)P₂ and PI(3,4,5)P₃ concentrations in a temporally well-controlled manner.

4.2.1 Comparison of our method with previously described PI manipulation techniques

Widely used methods for acutely altering PI concentrations are based on the recruitment of PI metabolizing enzymes to the membrane through a dimerization strategy, triggered either by rapamycin (Suh et al., 2006; Varnai et al., 2006) or via an optogenetic approach (Idevall-Hagren et al., 2012). Compared to these methods, the main advantage of the VSP-based approach is the reversibility of PI changes with times for 50 % recovery of 12 to 28 seconds. In contrast, the rapamycin system is virtually irreversible and with the optogenetic method half-maximal recovery of PI(4,5)P₂ requires several minutes (Idevall-Hagren et al., 2012). One additional disadvantage of the optogenetic approach is that its sensitivity to blue and green light places restrictions on which fluorophores can be used for imaging/monitoring purposes. On the other hand it allows for subcellular manipulation of PI concentrations, whereas VSP activation in our system always affects the entire plasma membrane of the cell. We further note that activation of VSPs by each of the tested ion channels allowed for a graded depletion of PI(4,5)P₂. This high level of control over PI(4,5)P₂ levels may be used to compare the apparent affinity of intracellular PI(4,5)P₂ effectors in a semi-quantitative manner, as demonstrated in this laboratory earlier (Halaszovich et al., 2009).

4.2.2 Three different cation channels for induction of membrane depolarization

Each of the three classes of channels explored here activated Ci-VSP with similar efficacy. Advantages and limitations of each channel type mostly relate to the technical aspects of channel activation. Depolarization through constitutively open K^+ channels requires full exchange of bath solution to alter the K^+ concentration; in some cases, high extracellular K^+ concentrations interfered with GFP fluorescence (Fig. 3.15C). Activation of ligand gated channels does not necessarily require complete bath exchange, since the ligand can be added to the bath solution, especially when small concentrations can be used; for the TRPV1 channel used here, an agonist concentration as low as 100 nM was sufficient for maximal effect. A disadvantage of using TRPV1 is the requirement for a Ca^{2+} -free bath solution, although in many cases this will not be a severe restriction. Also, use of TRPV1 was the method showing the slowest kinetics, which is probably related to ligand permeation and binding/unbinding. Manipulations of the bath solution can be avoided altogether when the optogenetic approach using a light gated channel (ChR2) is used. Here, we achieved the fastest response times. Disadvantages of using ChR2 are that a low pH (6.5) and Ca^{2+} -free bath solution had to be used and that the spectral characteristics of ChR2 preclude the use of certain wavelengths for excitation of fluorophores. Notably, we were not able to use GFP-tagged PI-sensors.

4.2.3 Analysis of PTEN mutants and inhibitors

Beyond manipulation of $PI(4,5)P_2$ and $PI(3,4)P_2/PI(3,4,5)P_3$ levels, the availability of $PTEN_{CIV}$ considerably extends the range of useful applications of the method presented here. The role of PTEN in pathological conditions like tumors of sporadic and germline origin and ASDs is well established (Hollander et al., 2011; Varga et al., 2009; Cantley and Neel, 1999). Biochemical *in vitro* techniques or a heterologous yeast reconstitution system have usually been used to investigate the effect of mutations on protein function or to study chemical PTEN inhibitors and activators.

The method we present should provide a useful complementation to the current spectrum of methods. We note several potential advantages of this approach. First, our method proved to be more sensitive than the published yeast-based method (Rodríguez-Escudero et al., 2011), in assessing the effect of PTEN mutations (see below). Second, in the living mammalian cell, PTEN acts on its substrates in the native membrane environment, which can differ substantially from the composition of vesicles used to present the substrates or even soluble substrate analogs used in *in vitro* assays. This might affect activity or substrate specificity inferred from such experiments, as demonstrated for hVSP1 which was first described as a 3-phosphatase based on *in vitro* data (Walker et al., 2001) but performed as a 5-phosphatase in living cells. Finally, the new method is applicable to a wide range of cell types, including cell lines derived from human tumors, once heterologous expression of the molecular components (VSP and cation channel) can be achieved in that cell line.

To explore the potential of the method, we studied PTEN mutations, including known oncogenic mutations. For some of these PTEN mutations, results obtained with the PTEN_{CIV} approach were consistent with previously published findings from *in vitro* and yeast assays (Rodríguez-Escudero et al., 2011). Thus, PI(3,4,5)P₃ phosphatase activity was strongly decreased for PTEN_{CIV} K125L and abrogated for PTEN_{CIV} K125N (Fig. 3.16B,C). However, the yeast survival method previously did not detect any defect of the PTEN K125R (Rodríguez-Escudero et al., 2011), although the mutant is annotated as an oncogenic mutation. Our approach indeed detected a decrease of phosphatase activity by 40%. This finding might explain the tumorigenic effect of that mutation and also highlights the sensitivity of the VSP approach. As ASDs related mutations have been shown to decrease but not abrogate PTEN phosphatase activity (Rodríguez-Escudero et al., 2011) this high sensitivity should render our method a well-suited tool for testing ASDs and tumor associated PTEN mutations.

Similarly, the PTEN_{CIV} method enabled analysis of pharmacological manipulation of PTEN. *In vitro* and *in vivo*, bpV compounds inhibit PTEN at nanomolar concentrations with minimal cytotoxicity (Schmid et al., 2004). In that study, more indirect methods like assessing the phosphorylation state of AKT were used, whereas we directly

monitored PTEN's substrate PI(3,4,5)P₃ to determine the effect of these inhibitors in living cells. The bpV compounds have been used to study the involvement of PTEN in signaling, proliferation, apoptosis, and neurogenesis, (Band et al., 1997; Batty et al., 2007; Tian et al., 2012; Becker et al., 2013) however, higher concentrations (200 nM – 100 μM) were required. We found comparable concentrations to effectively inhibit PTEN activity in our live cell assay. Moreover, because the PTEN_{CIV} method is essentially a real-time approach in living cells, it can yield insights into the temporal cellular dynamics of PI(3,4)P₂ and PI(3,4,5)P₃ signaling that are difficult to obtain with a purely biochemical approach. As an example, we showed that down-regulation of PI(3,4,5)P₃ (and PI(3,4)P₂) concentration resulted in a surprisingly rapid switching-off of signaling by dephosphorylation of intermediates within the AKT signaling cascade, which (to our knowledge) has not been appreciated before. This finding points to a rather high activity of the protein phosphatase(s) that antagonize AKT kinase activity. In summary, this work established novel, simple to use, and broadly applicable methods that provide temporal control of VSPs. This allows for manipulation of PI levels and subsequently manipulation of their downstream targets. Moreover, using the engineered voltage sensitive enzyme PTEN_{CIV} we suggest a novel method for characterizing this critical tumor suppressor in a population of living mammalian cells, fast and ingeniously. This method complements the already used *in vitro* and non-mammalian PTEN activity assays and eases the study of this important tumor suppressor.

4.3 Outlook

In this thesis we extended our knowledge regarding several aspects of VSPs' function and regulation but many questions remain unanswered and further investigation is required to complete this work.

In the first part of this thesis we demonstrated for the first time the pH dependence of VSPs' activity but the exact mechanism by which this occurs remains unknown. We speculated that the pH sensitivity observed affects the phosphatase activity, presumably by facilitating the catalysis. However we did not succeed in identifying the

histidine that plays the role of pH sensor. Of course other amino acids may also be able to sense pH changes, because the pKa values of amino acids in solutions often differ from the pKa values in a protein environment. For example amino acids with far from the physiological pKa values such as lysine, arginine and aspartic acid have been found to determine the pH dependence of proteins (Wragg and Drickamer, 1999; Niemeyer et al., 2010). To compute the pKa values of amino acids side chains in proteins several computation methods are available, for example the FDPB-based method (*FDPB* is for Finite Difference Poisson-Boltzmann) or molecular dynamics-based methods. This could facilitate the selection of possible candidates that act as pH sensors in VSPs.

An alternative way to test the pH sensitivity of VSPs would be by *in vitro* phosphatase assays i.e. the malachite green phosphatase assay (Murata et al., 2005; Matsuda et al., 2011), where we could estimate the efficiency of the phosphatase domain of VSPs to dephosphorylate soluble PI substrates at different pH conditions. This would allow the study of the pH influence without the involvement of parameters such as the sensing, kinases and pH domain binding, reassuring that pH directly affects the phosphatase.

Another interesting question to be answered is if pH could directly activate VSPs. The data in section 3.1.3 provided evidence that pH can increase phosphatase activity during voltage activation. But can pH alone activate VSPs? This question is particularly relevant for hVSP1 which is expressed in testis and stomach, organs where voltage regulation is not straightforward. One way to test for this hypothesis would be to change in real time the intracellular pH value and simultaneous record the phosphatase activity. As shown in a study for pH sensitive TASK channels (Niemeyer et al., 2010) rapid intracellular acidification can be achieved using $\text{CO}_2\text{-HCO}_3$, while alkalization of the cell interior can be achieved with NH_4Cl^- .

In the second part of this thesis we reported the development of a novel approach for studying the tumor suppressor PTEN, in living mammalian cells and without electrophysiology. In our experiments, we were able to analyze mutations and pharmacological inhibition of PTEN in a small population of cells. However, the technique might as well be used in high through-put mutation screens and screens for novel substances with pharmacological activity towards PTEN. As shown in Figure 3.14,

the phosphatase activity of VSPs can be monitored using a FRET-based system that is independent of translocation of PI sensors, and therefore independent from image analysis by the experimenter. Accordingly, the system for PTEN_{CIV} activation combined with an optimized FRET sensor can be employed for 96-well plates with automated solution exchange and automated fluorescence detection in standard multi-plate readers.

In this work we contributed to increasing the understanding of some aspects of VSPs' function and regulation, as well as expanding their applicability as PI manipulating tools. Certainly, there is still a lot to learn about these fascinating “Janus Bifrons” (Villalba-Galea, 2012) proteins, first and foremost their physiological role in biological systems.

5 References

- Aitken, R.J., M. Paterson, H. Fisher, D.W. Buckingham, and M. van Duin. 1995. Redox regulation of tyrosine phosphorylation in human spermatozoa and its role in the control of human sperm function. *J Cell Sci.* 108 (Pt 5:2017–2025.
- Axelrod, D. 1981. Cell-substrate contacts illuminated by total internal reflection fluorescence. *J. Cell Biol.* 89:141–145. doi:10.1083/jcb.89.1.141.
- Balla, T. 2013. Phosphoinositides: tiny lipids with giant impact on cell regulation. *Physiol. Rev.* 93:1019–137. doi:10.1152/physrev.00028.2012.
- Baltz, J.M., Y. Zhao, and K.P. Phillips. 1995. Intracellular pH and its regulation during fertilization and early embryogenesis. *Theriogenology.* 44:1133–1144. doi:10.1016/0093-691X(95)00325-3.
- Band, C.J., B.I. Posner, V. Dumas, and J.O. Contreres. 1997. Early signaling events triggered by peroxovanadium [bpV(phen)] are insulin receptor kinase (IRK)-dependent: specificity of inhibition of IRK-associated protein tyrosine phosphatase(s) by bpV(phen). *Mol. Endocrinol.* 11:1899–910.
- Batty, I.H., J. van der Kaay, A. Gray, J.F. Telfer, M.J. Dixon, and C.P. Downes. 2007. The control of phosphatidylinositol 3,4-bisphosphate concentrations by activation of the Src homology 2 domain containing inositol polyphosphate 5-phosphatase 2, SHIP2. *Biochem. J.* 407:255–66. doi:10.1042/BJ20070558.
- Becker, L., J. Peterson, S. Kulkarni, and P.J. Pasricha. 2013. Ex vivo neurogenesis within enteric ganglia occurs in a PTEN dependent manner. *PLoS One.* 8:e59452. doi:10.1371/journal.pone.0059452.
- Bevans, C.G., and A.L. Harris. 1999. Regulation of connexin channels by pH: Direct action of the protonated form of taurine and other aminosulfonates. *J. Biol. Chem.* 274:3711–3719. doi:10.1074/jbc.274.6.3711.
- Bezanilla, F. 2008. How membrane proteins sense voltage. *Nat. Rev. Mol. Cell Biol.* 9:323–332. doi:10.1038/nrm2376.
- Brazil, D.P., Z.-Z. Yang, and B. a Hemmings. 2004. Advances in protein kinase B signalling: AKTion on multiple fronts. *Trends Biochem. Sci.* 29:233–42. doi:10.1016/j.tibs.2004.03.006.
- Brown, E.J., M.W. Albers, T.B. Shin, K. Ichikawa, C.T. Keith, W.S. Lane, and S.L. Schreiber. 1994. A mammalian protein targeted by G1-arresting rapamycin-receptor complex. *Nature.* 369:756–758. doi:10.1038/369756a0.
- Cantley, L.C., and B.G. Neel. 1999. New insights into tumor suppression: PTEN suppresses tumor formation by restraining the phosphoinositide 3-kinase/AKT pathway. *Proc. Natl. Acad. Sci. U. S. A.* 96:4240–5.
- Casey, J.R., S. Grinstein, and J. Orlowski. 2010. Sensors and regulators of intracellular pH. *Nat. Rev. Mol. Cell Biol.* 11:50–61. doi:10.1038/nrm2820.
- Caterina, M.J., M. a Schumacher, M. Tominaga, T. a Rosen, J.D. Levine, and D. Julius. 1997. The capsaicin receptor: a heat-activated ion channel in the pain pathway. *Nature.* 389:816–24. doi:10.1038/39807.
- Chalhoub, N., and S.J. Baker. 2009. PTEN and the PI3-kinase pathway in cancer. *Annu. Rev.*

- Pathol.* 4:127–50. doi:10.1146/annurev.pathol.4.110807.092311.
- Chambard, J.-M., and J.F. Ashmore. 2005. Regulation of the voltage-gated potassium channel KCNQ4 in the auditory pathway. *Pflugers Arch.* 450:34–44. doi:10.1007/s00424-004-1366-2.
- Chen, H., C. Rossier, M. a. Morris, H.S. Scott, a. Gos, a. Bairoch, and S.E. Antonarakis. 1999. A testis-specific gene, TPTE, encodes a putative transmembrane tyrosine phosphatase and maps to the pericentromeric region of human chromosomes 21 and 13, and to chromosomes 15, 22, and Y. *Hum. Genet.* 105:399–409. doi:10.1007/s004390051122.
- Cid, V.J., I. Rodríguez-Escudero, a Andrés-Pons, C. Romá-Mateo, a Gil, J. den Hertog, M. Molina, and R. Pulido. 2008. Assessment of PTEN tumor suppressor activity in nonmammalian models: the year of the yeast. *Oncogene.* 27:5431–42. doi:10.1038/onc.2008.240.
- Costa, H. a., M.G. Leitner, M.L. Sos, A. Mavrantoni, A. Rychkova, J.R. Johnson, B.W. Newton, M.-C. Yee, F.M. De La Vega, J.M. Ford, N.J. Krogan, K.M. Shokat, D. Oliver, C.R. Halaszovich, and C.D. Bustamante. 2015. Discovery and functional characterization of a neomorphic PTEN mutation. *Proc. Natl. Acad. Sci.* 201422504. doi:10.1073/pnas.1422504112.
- Coutinho-Budd, J.C., S.B. Snider, B.J. Fitzpatrick, J.E. Rittiner, and M.J. Zylka. 2013. Biological constraints limit the use of rapamycin-inducible FKBP12-Inp54p for depleting PIP2 in dorsal root ganglia neurons. *J. Negat. Results Biomed.* 12:13. doi:10.1186/1477-5751-12-13.
- Das, S., J.E. Dixon, and W. Cho. 2003. Membrane-binding and activation mechanism of PTEN. *Proc. Natl. Acad. Sci. U. S. A.* 100:7491–6. doi:10.1073/pnas.0932835100.
- Devereaux, K., and G. Di Paolo. 2013. PI5P migrates out of the PIP shadow. *EMBO Rep.* 14:214–5. doi:10.1038/embor.2013.2.
- Enyedi, P., and G. Czirják. 2010. Molecular background of leak K⁺ currents: two-pore domain potassium channels. *Physiol. Rev.* 90:559–605. doi:10.1152/physrev.00029.2009.
- Falkenburger, B.H., J.B. Jensen, E.J. Dickson, B.-C. Suh, and B. Hille. 2010a. Phosphoinositides: lipid regulators of membrane proteins. *J. Physiol.* 588:3179–85. doi:10.1113/jphysiol.2010.192153.
- Falkenburger, B.H., J.B. Jensen, and B. Hille. 2010b. Kinetics of PIP2 metabolism and KCNQ2/3 channel regulation studied with a voltage-sensitive phosphatase in living cells. *J. Gen. Physiol.* 135:99–114. doi:10.1085/jgp.200910345.
- Fish, K.N. 2009. Total internal reflection fluorescence (TIRF) microscopy. *Curr. Protoc. Cytom.* Chapter 12:Unit12.18. doi:10.1002/0471142956.cy1218s50.
- Gao, X., and J. Zhang. 2008. Spatiotemporal Analysis of Differential Akt Regulation in Plasma Membrane Microdomains. *Mol. Biol. Cell.* 19:4366–4373. doi:10.1091/mbc.E08.
- Garcia-Junco-Clemente, P., and P. Golshani. 2014. PTEN: A master regulator of neuronal structure, function, and plasticity. *Commun. Integr. Biol.* 7. doi:10.4161/cib.28358.
- Halaszovich, C.R., M.G. Leitner, A. Mavrantoni, A. Le, L. Frezza, A. Feuer, D.N. Schreiber, C. a Villalba-Galea, and D. Oliver. 2012. A human phospholipid phosphatase activated by a transmembrane control module. *J. Lipid Res.* 53:2266–74. doi:10.1194/jlr.M026021.
- Halaszovich, C.R., D.N. Schreiber, and D. Oliver. 2009. Ci-VSP is a depolarization-activated phosphatidylinositol-4,5-bisphosphate and phosphatidylinositol-3,4,5-trisphosphate 5'-

- phosphatase. *J. Biol. Chem.* 284:2106–13. doi:10.1074/jbc.M803543200.
- Hamill, O.P., A. Marty, E. Neher, B. Sakmann, and F.J. Sigworth. 1981. Improved patch-clamp techniques for high-resolution current recording from cells and cell-free membrane patches. *Pflügers Arch. Eur. J. Physiol.* 391:85–100. doi:10.1007/BF00656997.
- Hertel, F., A. Switalski, E. Mintert-Jancke, K. Karavassilidou, K. Bender, L. Pott, and M.-C. Kienitz. 2011. A genetically encoded tool kit for manipulating and monitoring membrane phosphatidylinositol 4,5-bisphosphate in intact cells. *PLoS One.* 6:e20855. doi:10.1371/journal.pone.0020855.
- Hobiger, K., T. Utesch, M.A. Mroginski, and T. Friedrich. 2012. Coupling of Ci-VSP modules requires a combination of structure and electrostatics within the linker. *Biophys. J.* 102:1313–22. doi:10.1016/j.bpj.2012.02.027.
- Hobiger, K., T. Utesch, M.A. Mroginski, G. Seebohm, and T. Friedrich. 2013. The Linker Pivot in Ci-VSP: The Key to Unlock Catalysis. *PLoS One.* 8. doi:10.1371/journal.pone.0070272.
- Hollander, M.C., G.M. Blumenthal, and P.A. Dennis. 2011. PTEN loss in the continuum of common cancers, rare syndromes and mouse models. *Nat. Rev. Cancer.* 11:289–301.
- Holmström, K.M., and T. Finkel. 2014. Cellular mechanisms and physiological consequences of redox-dependent signalling. *Nat. Rev. Mol. Cell Biol.* 15:411–21. doi:10.1038/nrm3801.
- Hossain, M.I., H. Iwasaki, Y. Okochi, M. Chahine, S. Higashijima, K. Nagayama, and Y. Okamura. 2008. Enzyme Domain Affects the Movement of the Voltage Sensor in Ascidian and Zebrafish Voltage-sensing Phosphatases. *J. Biol. Chem.* 283:18248–18259. doi:10.1074/jbc.M706184200.
- Idevall-Hagren, O., E.J. Dickson, B. Hille, D.K. Toomre, and P. De Camilli. 2012. Optogenetic control of phosphoinositide metabolism. *Proc. Natl. Acad. Sci. U. S. A.* 109:E2316–23. doi:10.1073/pnas.1211305109.
- Kimber, W.A., L. Trinkle-Mulcahy, P.C.F. Cheung, M. Deak, L.J. Marsden, A. Kieloch, S. Watt, R.T. Javier, A. Gray, C.P. Downes, J.M. Lucocq, and D.R. Alessi. 2002. Evidence that the tandem-pleckstrin-homology-domain-containing protein TAPP1 interacts with Ptd(3,4)P2 and the multi-PDZ-domain-containing protein MUPP1 in vivo. *Biochem. J.* 361:525–536. doi:10.1042/0264-6021:3610525.
- Klarlund, J.K., A. Guilherme, J.J. Holik, J. V Virbasius, A. Chawla, and M.P. Czech. 1997. Signaling by phosphoinositide-3,4,5-trisphosphate through proteins containing pleckstrin and Sec7 homology domains. *Science.* 275:1927–1930. doi:10.1126/science.275.5308.1927.
- Kohout, S.C., S.C. Bell, L. Liu, Q. Xu, D.L. Minor, and E.Y. Isacoff. 2010. Electrochemical coupling in the voltage-dependent phosphatase Ci-VSP. *Nat. Chem. Biol.* 6:369–75. doi:10.1038/nchembio.349.
- Kohout, S.C., M.H. Ulbrich, S.C. Bell, and E.Y. Isacoff. 2008. Subunit organization and functional transitions in Ci-VSP. *Nat. Struct. Mol. Biol.* 15:106–108. doi:10.1038/nsmb1320.
- Kooijman, E.E., K.E. King, M. Gangoda, and A. Gericke. 2009. Ionization properties of phosphatidylinositol polyphosphates in mixed model membranes. *Biochemistry.* 48:9360–9371. doi:10.1021/bi9008616.
- Kurokawa, T., S. Takasuga, S. Sakata, S. Yamaguchi, S. Horie, K.J. Homma, T. Sasaki, and Y. Okamura. 2012. 3' Phosphatase activity toward phosphatidylinositol 3,4-bisphosphate [PI(3,4)P2] by voltage-sensing phosphatase (VSP). *Proc. Natl. Acad. Sci. U. S. A.* 109:10089–94. doi:10.1073/pnas.1203799109.

- Lacroix, J., C.R. Halaszovich, D.N. Schreiber, M.G. Leitner, F. Bezanilla, D. Oliver, and C. a Villalba-Galea. 2011. Controlling the activity of a phosphatase and tensin homolog (PTEN) by membrane potential. *J. Biol. Chem.* 286:17945–53. doi:10.1074/jbc.M110.201749.
- de Lamirande, E., and C. O’Flaherty. 2008. Sperm activation: Role of reactive oxygen species and kinases. *Biochim. Biophys. Acta - Proteins Proteomics.* 1784:106–115. doi:10.1016/j.bbapap.2007.08.024.
- Lee, J., H. Yang, and M. Georgescu. 1999. Crystal structure of the PTEN tumor suppressor: implications for its phosphoinositide phosphatase activity and membrane association. *Cell.* 99:323–34.
- Lee, S.R., K.S. Yang, J. Kwon, C. Lee, W. Jeong, and S.G. Rhee. 2002. Reversible inactivation of the tumor suppressor PTEN by H₂O₂. *J. Biol. Chem.* 277:20336–20342. doi:10.1074/jbc.M111899200.
- Levine, T.P., and S. Munro. 1998. The pleckstrin homology domain of oxysterol-binding protein recognises a determinant specific to Golgi membranes. *Curr. Biol.* 8:729–739. doi:10.1016/S0960-9822(98)70296-9.
- Li, Q., S. Wanderling, M. Paduch, D. Medovoy, A. Singharoy, R. McGreevy, C. a Villalba-Galea, R.E. Hulse, B. Roux, K. Schulten, A. Kossiakoff, and E. Perozo. 2014. Structural mechanism of voltage-dependent gating in an isolated voltage-sensing domain. *Nat. Struct. Mol. Biol.* 21:244–52. doi:10.1038/nsmb.2768.
- Liem, L.K., J.M. Simard, Y. Song, K. Tewari, W. Young, and R.G. Dacey. 1995. The patch clamp technique. *Neurosurgery.* 36:382–392. doi:10.1227/00006123-199502000-00020.
- Lin, J.Y. 2011. A user’s guide to channelrhodopsin variants: features, limitations and future developments. *Exp. Physiol.* 96:19–25. doi:10.1113/expphysiol.2009.051961.
- Lin, J.Y., M.Z. Lin, P. Steinbach, and R.Y. Tsien. 2009. Characterization of engineered channelrhodopsin variants with improved properties and kinetics. *Biophys. J.* 96:1803–1814. doi:10.1016/j.bpj.2008.11.034.
- Lindner, M., M.G. Leitner, C.R. Halaszovich, G.R. V Hammond, and D. Oliver. 2011. Probing the regulation of TASK potassium channels by PI₄,5P₂ with switchable phosphoinositide phosphatases. *J. Physiol.* 589:3149–62. doi:10.1113/jphysiol.2011.208983.
- Liu, L., S.C. Kohout, Q. Xu, S. Müller, C.R. Kimberlin, E.Y. Isacoff, and D.L. Minor. 2012. A glutamate switch controls voltage-sensitive phosphatase function. *Nat. Struct. Mol. Biol.* 19:633–41. doi:10.1038/nsmb.2289.
- Liu, Y., and V.A. Bankaitis. 2010. Phosphoinositide phosphatases in cell biology and disease. *Prog. Lipid Res.* 49:201–217. doi:10.1016/j.plipres.2009.12.001.
- Lukin, J. a, and C. Ho. 2004. The structure--function relationship of hemoglobin in solution at atomic resolution. *Chem. Rev.* 104:1219–30. doi:10.1021/cr940325w.
- Maehama, T., and J.E. Dixon. 1998. The Tumor Suppressor, PTEN/MMAC1, Dephosphorylates the Lipid Second Messenger, Phosphatidylinositol 3,4,5-Trisphosphate. *J. Biol. Chem.* 273:13375–13378. doi:10.1074/jbc.273.22.13375.
- Matsuda, M., K. Takeshita, T. Kurokawa, S. Sakata, M. Suzuki, E. Yamashita, Y. Okamura, and A. Nakagawa. 2011. Crystal structure of the cytoplasmic phosphatase and tensin homolog (PTEN)-like region of *Ciona intestinalis* voltage-sensing phosphatase provides insight into substrate specificity and redox regulation of the phosphoinositide phosphatase activity. *J. Biol. Chem.* 286:23368–77. doi:10.1074/jbc.M110.214361.

- McCrea, H.J., and P. De Camilli. 2009. Mutations in phosphoinositide metabolizing enzymes and human disease. *Physiology (Bethesda)*. 24:8–16. doi:10.1152/physiol.00035.2008.
- Miura, T., A. Hori-I, H. Mototani, and H. Takeuchi. 1999. Raman spectroscopic study on the copper(II) binding mode of prion octapeptide and its pH dependence. *Biochemistry*. 38:11560–11569. doi:10.1021/bi9909389.
- Molleman, A. 2003. Patch Clamping: An Introductory Guide to Patch Clamp Electrophysiology. 2003. 186 pp.
- Murata, Y., H. Iwasaki, M. Sasaki, K. Inaba, and Y. Okamura. 2005. Phosphoinositide phosphatase activity coupled to an intrinsic voltage sensor. *Nature*. 435:1239–43. doi:10.1038/nature03650.
- Murata, Y., and Y. Okamura. 2007. Depolarization activates the phosphoinositide phosphatase Ci-VSP, as detected in *Xenopus* oocytes coexpressing sensors of PIP₂. *J. Physiol.* 583:875–89. doi:10.1113/jphysiol.2007.134775.
- Nagel, G., T. Szellas, W. Huhn, S. Kateriya, N. Adeishvili, P. Berthold, D. Ollig, P. Hegemann, and E. Bamberg. 2003. Channelrhodopsin-2, a directly light-gated cation-selective membrane channel. *Proc. Natl. Acad. Sci. U. S. A.* 100:13940–13945. doi:10.1073/pnas.1936192100.
- Neher, E., and B. Sakmann. 1976. Single-channel currents recorded from membrane of denervated frog muscle fibres. *Nature*. 260:799–802. doi:10.1038/260799a0.
- Neuhaus, H., and T. Hollemann. 2009. Kidney specific expression of cTPTE during development of the chick embryo. *Gene Expr. Patterns*. 9:568–71. doi:10.1016/j.gep.2009.09.002.
- Niemeyer, M.I., L.P. Cid, G. Peña-Münzenmayer, and F. V. Sepúlveda. 2010. Separate gating mechanisms mediate the regulation of K₂P potassium channel TASK-2 by intra- and extracellular pH. *J. Biol. Chem.* 285:16467–16475. doi:10.1074/jbc.M110.107060.
- Nishigaki, T., O. José, A.L. González-Cota, F. Romero, C.L. Treviño, and A. Darszon. 2014. Intracellular pH in sperm physiology. *Biochem. Biophys. Res. Commun.* 450:1149–1158. doi:10.1016/j.bbrc.2014.05.100.
- Ogasawara, M., M. Sasaki, N. Nakazawa, A. Nishino, and Y. Okamura. 2011. Gene expression profile of Ci-VSP in juveniles and adult blood cells of ascidian. *Gene Expr. Patterns*. 11:233–238. doi:10.1016/j.gep.2010.12.004.
- Oikawa, T., and T. Takenawa. 2009. PtdIns(3,4)P₂ instigates focal adhesions to generate podosomes. *Cell Adhes. Migr.* 3:195–197. doi:10.4161/cam.3.2.7510.
- Qu, Z., Z. Yang, N. Cui, G. Zhu, C. Liu, H. Xu, S. Anchevalap, W. Shen, J. Wu, Y. Li, and C. Jiang. 2000. Gating of inward rectifier K⁺ channels by proton-mediated interactions of N- and C-terminal domains. *J Biol Chem.* 275:31573–80. doi:10.1074/jbc.M003473200.
- Quinn, K. V, P. Behe, and A. Tinker. 2008. Monitoring changes in membrane phosphatidylinositol 4,5-bisphosphate in living cells using a domain from the transcription factor tubby. *J. Physiol.* 586:2855–2871. doi:10.1113/jphysiol.2008.153791.
- Raab-Graham, K.F., C.M. Radeke, and C.A. Vandenberg. 1994. Molecular cloning and expression of a human heart inward rectifier potassium channel. *Neuroreport*. 5:2501–2505.
- Rahdar, M., T. Inoue, T. Meyer, J. Zhang, F. Vazquez, and P.N. Devreotes. 2009. A phosphorylation-dependent intramolecular interaction regulates the membrane association and activity of the tumor suppressor PTEN. *Proc. Natl. Acad. Sci. U. S. A.* 106:480–485. doi:10.1073/pnas.0811212106.

- Ratzan, W.J., A. V Evsikov, Y. Okamura, and L.A. Jaffe. 2011. Voltage sensitive phosphoinositide phosphatases of *Xenopus*: their tissue distribution and voltage dependence. *J. Cell. Physiol.* 226:2740–6. doi:10.1002/jcp.22854.
- Rebecchi, M.J., and S.N. Pentylala. 2000. Structure, function, and control of phosphoinositide-specific phospholipase C. *Physiol Rev.* 80:1291–1335.
- Rodríguez-Escudero, I., M.D. Oliver, A. Andrés-Pons, M. Molina, V.J. Cid, and R. Pulido. 2011. A comprehensive functional analysis of PTEN mutations: implications in tumor- and autism-related syndromes. *Hum. Mol. Genet.* 20:4132–42. doi:10.1093/hmg/ddr337.
- Rodriguez-Viciano, P., P.H. Warne, B. Vanhaesebroeck, M.D. Waterfield, and J. Downward. 1996. Activation of phosphoinositide 3-kinase by interaction with Ras and by point mutation. *Eur. Mol. Biol. Organ. J.* 15:2442–2451.
- Sakata, S., M.I. Hossain, and Y. Okamura. 2011. Coupling of the phosphatase activity of Ci-VSP to its voltage sensor activity over the entire range of voltage sensitivity. *J. Physiol.* 589:2687–705. doi:10.1113/jphysiol.2011.208165.
- Salim, K., M.J. Bottomley, E. Querfurth, M.J. Zvelebil, I. Gout, R. Scaife, R.L. Margolis, R. Gigg, C.I. Smith, P.C. Driscoll, M.D. Waterfield, and G. Panayotou. 1996. Distinct specificity in the recognition of phosphoinositides by the pleckstrin homology domains of dynamin and Bruton's tyrosine kinase. *EMBO J.* 15:6241–6250.
- Santagata, S., T.J. Boggon, C.L. Baird, C. a Gomez, J. Zhao, W.S. Shan, D.G. Myszka, and L. Shapiro. 2001. G-protein signaling through tubby proteins. *Science.* 292:2041–50. doi:10.1126/science.1061233.
- Schmid, A.C., R.D. Byrne, R. Vilar, and R. Woscholski. 2004. Bisperoxovanadium compounds are potent PTEN inhibitors. *FEBS Lett.* 566:35–38.
- Servant, G., O.D. Weiner, P. Herzmark, T. Balla, J.W. Sedat, and H.R. Bourne. 2000. Polarization of chemoattractant receptor signaling during neutrophil chemotaxis. *Science.* 287:1037–1040. doi:10.1126/science.287.5455.1037.
- Shacter, E. 2000. Quantification and significance of protein oxidation in biological samples. *Drug Metab. Rev.* 32:307–326. doi:10.1081/DMR-100102336.
- Srivastava, J., D.L. Barber, and M.P. Jacobson. 2007. Intracellular pH sensors: design principles and functional significance. *Physiology (Bethesda).* 22:30–39. doi:10.1152/physiol.00035.2006.
- Suh, B.-C., T. Inoue, T. Meyer, and B. Hille. 2006. Rapid chemically induced changes of PtdIns(4,5)P₂ gate KCNQ ion channels. *Science.* 314:1454–7. doi:10.1126/science.1131163.
- Sutton, K. a, M.K. Jungnickel, L. Jovine, and H.M. Florman. 2012. Evolution of the voltage sensor domain of the voltage-sensitive phosphoinositide phosphatase VSP/TPTE suggests a role as a proton channel in eutherian mammals. *Mol. Biol. Evol.* 29:2147–55. doi:10.1093/molbev/mss083.
- Szentpetery, Z., A. Balla, Y.J. Kim, M.A. Lemmon, and T. Balla. 2009. Live cell imaging with protein domains capable of recognizing phosphatidylinositol 4,5-bisphosphate; a comparative study. *BMC Cell Biol.* 10:67. doi:10.1186/1471-2121-10-67.
- Tapparel, C., A. Reymond, C. Girardet, L. Guillou, R. Lyle, C. Lamon, P. Hutter, and S.E. Antonarakis. 2003. The TPTE gene family: cellular expression, subcellular localization and alternative splicing. *Gene.* 323:189–199. doi:10.1016/j.gene.2003.09.038.

- Tian, Y., A. Daoud, and J. Shang. 2012. Effects of bpV(pic) and bpV(phen) on H9c2 cardiomyoblasts during both hypoxia/reoxygenation and H₂O₂-induced injuries. *Mol. Med. Rep.* 5:852–8. doi:10.3892/mmr.2011.737.
- Varga, E. a, M. Pastore, T. Prior, G.E. Herman, and K.L. McBride. 2009. The prevalence of PTEN mutations in a clinical pediatric cohort with autism spectrum disorders, developmental delay, and macrocephaly. *Genet. Med.* 11:111–7. doi:10.1097/GIM.0b013e31818fd762.
- Várnai, P., and T. Balla. 1998. Visualization of phosphoinositides that bind pleckstrin homology domains: Calcium- and agonist-induced dynamic changes and relationship to myo-[³H]inositol-labeled phosphoinositide pools. *J. Cell Biol.* 143:501–510. doi:10.1083/jcb.143.2.501.
- Várnai, P., and T. Balla. 2006. Live cell imaging of phosphoinositide dynamics with fluorescent protein domains. *Biochim. Biophys. Acta.* 1761:957–67. doi:10.1016/j.bbali.2006.03.019.
- Várnai, P., B. Thyagarajan, T. Rohacs, and T. Balla. 2006. Rapidly inducible changes in phosphatidylinositol 4,5-bisphosphate levels influence multiple regulatory functions of the lipid in intact living cells. *J. Cell Biol.* 175:377–82. doi:10.1083/jcb.200607116.
- Villalba-Galea, C. a. 2012. Voltage-Controlled Enzymes: The New JanusBifrons. *Front. Pharmacol.* 3:161. doi:10.3389/fphar.2012.00161.
- Villalba-Galea, C. a, F. Miceli, M. Tagliatalata, and F. Bezanilla. 2009. Coupling between the voltage-sensing and phosphatase domains of Ci-VSP. *J. Gen. Physiol.* 134:5–14. doi:10.1085/jgp.200910215.
- Villalba-Galea, C. a, W. Sandtner, D.M. Starace, and F. Bezanilla. 2008. S4-based voltage sensors have three major conformations. *Proc. Natl. Acad. Sci. U. S. A.* 105:17600–7. doi:10.1073/pnas.0807387105.
- Walker, S.M., C.P. Downes, and N.R. Leslie. 2001. TPIP : a novel phosphoinositide 3-phosphatase. 283:277–283.
- Wragg, S., and K. Drickamer. 1999. Identification of amino acid residues that determine pH dependence of ligand binding to the asialoglycoprotein receptor during endocytosis. *J. Biol. Chem.* 274:35400–35406.
- Wu, Y., D. Dowbenko, M.T. Pisabarro, L. Dillard-Telm, H. Koeppen, and L. a Lasky. 2001. PTEN 2, a Golgi-associated testis-specific homologue of the PTEN tumor suppressor lipid phosphatase. *J. Biol. Chem.* 276:21745–53. doi:10.1074/jbc.M101480200.
- Yamaguchi, S., T. Kurokawa, I. Taira, N. Aoki, S. Sakata, Y. Okamura, and K.J. Homma. 2014. Potential role of voltage-sensing phosphatases in regulation of cell structure through the production of PI(3,4)P₂. *J. Cell. Physiol.* 229:422–33. doi:10.1002/jcp.24463.
- Yoshizaki, H., N. Mochizuki, Y. Gotoh, and M. Matsuda. 2007. Akt – PDK1 Complex Mediates Epidermal Growth Factor-induced Membrane Protrusion through Ral Activation. *Mol. Biol. Cell.* 18:119–128. doi:10.1091/mbc.E06.
- Yudin, Y., V. Lukacs, C. Cao, and T. Rohacs. 2011. Decrease in phosphatidylinositol 4,5-bisphosphate levels mediates desensitization of the cold sensor TRPM8 channels. *J. Physiol.* 589:6007–27. doi:10.1113/jphysiol.2011.220228.
- Zeng, Y., J.A. Oberdorf, and H.M. Florman. 1996. pH regulation in mouse sperm: identification of Na(+)-, Cl(-)-, and HCO₃(-)-dependent and arylaminobenzoate-dependent regulatory mechanisms and characterization of their roles in sperm capacitation. *Dev. Biol.* 173:510–520.

6 Acknowledgments

I would like to sincerely thank Dr. Christian Halaszovich and Prof. Dr. Dominik Oliver for providing my research topic and giving me the opportunity to work in this group, as well as for the scientific guidance and support that they provided throughout my thesis.

In particular I want to express my gratitude to Dr. Christian Halaszovich for his close supervision including scientific discussions, technical guidance, answering questions, reviewing my paper and thesis, and for his encouragement and support throughout my PhD. Moreover I thank Dr. Michael Leitner for kindly providing great help in numerous occasions.

I thank all the scientific members of our group: Anja Feuer, Aileen Franke, Bettina Wilke, Florian Nies, Julia Hartmann, Marlen Dierich, Veronika Thallmair, Dr. Daniela Schreiber, Dr. Kirstin Hobiger and Dr. Dmitri Gorbunov for the help and the nice cooperation.

I would also like to thank the technical assistants: Gisela Fischer, Eva Naudascher, Olga Ebers and Matthias Bauer for their support in molecular biology and cell culture.

In addition, I would like to thank the following for providing plasmid DNA: T. Balla for the gift of PLC δ 1-PH, Btk-PH, Akt1-PH, and GRP1-PH, L. Shapiro for tubbyC, M. Matsuda for Pippi-PI(4,5)P₂, J. Zhang for AktAR, T. Jentsch for KCNQ4, J. Daut for TASK-3, T. Plant for TRPV1, K. Deisseroth for ChR2 H134R, Y. Okamura for Ci-VSP and J. Downward for p110 α K227E.

This project was supported by University Medical Center Giessen and Marburg grant UKGM 32/2011 MR to C. Halaszovich., grant UKGM 17/2013 to M. Leitner, and Deutsche Forschungsgemeinschaft / DFG grant SFB593 TP A12 to Dominik Oliver.

7 Publications

Mavrantoni A., Thallmair V., Leitner M.G., Schreiber D.N., Oliver D., Halaszovich C.R. (2015). A method to control phosphoinositides and to analyze PTEN function in living cells using voltage sensitive phosphatases. *Front Pharmacol*, 31;6:68. doi: 10.3389/fphar.2015.00068

Costa H., Leitner M., Sos M., **Mavrantoni A.**, Rychkova A., Johnson J., Newton B., Yee M., De La Vega F., Ford J., Krogan N., Shokat K. , Oliver D., Halaszovich C., and Bustamante C. (2015). Discovery and functional characterization of a neomorphic PTEN mutation. *Proc Natl Acad Sci U S A*, 10;112(45):13976-81. doi: 10.1073/pnas.1422504112

Halaszovich, C. R., Leitner, M. G., **Mavrantoni, A.**, Le, A., Frezza, L., Feuer, A. Schreiber, D. N. Villalba-Galea, C. A. Oliver, D. (2012). A human phospholipid phosphatase activated by a transmembrane control module. *Journal of Lipid Research*, 53(11), 2266–74. doi:10.1194/jlr.M026021

8 Curriculum vitae

Name : Angeliki Mavrantoni

Email: angelikimavrantoni@gmail.com

Address: Coschützer Str. 23, 01187, Dresden

Tel: +49 152 59522010

Date and place of birth: 30.01.1987, Corfu, Greece

EDUCATION

Sept.2011-Feb.2015 **PhD in Physiology**, Philipps University, Department of Physiology, Marburg, Germany.

Sept. 2010-Aug. 2011 **Master's in Biomedical Science**, Glasgow University, Glasgow, UK.

Sept. 2004-Feb. 2009 **Bachelor's in Molecular Biology and Genetics**, Democritus University, Alexandroupolis, Greece.

RESEARCH EXPERIENCE

Doctoral research, Philipps University, Marburg. September 2011-February 2015.

"Voltage Sensitive Phosphatases: understanding their function and expanding their potential use". Research involves molecular cloning, confocal microscopy, TIRF microscopy, FRET, patch clamping.

Master's research, project 1, Glasgow University, UK, October 2010-March 2011. "Mosaicism of MeCP2 expression in the brain and in peripheral tissues". Research involved sectioning, histological processing, immunocytochemistry and confocal microscopy.

Master's research, project 2, Glasgow University, UK, April -August 2011.

"The effects of proteinase K on the synaptic activity and synaptic proteins of rodent hippocampus". Research involved hippocampus extracellular recordings and western blotting.

Bachelor's research: Seattle Biomedical Research Institute, Seattle, USA, March 2008- August 2008. "Cross-reactive neutralizing antibodies against HIV-1" Research involved molecular cloning, cell culture, ELISA and neutralization assays.

CONFERENCES

Poster presentation: German Physiological Society, Mainz, March 2014.

"The effect of intracellular pH and redox state on the catalytic activity of voltage sensitive phosphatases". Mavrantoni A., Oliver D., Halaszovich C.R.

Poster presentation: Biophysical Society, Philadelphia, February 2013. "

Activation of voltage sensitive phosphatases with pharmacological and optogenetic methods". Mavrantoni A., Oliver D., Halaszovich C.R.

Oral presentation: German Physiological Society, Dresden, March 2012.

"Studying voltage sensitive phosphatases in population of living cells without the need for electrophysiological instrumentation". Mavrantoni A., Oliver D., Halaszovich C.R.

9 List of academic teachers

My academic teachers were the following ladies and gentlemen in:

Marburg

Halaszovich, Oliver

Glasgow

Cobb, Hughes, Maxwell D., Maxwell W. ,McInerny, Riddley,Stone, Wilson

Alexandroupolis

Agianian, Boukouvala, Chlichlia, Fakis, Fylaktakidou, Galanis, Glykos, Grigoriou, Kastani, Kourkoutas, Koffa, Pappa, Pasxou, Skavdis, Sandaltzopoulos

10 Ehrenwörtliche Erklärung

Ich erkläre ehrenwörtlich, dass ich die dem Fachbereich Medizin Marburg zur Promotionsprüfung eingereichte Arbeit mit dem Titel:

“Voltage sensitive phosphatases: understanding their function and expanding their potential use.”

im Institut für Physiologie und Pathophysiologie unter Leitung von Prof. Dr. Dr. Daut mit Unterstützung durch Prof. Dr. Oliver und Dr. Halaszovich ohne sonstige Hilfe selbstdurchgeführt und bei der Abfassung der Arbeit keine anderen als die in der Dissertation aufgeführten Hilfsmittel benutzt habe. Ich habe bisher an keinem in-oder ausländischen Medizinischen Fachbereich ein Gesuch um Zulassung zur Promotion eingereicht, noch die vorliegende oder eine andere Arbeit als Dissertation vorgelegt.

Marburg am.....

Angeliki Mavrantoni